

**A D - 759 765**

**RAPID COMPUTATION BY WAVE THEORY OF  
PROPAGATION LOSS IN THE ARCTIC OCEAN**

**Henry W. Kutschale**

**Lamont-Doherty Geological Observatory**

**Prepared for:**

**Office of Naval Research**

**March 1973**

**DISTRIBUTED BY:**



**National Technical Information Service  
U. S. DEPARTMENT OF COMMERCE  
5285 Port Royal Road, Springfield Va. 22151**

AD 759765

LAMONT-DOMINITY GEOLOGICAL OBSERVATORY OF COLUMBIA UNIVERSITY  
Palisades, New York

10964

RAPID COMPUTATION BY WAVE THEORY  
OF PROPAGATION LOSS IN THE ARCTIC OCEAN

by

Henry W. Kutschale

CU-8-73

Technical Report No. 8

CONTRACT N00014-67-A-0108-0016



Research Supported by the Office  
of Naval Research and the  
Advanced Research Projects Agency

Reproduction of this document in  
whole or in part is permitted for  
any purpose of the U. S. Government.

March, 1973

Reproduced by  
NATIONAL TECHNICAL  
INFORMATION SERVICE  
U.S. Department of Commerce  
Springfield VA 22151

DISTRIBUTION STATEMENT A

Approved for public release;  
Distribution Unlimited

103 R

Inclassified

Security Classification

DOCUMENT CONTROL DATA - R & D

(Security classification of title, body of abstract and indexing annotation must be entered when the overall report is classified)

1. ORIGINATING ACTIVITY (Name, city, state)	2a. REPORT NUMBER	2b. GROUP
	Unclassified Arctic	

3. REPORT TITLE

Rapid Computation by Wave Theory of Propagation Loss in the Arctic Ocean.

4. DESCRIPTIVE NOTES (Type of report and inclusive dates)

Technical Report

5. AUTHOR(S) (First name, middle initial, last name)

Henry W. Kutschale

6. REPORT DATE	7a. TOTAL NO. OF PAGES	7b. NO. OF REFS
March 1973	99	15
8a. CONTRACT OR GRANT NO.	9a. ORIGINATOR'S REPORT NUMBER(S)	
N00014-67-A-0108-0016	CU-8-73	
b. PROJECT NO.		
c. NR 307-320/1-6-69 (415)		
d.	9b. OTHER REPORT NO(S) (Any other numbers that may be assigned this report)	

10. DISTRIBUTION STATEMENT

Reproduction of this document in whole or in part is permitted for any purpose of the U. S. Government.

11. SUPPLEMENTARY NOTES	12. SPONSORING MILITARY ACTIVITY
	Office of Naval Research and Advanced Research Projects Agency

13. ABSTRACT

A rapid, accurate method was developed of computing propagation loss as a function of range in the ice covered Arctic Ocean. Input parameters to the propagation model are source and detector depth, wave frequency, ice roughness, bottom topography, and the velocity structure as a function of depth in the ice, water, and bottom. Computation is done by direct integration of the exact integral solution of the wave equation derived from a harmonic point source located in a multilayered, interbedded liquid-solid half space. The integration technique, introduced by H. W. Marsh, employs the Fast Fourier Transform for very rapid evaluation of the integral solution. Computed propagation loss as a function of range is in good agreement with field data.

Unclassified  
Security Classification

14  KEY WORDS	LINK A		LINK B		LINK C	
	ROLE	WT	ROLE	WT	ROLE	WT
Arctic Hydroacoustics Propagation Loss Numerical Computations Fast Field Program Fast Fourier Transform Layered Media Matrix Integral Solution Digital Computer Wave Theory						

## TABLE OF CONTENTS

	Pages
<b>Abstract</b>	1
<b>Captions for Figures</b>	2- 5
<b>Introduction</b>	6- 8
<b>Comparison with Normal-Mode Theory</b>	8- 9
<b>Computation of Propagation Loss</b>	9-13
<b>Comparison with Field Data</b>	13-14
<b>Comparison with Ray Theory</b>	14-15
<b>Acknowledgements</b>	16
<b>Tables I to VI</b>	17-22
<b>Figures 1 to 41</b>	23-63
<b>Definition of Symbols for Appendix A and Appendix B</b>	64-66
<b>Appendix A</b>	67-92
<b>Appendix B</b>	93-97
<b>References</b>	98-99

**ABSTRACT**

A rapid, accurate method was developed of computing propagation loss as a function of range in the ice covered Arctic Ocean. Input parameters to the propagation model are source and detector depth, wave frequency, ice roughness, bottom topography, and the velocity structure as a function of depth in the ice, water, and bottom. Computation is done by direct integration of the exact integral solution of the wave equation derived from a harmonic point source located in a multilayered, interbedded liquid-solid half space. The integration technique introduced by H. W. Marsh, employs the Fast Fourier Transform for very rapid evaluation of the integral solution. Computed propagation loss as a function of range is in good agreement with field data.

CAPTIONS FOR FIGURES

**Figure 1.** Typical ray paths for a source 100 m deep in the central Arctic Ocean. Forty rays computed at 1 degree intervals at the source. Angles at the source go from 20 degrees above to 20 degrees below the horizontal.

**Figure 2.** Oscillogram of signal from 9 lb. charge of TNT fired at a depth of 152 m. Hydrophone at a depth of 61 m. Passband of listening system 10-21 Hz.

**Figure 3.** Comparison of observed and computed group-velocity dispersion for first three modes. Range 578.6 km. 5-lb. TNT charge at 66 m, hydrophone at 46 m.

**Figure 4.** Vertical sound velocity profile for model of Table I.

**Figure 5.** Propagation loss as a function of range at 10 Hz for model of Table I. Direct integration (FFP). Source depth 150 m, hydrophone depth 100 m.

**Figure 6.** Propagation loss as a function of range at 25 Hz for model of Table I. Direct integration (FFP). Source depth 150 m, hydrophone depth 100 m.

**Figure 7.** Propagation loss as a function of range at 10 Hz for model of Table I. Normal-mode theory. Source depth 150 m, hydrophone depth 100 m.

**Figure 8.** Propagation loss as a function of range at 25 Hz for model of Table I. Normal-mode theory. Source depth 150 m, hydrophone depth 100 m.

**Figure 9.** Absolute value of integrand at 10 Hz corresponding to Figure 5.

**Figure 10.** Absolute value of integrand at 25 Hz corresponding to Figure 6.

**Figure 11.** Propagation loss as a function of range for model of Table 2 at 10 Hz. Source depth 50, hydrophone depth 50 m. Surface roughness 3 m RMS.

## CAPTIONS FOR FIGURES (cont'd)

- Figure 12. Propagation loss as a function of range for model of Table II at 15 Hz. Source depth 50 m, hydrophone depth 50 m. Surface roughness 3 m RMS.
- Figure 13. Propagation loss as a function of range for model of Table II at 20 Hz. Source depth 50 m, hydrophone depth 50 m. Surface roughness 3 m RMS.
- Figure 14. Propagation loss as a function of range for model of Table II at 30 Hz. Source depth 50 m, hydrophone depth 50 m. Surface roughness 3 m RMS.
- Figure 15. Propagation loss as a function of range for model of Table II at 60 Hz. Source depth 50 m, hydrophone depth 50 m. Surface roughness 3 m RMS.
- Figure 16. Propagation loss as a function of range for model of Table III at 10 Hz. Source depth 50 m, hydrophone depth 50 m. Ice roughness 3 m RMS.
- Figure 17. Propagation loss as a function of range for model of Table III at 15 Hz. Source depth 50 m, hydrophone depth 50 m. Ice roughness 3 m RMS.
- Figure 18. Propagation loss as a function of range for model of Table III at 20 Hz. Source depth 50 m, hydrophone depth 50 m. Ice roughness 3 m RMS.
- Figure 19. Propagation loss as a function of range for model of Table III at 30 Hz. Source depth 50 m, hydrophone depth 50 m. Ice roughness 3 m RMS.
- Figure 20. Propagation loss as a function of range for model of Table III at 60 Hz. Source depth 50 m, hydrophone depth 50 m. Ice roughness 3 m RMS.
- Figure 21. Propagation loss as a function of range for model of Table IV at 10 Hz. Source depth 50 m, hydrophone depth 50 m. Surface roughness 3 m RMS.

CAPTIONS FOR FIGURES (cont'd)

**Figure 22.** Propagation loss as a function of range for model of Table IV at 15 Hz. Source depth 50 m, hydrophone depth 50 m. Surface roughness 3 m RMS.

**Figure 23.** Propagation loss as a function of range for model of Table IV at 20 Hz. Source depth 50 m, hydrophone depth 50 m. Surface roughness 3 m RMS.

**Figure 24.** Propagation loss as a function of range for model of Table IV at 30 Hz. Source depth 50 m, hydrophone depth 50 m. Surface roughness 3 m RMS.

**Figure 25.** Propagation loss as a function of range for model of Table IV at 60 Hz. Source depth 50 m, hydrophone depth 50 m. Surface roughness 3 m RMS.

**Figure 26.** Propagation loss as a function of range for model of Table V at 10 Hz. Source depth 50 m, hydrophone depth 50 m. Ice roughness 3 m RMS.

**Figure 27.** Propagation loss as a function of range for model of Table V at 15 Hz. Source depth 50 m, hydrophone depth 50 m. Ice roughness 3 m RMS.

**Figure 28.** Propagation loss as a function of range for model of Table V at 20 Hz. Source depth 50 m, hydrophone depth 50 m. Ice roughness 3 m RMS.

**Figure 29.** Propagation loss as a function of range for model of Table V at 30 Hz. Source depth 50 m, hydrophone depth 50 m. Ice roughness 3 m RMS.

**Figure 30.** Propagation loss as a function of range for model of Table V at 60 Hz. Source depth 50 m, hydrophone depth 50 m. Ice roughness 3 m RMS.

**Figure 31.** Propagation loss as a function of range for model of Table III at 15 Hz. Source depth 100 m, hydrophone depth 50 m. Ice roughness 3 m RMS.

## CAPTIONS FOR FIGURES (cont'd)

- Figure 32. Propagation loss as a function of range for model of Table III at 15 Hz. Source depth 150 m, hydrophone depth 50 m. Ice roughness 3 m RMS.
- Figure 33. Average propagation loss as a function of range for model of Table III at 15 Hz. Source 50 m, hydrophone depth 50 m. Ice roughness 3 m RMS. Averaging interval 11.5 km.
- Figure 34. Average propagation loss as a function of range for model of Table III at 15 Hz. Source 100 m, hydrophone depth 50 m. Ice roughness 3 m RMS. Averaging interval 11.5 km.
- Figure 35. Average propagation loss as a function of range for model of Table III at 15 Hz. Source 150 m, hydrophone depth 50 m. Ice roughness 3 m RMS. Averaging interval 11.5 km.
- Figure 36. Propagation loss as a function of range for model of Table VI at 15 Hz. Source depth 50 m, hydrophone depth 50 m. Ice roughness 3 m RMS.
- Figure 37. Propagation loss as a function of range for model of Table VI at 30 Hz. Source depth 50 m, hydrophone depth 50 m. Ice roughness 3 m RMS.
- Figure 38. Propagation loss as a function of range for model of Table III at 15 Hz. Source depth 50 m, hydrophone depth 50 m. Ice roughness 4 m RMS.
- Figure 39. Average propagation loss as a function of range for model of Table III at 15 Hz. Source depth 50 m, hydrophone depth 50 m. Ice roughness 4 m RMS. Averaging interval 11.5 km.
- Figure 40. Average propagation loss as a function of range for model of Table III at 20 Hz. Source depth 50 m, hydrophone depth 50 m. Ice roughness 3 m RMS. Averaging interval 8.6 km.
- Figure 41. Comparison of propagation loss of field data with computed curve of Figure 40. Predictions by ray theory also shown.
- Figure A-1. Layered model.

## INTRODUCTION

The two features peculiar to the polar environment that most strongly influence underwater sound are the permanent ice cover and the velocity structure in the water. Ice movement generates ambient noise and the ice modifies propagation, particularly at high frequencies, by scattering waves from the rough ice boundaries. Sound velocity is a function of temperature, salinity, and pressure. The relationship among these variables in the central Arctic Ocean is such that sound velocity is generally an increasing function of depth from the surface to the bottom. Such a velocity profile is found only in polar waters. The sound velocity structure is very uniform both as a function of location and time of year. Sounds are transmitted to great ranges in this natural Arctic waveguide or sound channel by upward refraction in the water and repeated reflection from the ice canopy. Typical ray paths are shown in Fig. 1. A two-pound explosion of TNT has been heard at ranges exceeding 1,000 km (700 miles).

The surface sound channel of the Arctic is the polar extension of the deep sound channel or SOFAR channel of the nonpolar oceans, but the Arctic signals are often quite different from those observed in the deep channel, largely because of the predominance of low-frequency waves in the Arctic. A regular oscillatory wave train at long ranges from an underwater explosion is the result of interference of sounds traveling along the various paths between source and detector (Kutschale, 1961, 1969). The exact solution of the wave equation for propagation in multilayered media in terms of normal modes provides a useful method for describing these signals in detail (Kutschale,

1969, 1970). Figure 2 shows a typical signal with waves corresponding to the first and second normal modes. On Figure 3 a typical sound spectrogram is compared with a computed one. The agreement between the observed and computed group-velocity dispersion is excellent. Figures 2 and 3 show that the low-frequency waves traveling in the sound channel are coherent over long ranges. Thus a coherent summation of waves is appropriate for computing propagation loss from low-frequency continuous wave (cw) sources.

A rapid, accurate method is developed in Appendix A of computing propagation loss as a function of range in the ice covered Arctic Ocean. Important input parameters to the propagation model are wave frequency, source and detector depth, ice roughness, bottom topography, and the velocity structure as a function of depth in the ice, water, and bottom sediments. Computational speed is of the utmost importance to evaluate effects of variations of these parameters on propagation loss as a function of range since a large number of models must be considered.

Such a rapid, accurate computational method is the Fast Field Program (FFP) technique for wave theory introduced by Marsh (1967). The FFP was implemented for computation on a digital computer by Di-Napoli (1971) for propagation in an all-liquid waveguide. In the Arctic Ocean solid layers as well as liquid layers must be considered, and a convenient starting point for the FFP is the integral solution of the wave equation derived by matrix methods in Appendix A for propagation from point harmonic sources in a multilayered liquid-solid half space.

In the FFP technique the integral solution of the wave equation is evaluated rapidly as a function of range by numerical integration

employing the Fast Fourier Transform (FFT). Singularities in the integrand corresponding to the normal-mode poles are removed from the axis of integration by including attenuation coefficients for compressional and shear waves in each layer. In a liquid layer, of course, both the shear velocity and corresponding attenuation coefficient are zero.

Two computer programs were written in Fortran IV to evaluate the liquid-and solid-bottom integral solutions derived in Appendix A. A comparison of the FFP computations with those computations by normal-mode theory from the corresponding integral solution are identical, but the FFP technique is far more convenient and at least an order of magnitude faster, since the computations are done directly from the integral solution without first computing the roots of the dispersion equation and then summing the normal modes.

In the multilayered computations, the variation of compressional and shear velocities and density with depth in the ice, ocean, and sediments is represented by a series of plane parallel layers, each with constant velocities and density over the layer thickness. The last layer of the laminated half space is of infinite thickness. The number of layers is adjusted until no further significant change of computed results is obtained by a finer partitioning of the observed velocity and density data. In practice, 20 to 30 layers are usually sufficient to represent the velocity and density data in the deep ocean over the frequency band from 10 to 60 Hz. At higher frequencies more layers may be necessary.

#### Comparison with Normal-Mode Theory

The FFP approach integrates numerically the integral solution of the wave equation derived from a laminated half space. For guided

real wave number,  $k$ , axis corresponding to the normal-mode poles.

If attenuation coefficients are introduced in each layer, the poles are removed from the real  $k$  axis and the integration can be done numerically. The effect on propagation loss as a function of range of attenuation in each layer can be removed after the integral is computed so that the final result is the same as that computed by normal-mode theory with no attenuation present in each layer.

Table I lists the parameters of a model from which computations were done by normal-mode theory and the FFP (8192 points for the FFT). The velocity profile is shown in Figure 4. This shallow-water model exhibits the principal features of normal-mode propagation at low frequencies. It was chosen to speed the numerical work, since only between two and five normal modes propagate in the band from 10 to 25 Hz. Figures 5 to 8 show the comparisons by both methods of propagation loss as a function of range at 10 and 25 Hz. For the computations by the FFP the effect on propagation loss of the attenuation in each layer was removed after the integral was computed so that the computations from the integral solution by both methods should be identical. That this is the case is apparent from Figures 5 to 8 at 10 and 25 Hz.

At 10 Hz two normal modes propagate in the layered system and at 25 Hz five normal modes. The absolute value of the integrand at 10 and 25 Hz is shown in Figures 9 and 10. The peaks in the integrands correspond to the wave numbers computed by normal-mode theory. The first mode corresponds to the largest  $k$ . Progressively higher modes correspond to progressively lower  $k$  values.

#### Computation of Propagation Loss

This section presents computations of propagation loss as a function of range in the deep water of the central Arctic Ocean.

All integrations were made by the FFT with 8192 points. Great care was exercised to prevent aliasing in the FFT computations.

The following effects of the waveguide on propagation loss are investigated:

- 1) An ice layer at the surface
- 2) Rigidity in the bottom sediments
- 3) Source depth
- 4) Small changes in the sound-velocity profile  
in the upper 400 m of water
- 5) Variations of ice roughness along the path.

Table II gives a layered model for the deep Arctic Ocean. This model represents an average layering in the ocean based on about twenty individual sound velocity profiles observed at various locations and at different times of the year. The ocean velocity profile is partitioned into 23 layers. A finer partitioning would have a negligible effect on the computations over the frequency range from 10 to 60 Hz. The 4 km water depth represents propagation over the deep abyssal plains, such as the Canada Abyssal Plain.

Figures 11 to 15 show propagation loss as a function of range computed from the model of Table II. The fluctuating propagation loss from the cw source in the band from 10 to 60 Hz is in response to the multipath interference of waves traveling between source and detector. The integrations were carried out over a range of wave numbers to include all the normal modes as well as waves from which energy is refracted into the bottom (leaky modes). The contribution of the leaky modes to propagation loss is seen as a high-frequency oscillation at short ranges. At long ranges these waves have been eliminated because

of loss of energy to the bottom. The effect of attenuation in each layer was removed from the computations of Figures 11 to 15, as well as in all subsequent computations, since absorption of sound in the water is negligible at the very low frequencies of the computations over the range intervals used. However, a range dependent attenuation for a rough ice surface is included by multiplying the range dependence of pressure by the formula of Mellen and Marsh (1965).

In Figures 16 to 20 the computations are repeated for the layering in the water of Table II, but a solid ice sheet 3 m thick is placed at the surface. The model is given in Table III. The effect of this solid ice sheet on propagation loss as a function of range appears to be negligible over the frequency range 10 to 60 Hz.

Figures 21 to 30 show the effect of a solid bottom on propagation loss. The models are given in Tables IV and V. The layering in the water is the same as the model of Table II, but a shear velocity of 200 m/sec is included in the bottom sediments. Such low shear velocities are commonly measured in ocean-bottom sediments of deep basins (Sykes and Oliver, 1964). It is apparent that the effect on propagation loss of a solid bottom is small if the ice is neglected. When the ice sheet is included at the surface there is apparently wave coupling between the solid bottom and the solid surface layer observed as a high-frequency oscillation of propagation loss with range. However, the average propagation loss appears to be nearly the same as in the previous cases.

Figures 31 to 35 show the effect of source depth on propagation at 15 Hz. The effect of source depth on propagation loss is more apparent if the propagation loss for a cw source is smoothed with range.

This smoothing was done by taking a running average of propagation loss in range computed at the midpoint for each range interval. This was done for convenience rather than taking the running average with range of intensity and converting this to propagation loss. The latter approach is rigorously correct, but test cases showed that at 15 and 20 Hz the difference between the two methods of averaging was generally less than three dB. There is only a slight decrease of loss with range for the deeper sources.

Figures 36 and 37 show the effect on propagation loss at 15 and 30 Hz of small changes in stratification in the upper 400 m of water. The model is given in Table VI, and it corresponds to a single measured profile. It is apparent by comparing Figures 36 and 37 with Figures 17 and 19 that the detailed velocity structure in the upper layers has a significant effect on the fluctuations of the propagation loss with range, but the average loss as a function of range appears to be about the same in both cases.

Figures 38 and 39 show the effect on propagation loss of a rougher ice sheet than used in the previous computations. The effect on propagation loss of this rougher ice sheet is not apparent when compared with Figures 17 and 33, but it would be at longer ranges beyond 500 km or at higher frequencies over these same range intervals.

The effects of variable and rough bottom topography on propagation loss as a function of range were investigated, but not in detail. The method of approach is to assume that waves passing over all bottom topography without striking the bottom predominate in the signal. Such an assumption is substantiated by experimental data. This is implemented in the computations by two methods. In the first, the layered section is formed for the deepest portion of the propagation path. In

layers lying above all topography, low attenuation coefficients are used in each layer. For the deeper layers much higher attenuation coefficients are used. The effect of this high attenuation is to suppress waves with phase velocities greater than the speed of sound at the depth of the shallowest part of the bathymetric profile. The second method is to integrate only over the range of wave numbers corresponding to waves passing over all bottom topography. This method has the advantage of reducing computer time, since the integral is computed over a shorter range of wave numbers.

From the illustrations it is apparent that an ice sheet at the surface, a low rigidity bottom, or small changes in the velocity profile mainly affect fluctuations of propagation loss with range, but do not appear to alter significantly average values of loss as might be measured with explosive charges. As long as one is interested only in average propagation loss, the computations for an all-liquid guide appear to be satisfactory. On the other hand, if geophones are used as listening devices, the ice sheet must be included as a solid layer at the surface since the waves are elliptically polarized in the ice in the plane of propagation. Particle motion for guided hydroacoustic waves is retrograde elliptical at the surface and pro-grade elliptical at the bottom of the ice (Kutschale, 1972). The present theory has been extended to compute propagation loss to geophones on the ice surface or geophones buried at depth in the ice (Kutschale, in preparation).

#### Comparison with Field Data

In this section field data of propagation loss as 20 Hz are compared with the computed propagation loss. The comparisons are made for an average propagation loss as a function or range for both experiment and theory. Mellen and Marsh (1965) and Buck (1968) have

compiled average experimental curves. The measurements by Mellen and Marsh and Buck lump together various source depths between 40 and 200 m and propagation paths. This probably accounts for the spread of measurements at each frequency.

Since the measurements were made with explosive charges analyzed in various filter band widths reduced to a one Hz band, it is difficult to compare them with computations from a cw source. A meaningful basis for comparison is the smoothed propagation loss as a function of range computed from a running average. Such an average curve at 20 Hz is shown in Figure 40 for the model of Table III. Since the preceding computations show that the average loss is not affected much by a low shear velocity in the bottom, it was neglected. Field observations indicate that a root-mean-square (rms) ice roughness of 3 m is appropriate over the paths of the experiments.

In Figure 41 the average measured curves of Mellen and Marsh and Buck are compared with the average computed one. The agreement between the two sets of curves is quite good. A detailed comparison between experiment and theory would require close control of the experimental situation. Such experiments were made by Kutschale over the flat bottom of the Abyssal Canada Plain at ranges up to 1300 km by keeping the source and detector depths constant. These data will be analyzed for propagation loss, and they will be useful for a detailed comparison with the present theory.

#### Comparison with Ray Theory

Ray theory is commonly used to predict propagation loss in the ocean, and it was used by Aerophysics Research Corporation in their work. If only propagation loss at a single range point on a path

is required, it may be faster to use ray theory than the direct integration (FFP). The question is often raised, however, about the reliability of predictions by ray theory at very low frequencies. To attempt to answer this question, the FFP computations are compared with the ray predictions in Figure 41. Propagation loss by ray theory was computed by summing the intensities for each ray incoherently (phase was neglected). These computations should thus be compared with the smoothed propagation loss computations by the FFP. It is seen from Figure 41 that at ranges beyond 100 km the predictions by both methods agree reasonably well. At ranges less than 100 km the two sets of computations diverge. The ray theory predictions of loss are too low compared both to the field data and the FFP results. The reasonably good agreement at long ranges, however, is gratifying and supports the application of ray theory for the intensity computations at Aerophysics Research Corporation at ranges exceeding 500 km.

#### AKNOWLEDGMENTS

I am indebted to Harry Akers, Jr. for his assistance in writing the programs for computing and plotting propagation loss as a function of range. He also provided substantial assistance in preparing this report. Discussions with Dr. T. S. Chow of Aerophysics Research Corporation and Dr. F. R. DiNapoli of the Naval Underwater Systems Center, New London, Connecticut, were extremely helpful. Dr. T. S. Chow provided the computations of propagation loss by ray theory. Computing facilities were provided by the Columbia University Computing Center. This work was supported by the Office of Naval Research under Contract N00014-67-A-0108-0016 and by the Advanced Research Projects Agency by subcontract to Lamont-Doherty Geological Observatory from the Aerophysics Research Corporation, Bellevue, Washington.

TABLE ILayered Model, water depth 350 m

Layer	Compressional velocity, m/sec	Shear velocity, m/sec	Density, gm/cm <sup>3</sup>	Layer thickness, m
1	1434.0	0.0	1.03	50.0
2	1437.0	0.0	1.03	50.0
3	1440.0	0.0	1.03	50.0
4	1443.0	0.0	1.03	50.0
5	1446.4	0.0	1.03	50.0
6	1450.0	0.0	1.03	50.0
7	1453.2	0.0	1.03	50.0
8	1600.0	0.0	1.03	$\infty$

TABLE IILayered Model, water depth 4000 m, liquid bottom

Layer	Compressional velocity, m/sec	Shear velocity, m/sec	Density, gm/cm <sup>3</sup>	Layer thickness, m
1	1434.0	0.0	1.03	50.0
2	1437.0	0.0	1.03	50.0
3	1440.0	0.0	1.03	50.0
4	1443.0	0.0	1.03	50.0
5	1446.4	0.0	1.03	50.0
6	1450.0	0.0	1.03	50.0
7	1453.2	0.0	1.03	50.0
8	1456.0	0.0	1.03	250.0
9	1460.0	0.0	1.03	200.0
10	1463.0	0.0	1.03	200.0
11	1467.0	0.0	1.03	280.0
12	1472.0	0.0	1.03	220.0
13	1476.0	0.0	1.03	260.0
14	1480.0	0.0	1.03	240.0
15	1484.0	0.0	1.03	280.0
16	1489.0	0.0	1.03	320.0
17	1494.0	0.0	1.03	240.0
18	1498.0	0.0	1.03	200.0
19	1502.0	0.0	1.03	200.0
20	1506.0	0.0	1.03	280.0
21	1511.0	0.0	1.03	240.0
22	1515.0	0.0	1.03	240.0
23	1600.0	0.0	1.70	$\infty$

TABLE III

Layered Model, water depth plus ice thickness 4000 m,  
liquid bottom

Layer	Compressional velocity, m/sec	Shear velocity, m/sec	Density, gm. cm <sup>3</sup>	Layer thickness, m
1	3500.0	1800.0	0.90	3.0
2	1434.0	0.0	1.03	47.0
3	1437.0	0.0	1.03	50.0
4	1440.0	0.0	1.03	50.0
5	1443.0	0.0	1.03	50.0
6	1446.4	0.0	1.03	50.0
7	1450.0	0.0	1.03	50.0
8	1453.2	0.0	1.03	50.0
9	1456.0	0.0	1.03	250.0
10	1460.0	0.0	1.03	200.0
11	1463.0	0.0	1.03	200.0
12	1467.0	0.0	1.03	280.0
13	1472.0	0.0	1.03	220.0
14	1476.0	0.0	1.03	260.0
15	1480.0	0.0	1.03	240.0
16	1484.0	0.0	1.03	280.0
17	1489.0	0.0	1.03	320.0
18	1494.0	0.0	1.03	240.0
19	1498.0	0.0	1.03	200.0
20	1502.0	0.0	1.03	200.0
21	1506.0	0.0	1.03	280.0
22	1511.0	0.0	1.03	240.0
23	1515.0	0.0	1.03	240.0
24	1600.0	0.0	1.70	$\infty$

TABLE IV  
Layered Model, water depth 4000 m., solid bottom

Layer	Compressional velocity, m/sec	Shear velocity, m/sec	Density, gm/cm <sup>3</sup>	Layer thickness, m
1	1434.0	0.0	1.03	50.0
2	1437.0	0.0	1.03	50.0
3	1440.0	0.0	1.03	50.0
4	1443.0	0.0	1.03	50.0
5	1446.4	0.0	1.03	50.0
6	1450.0	0.0	1.03	50.0
7	1453.2	0.0	1.03	50.0
8	1456.0	0.0	1.03	250.0
9	1460.0	0.0	1.03	200.0
10	1463.0	0.0	1.03	200.0
11	1467.0	0.0	1.03	280.0
12	1472.0	0.0	1.03	220.0
13	1476.0	0.0	1.03	260.0
14	1480.0	0.0	1.03	240.0
15	1484.0	0.0	1.03	280.0
16	1489.0	0.0	1.03	320.0
17	1494.0	0.0	1.03	240.0
18	1498.0	0.0	1.03	200.0
19	1502.0	0.0	1.03	200.0
20	1506.0	0.0	1.03	280.0
21	1511.0	0.0	1.03	240.0
22	1515.0	0.0	1.03	240.0
23	1600.0	200.0	1.70	$\infty$

TABLE V

Layered Model, water plus ice depth 4000 m,

Layer	<u>solid bottom</u>			Layer thickness, m
	Compressional velocity, m/sec	Shear velocity, m/sec	Density, gm/cm <sup>3</sup>	
1	3500.0	1800.0	0.90	3.0
2	1434.0	0.0	1.03	47.0
3	1437.0	0.0	1.03	50.0
4	1440.0	0.0	1.03	50.0
5	1443.0	0.0	1.03	50.0
6	1446.4	0.0	1.03	50.0
7	1450.0	0.0	1.03	50.0
8	1453.2	0.0	1.03	50.0
9	1456.0	0.0	1.03	250.0
10	1460.0	0.0	1.03	200.0
11	1463.0	0.0	1.03	200.0
12	1467.0	0.0	1.03	280.0
13	1472.0	0.0	1.03	220.0
14	1476.0	0.0	1.03	260.0
15	1480.0	0.0	1.03	240.0
16	1484.0	0.0	1.03	280.0
17	1489.0	0.0	1.03	320.0
18	1494.0	0.0	1.03	240.0
19	1498.0	0.0	1.03	200.0
20	1502.0	0.0	1.03	200.0
21	1506.0	0.0	1.03	280.0
22	1511.0	0.0	1.03	240.0
23	1515.0	0.0	1.03	240.0
24	1600.0	200.0	1.70	$\infty$

**TABLE VI**  
**Layered Model, water plus ice depth 4000 m,**  
**liquid bottom**

<u>Layer</u>	<u>Compressional velocity, m/sec</u>	<u>Shear velocity, m/sec</u>	<u>Density, gm/cm<sup>3</sup></u>	<u>Layer thickness, m</u>
1	3500.0	1800.0	0.90	3.0
2	1435.2	0.0	1.03	37.0
3	1438.0	0.0	1.03	10.0
4	1438.0	0.0	1.03	30.0
5	1441.0	0.0	1.03	60.0
6	1443.0	0.0	1.03	40.0
7	1445.0	0.0	1.03	40.0
8	1449.0	0.0	1.03	40.0
9	1453.0	0.0	1.03	60.0
10	1455.0	0.0	1.03	40.0
11	1457.0	0.0	1.03	100.0
12	1459.5	0.0	1.03	140.0
13	1460.0	0.0	1.03	200.0
14	1463.0	0.0	1.03	200.0
15	1467.0	0.0	1.03	280.0
16	1472.0	0.0	1.03	220.0
17	1476.0	0.0	1.03	260.0
18	1480.0	0.0	1.03	240.0
19	1484.0	0.0	1.03	280.0
20	1489.0	0.0	1.03	320.0
21	1494.0	0.0	1.03	240.0
22	1498.0	0.0	1.03	200.0
23	1502.0	0.0	1.03	200.0
24	1506.0	0.0	1.03	280.0
25	1511.0	0.0	1.03	240.0
26	1515.0	0.0	1.03	240.0
27	1600.0	0.0	1.70	$\infty$

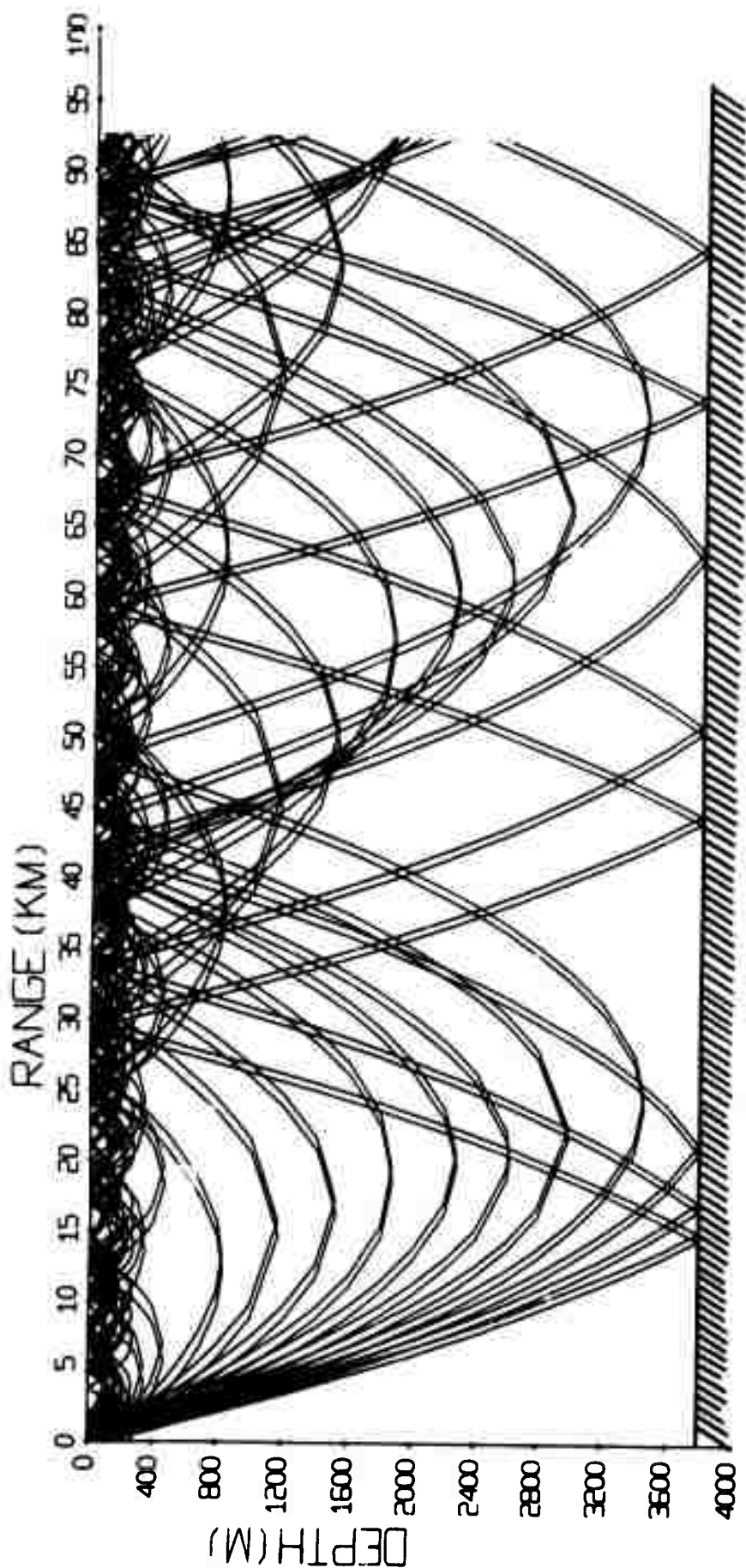


Fig. 1

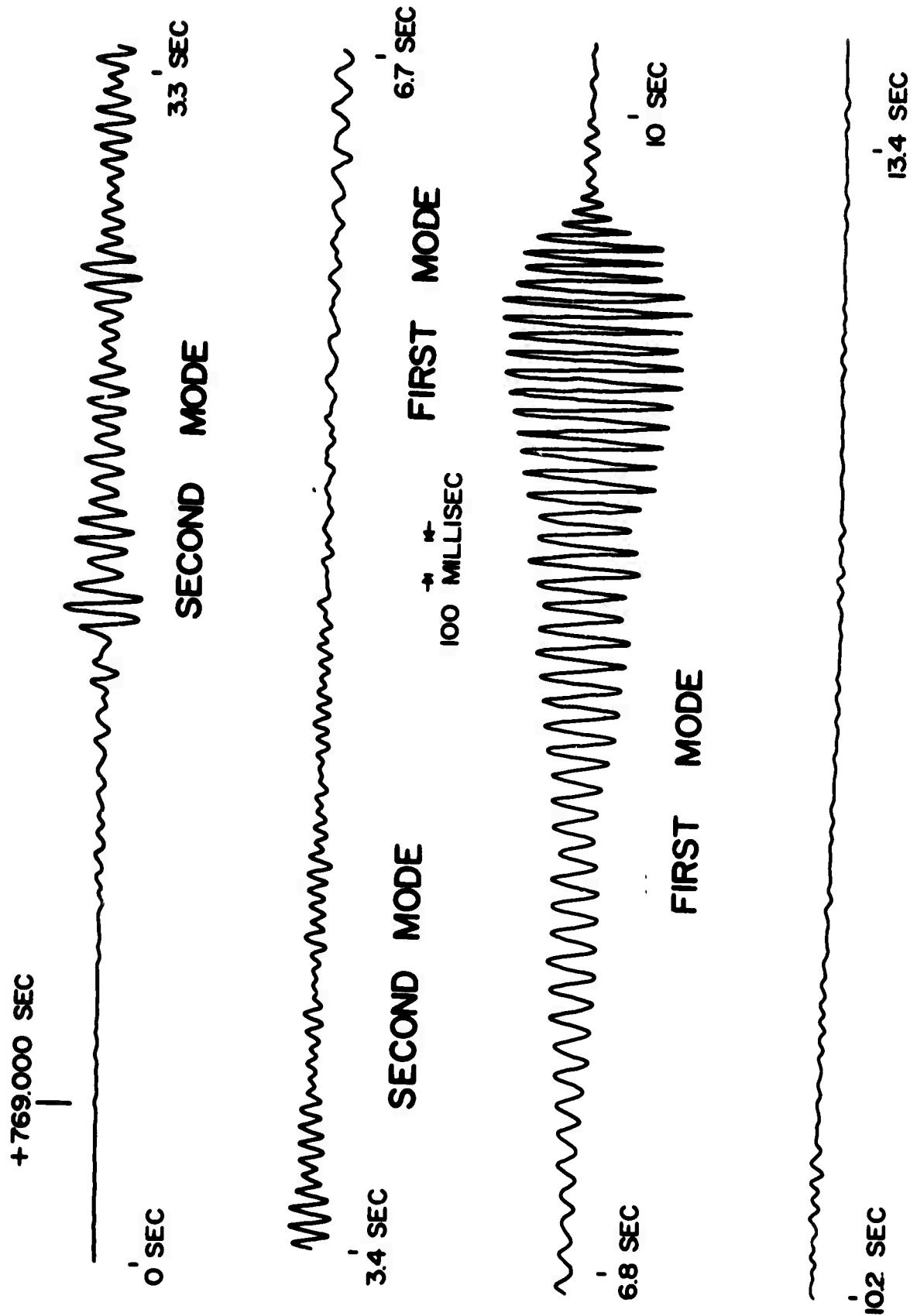


Fig. 2

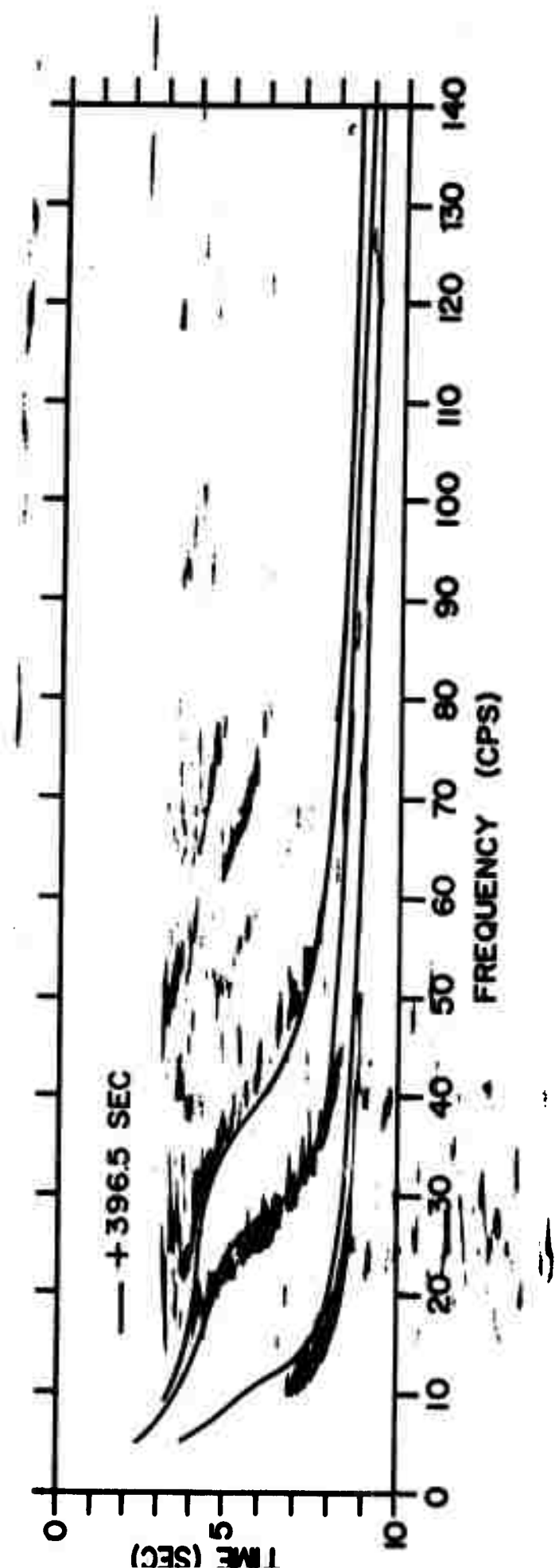


Fig. 3

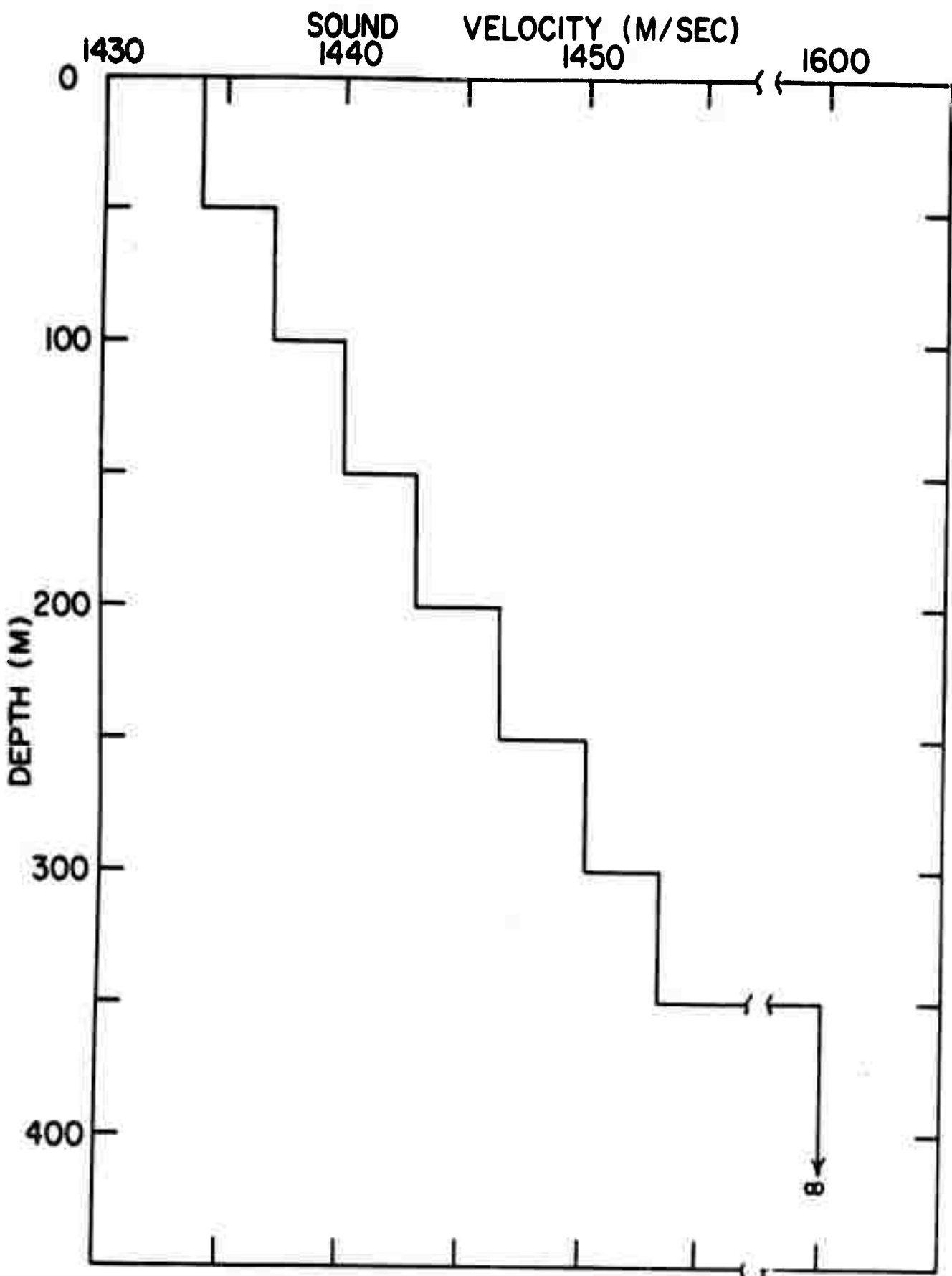
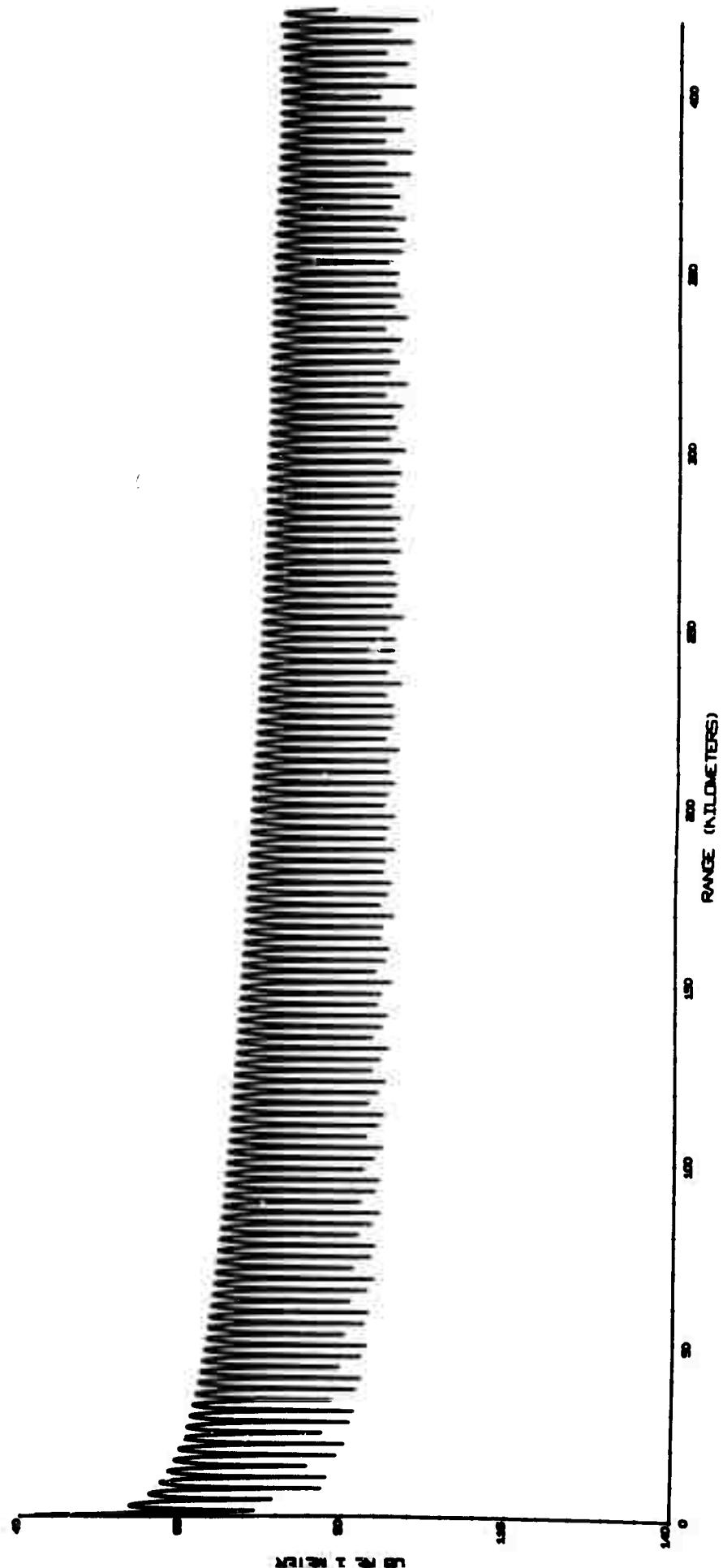


Fig. 4



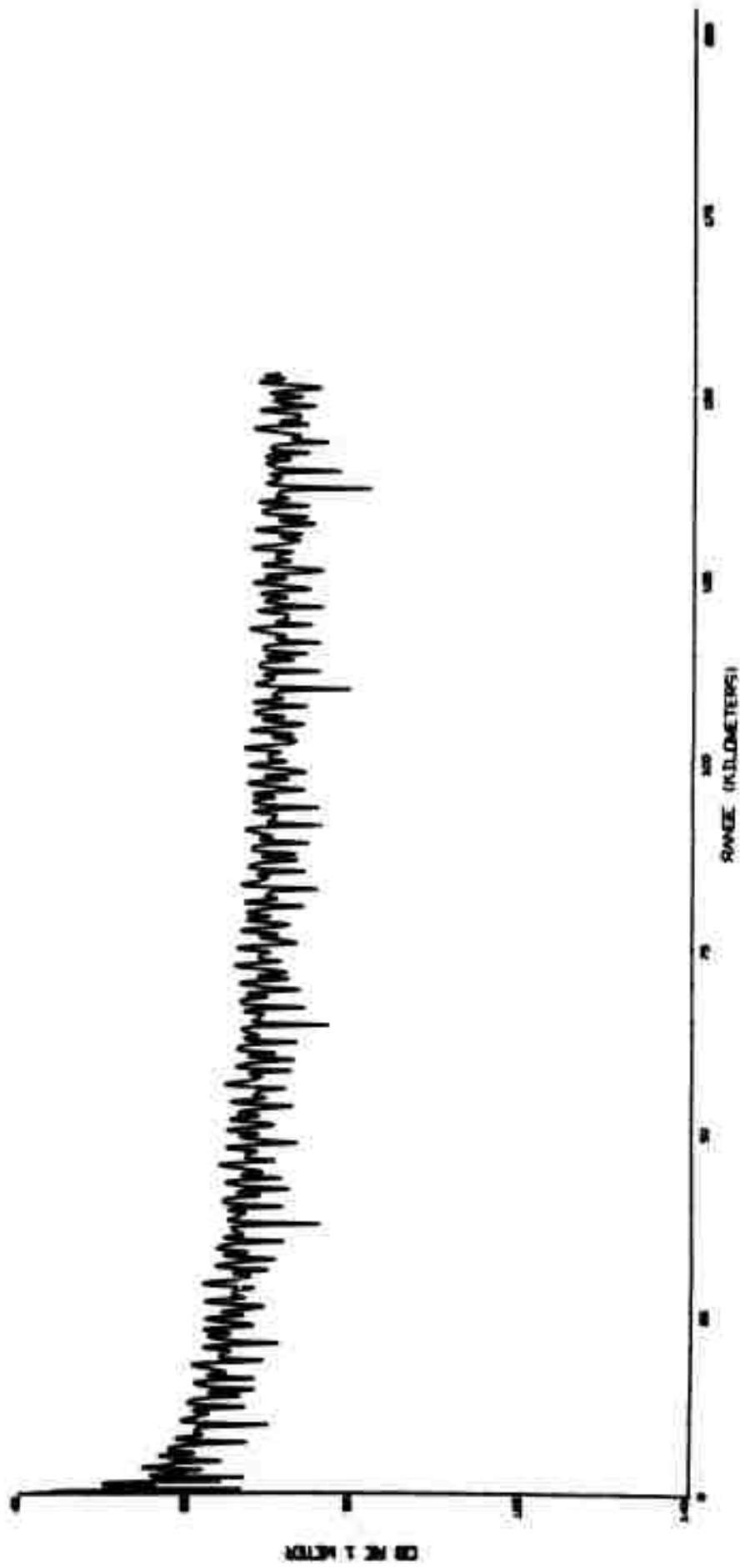


Fig. 6

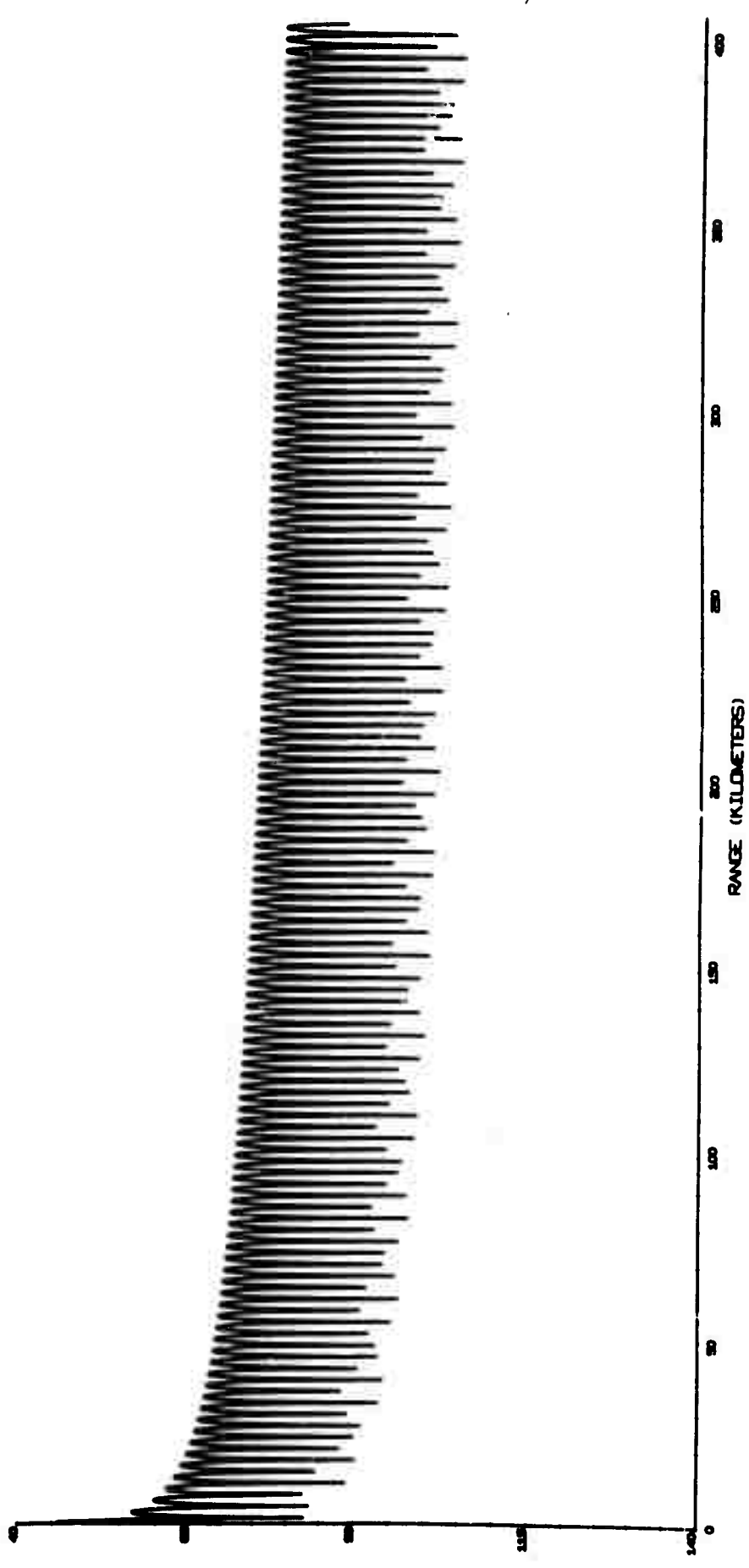
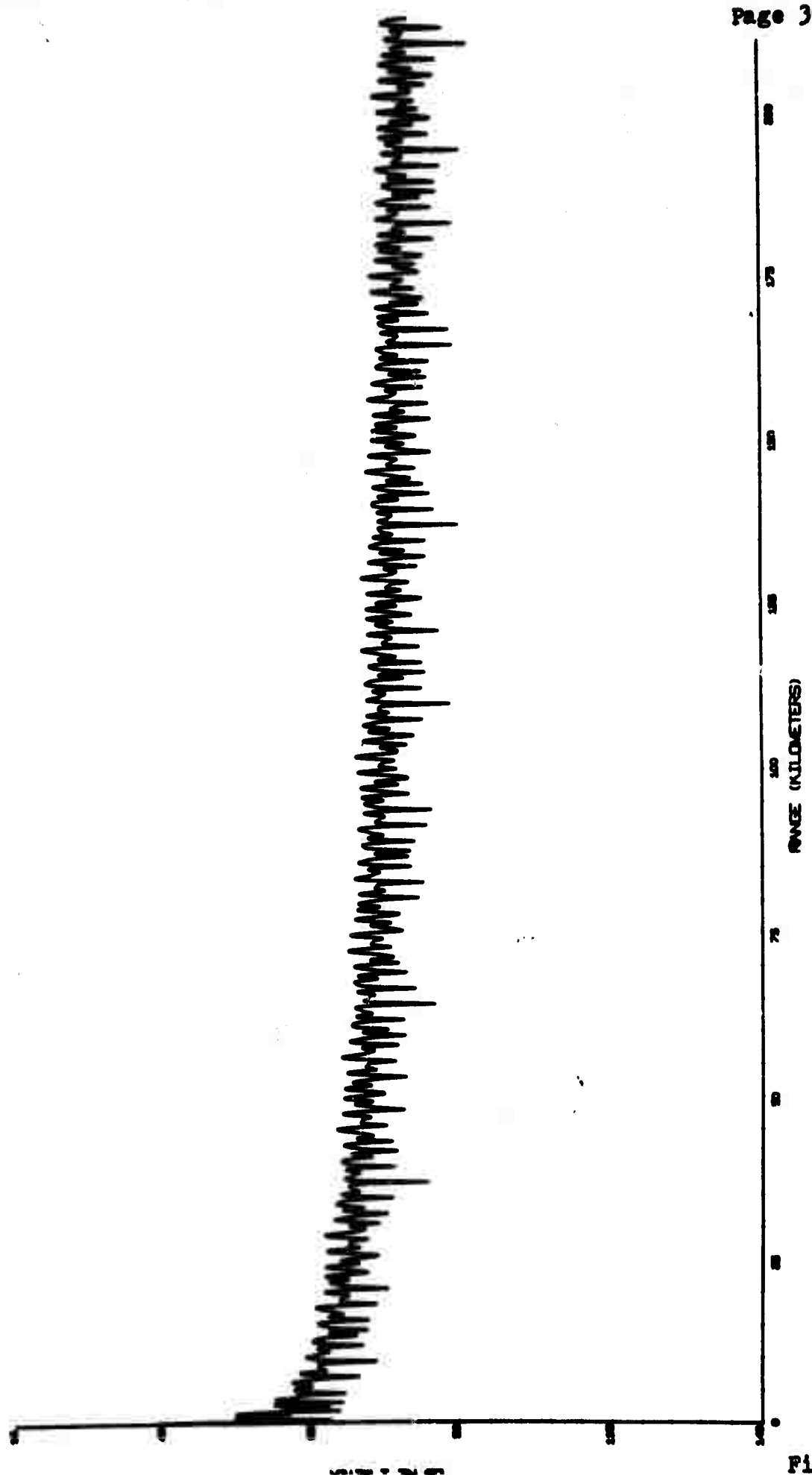


Fig. 7



TIME (KILODECIMETERS)

Fig. 8

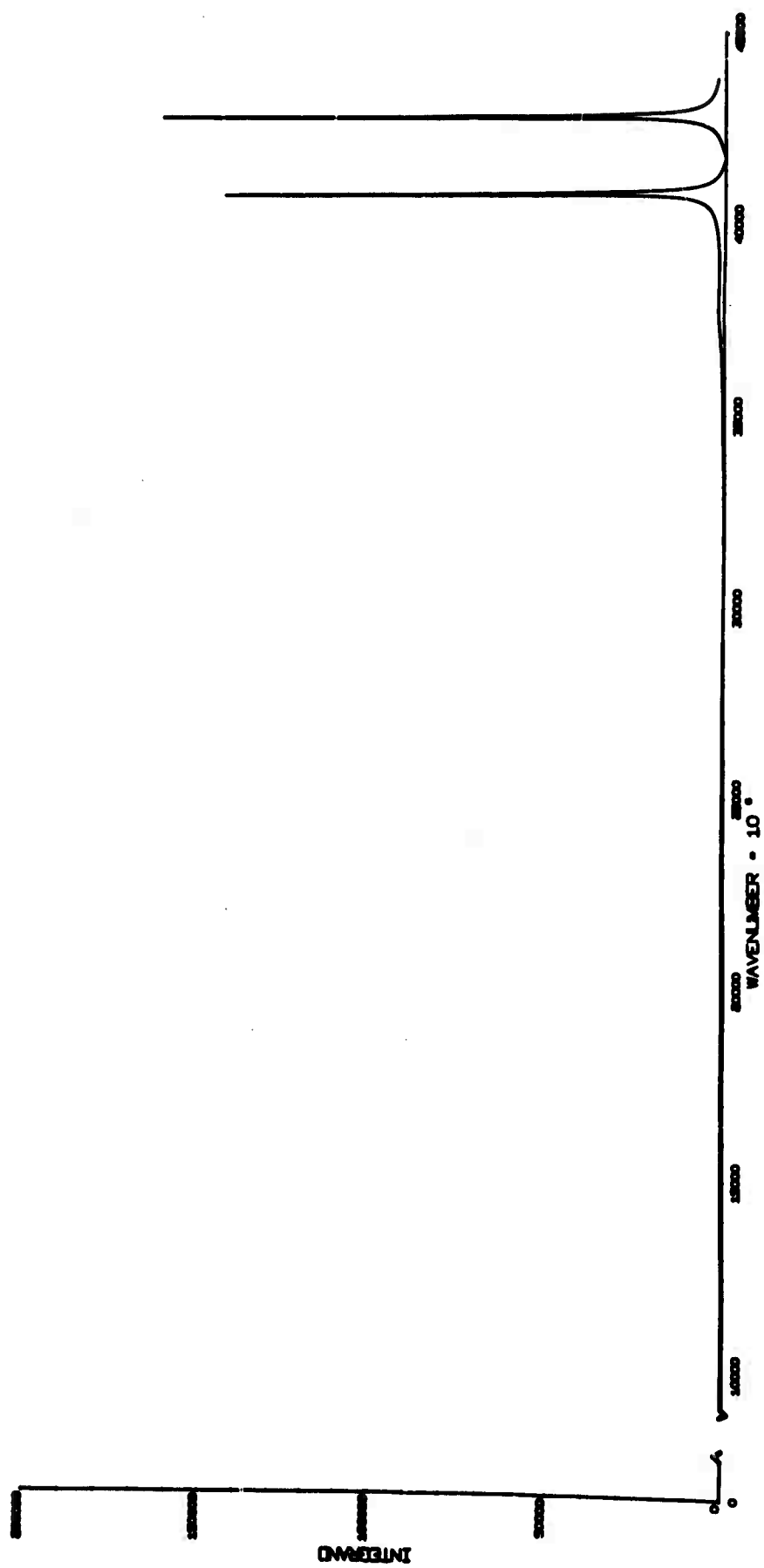


Fig. 9

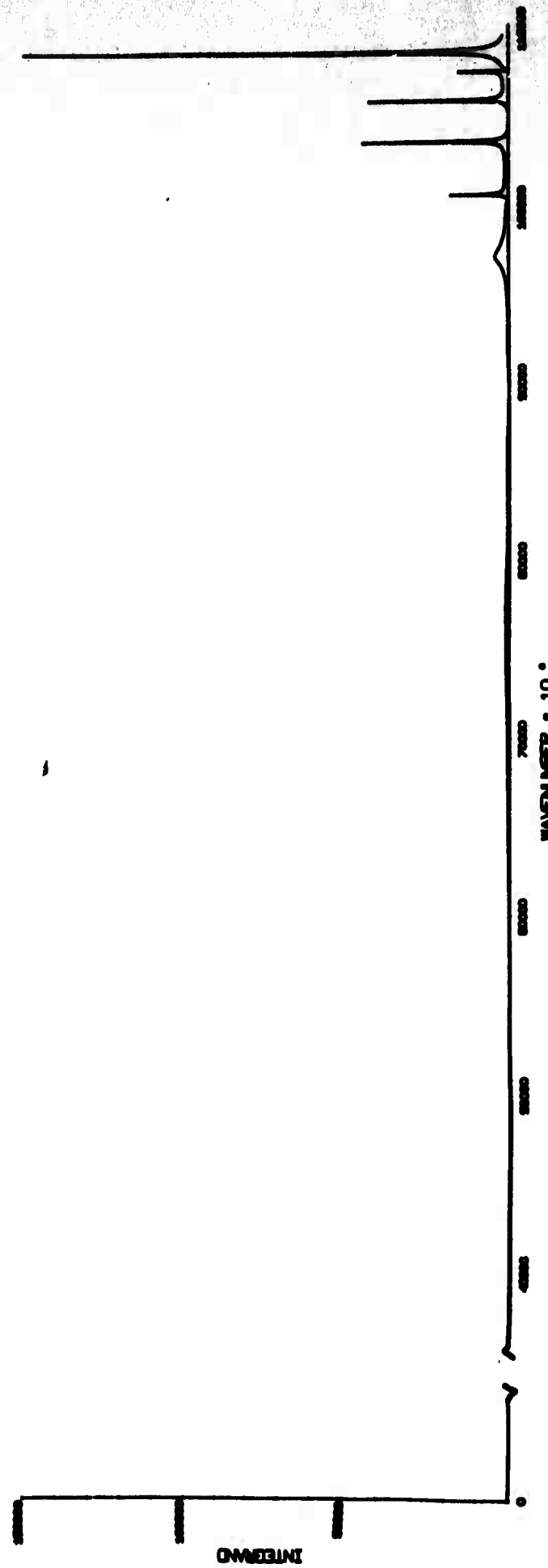


Fig. 10

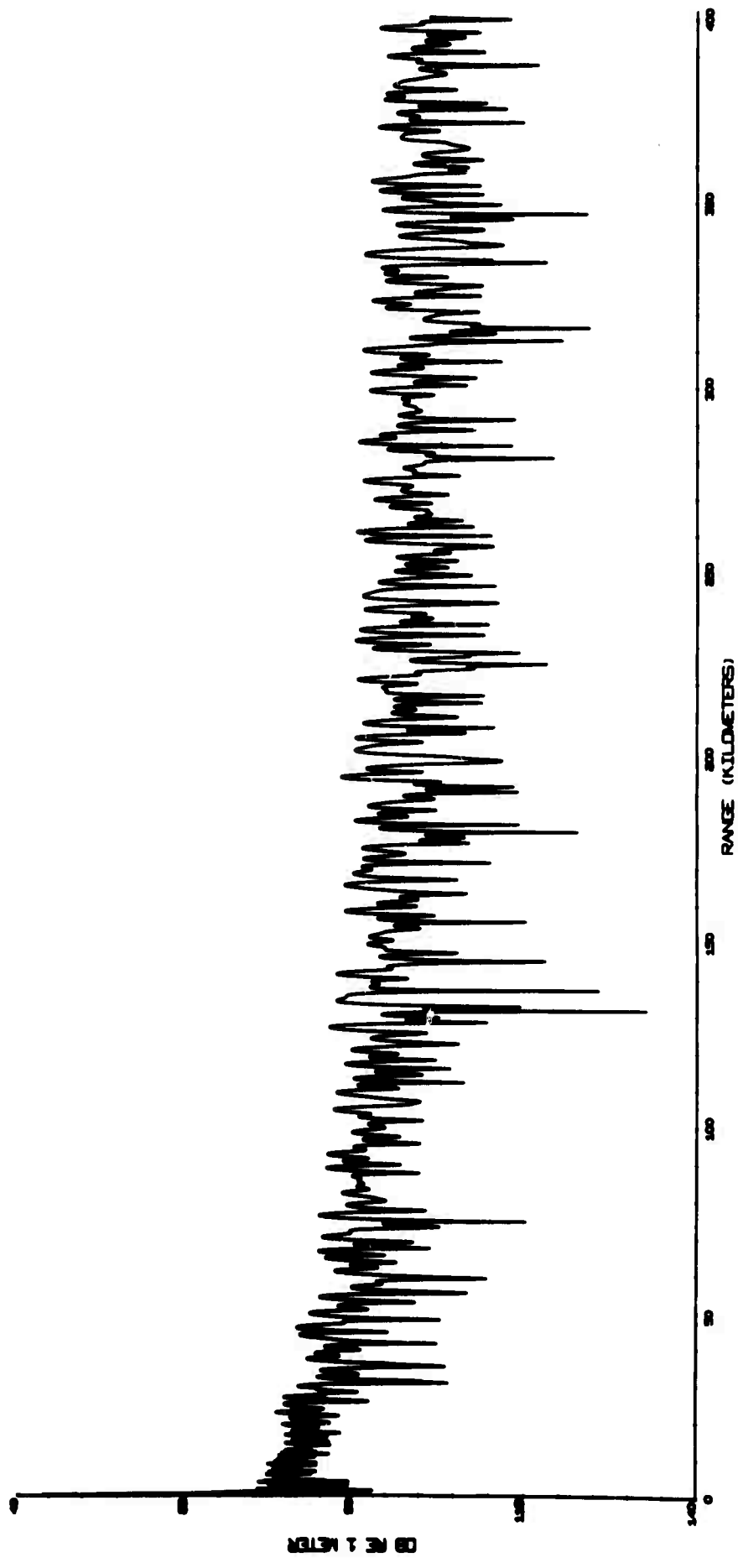
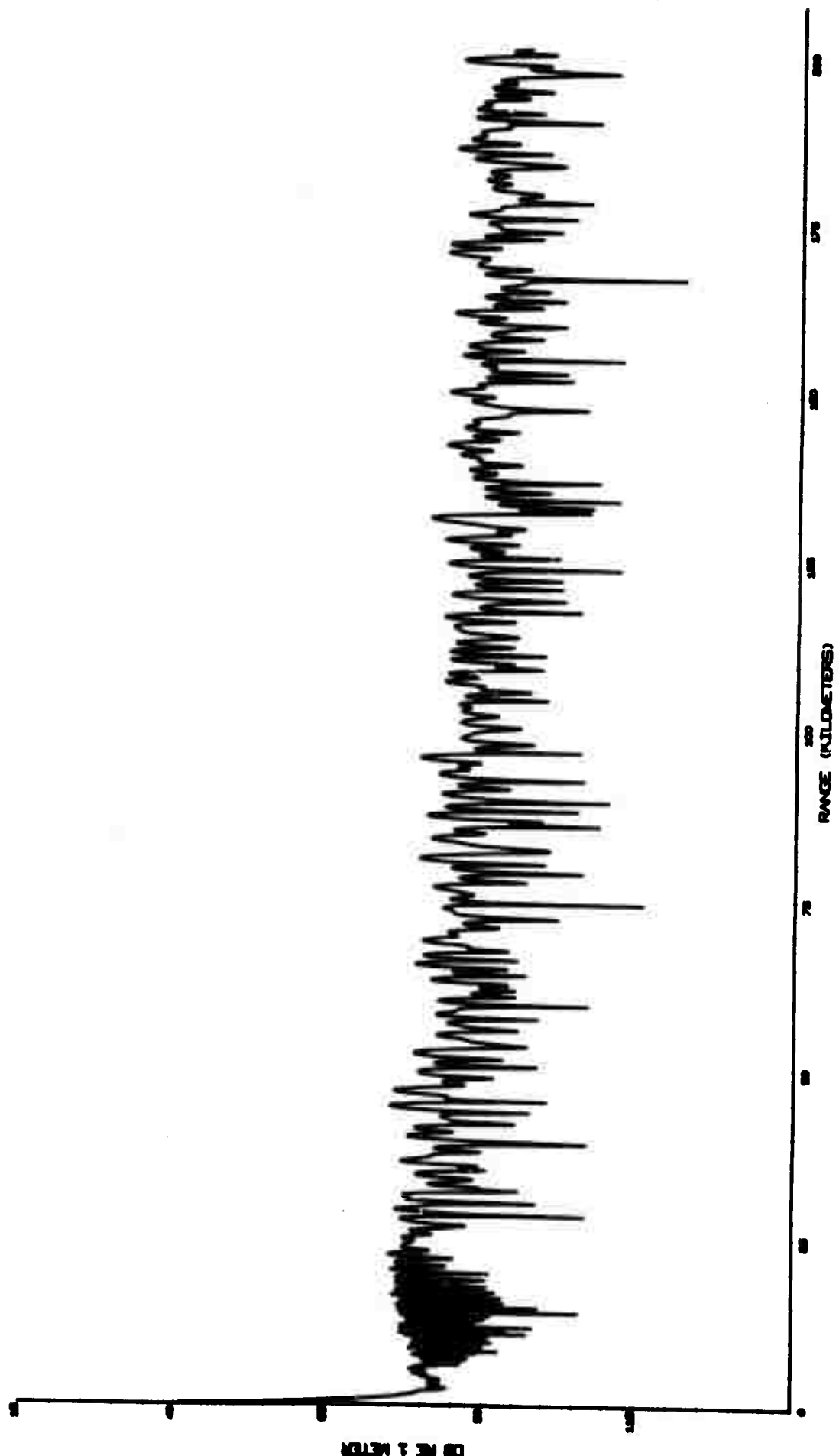


Fig. 11



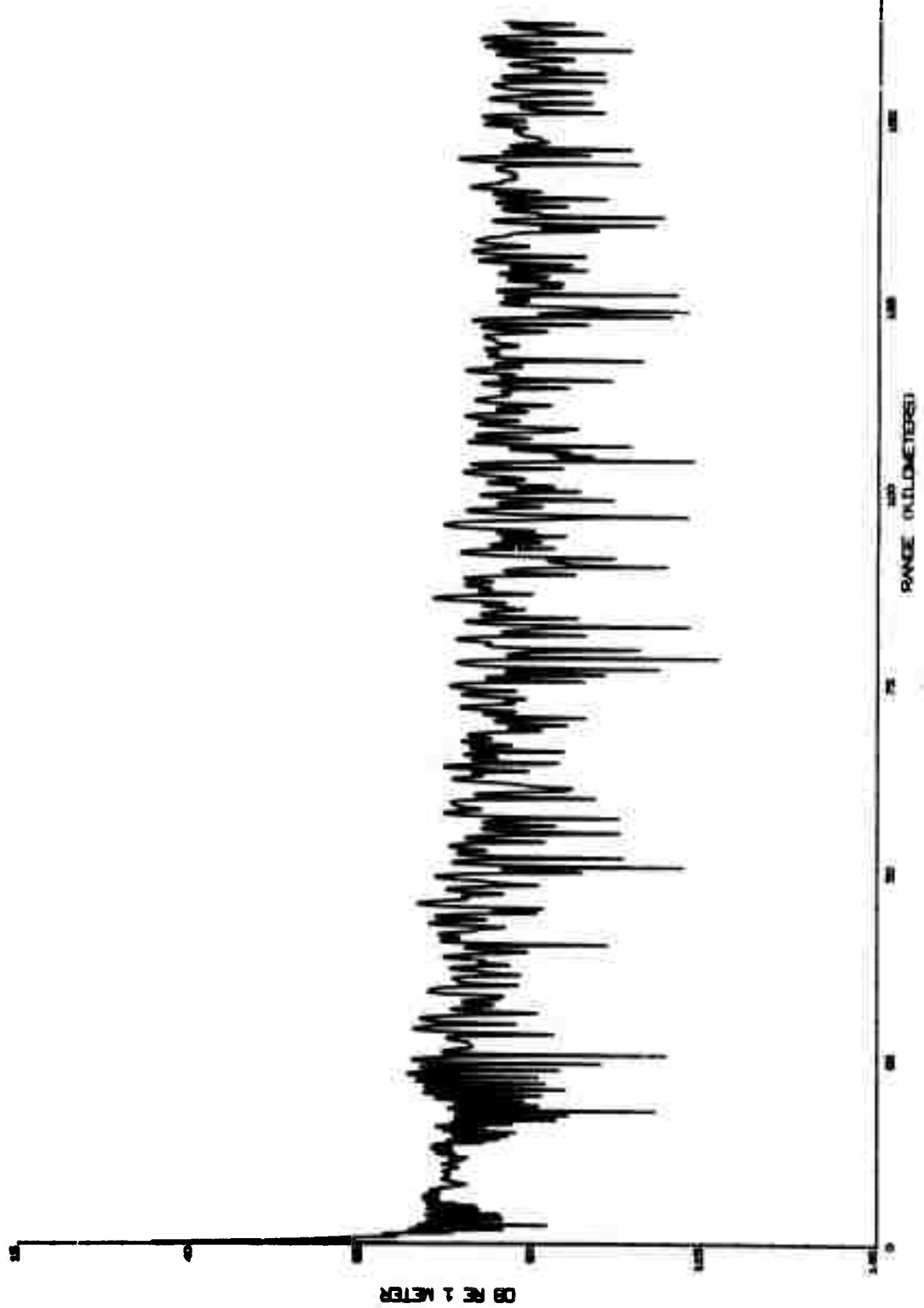
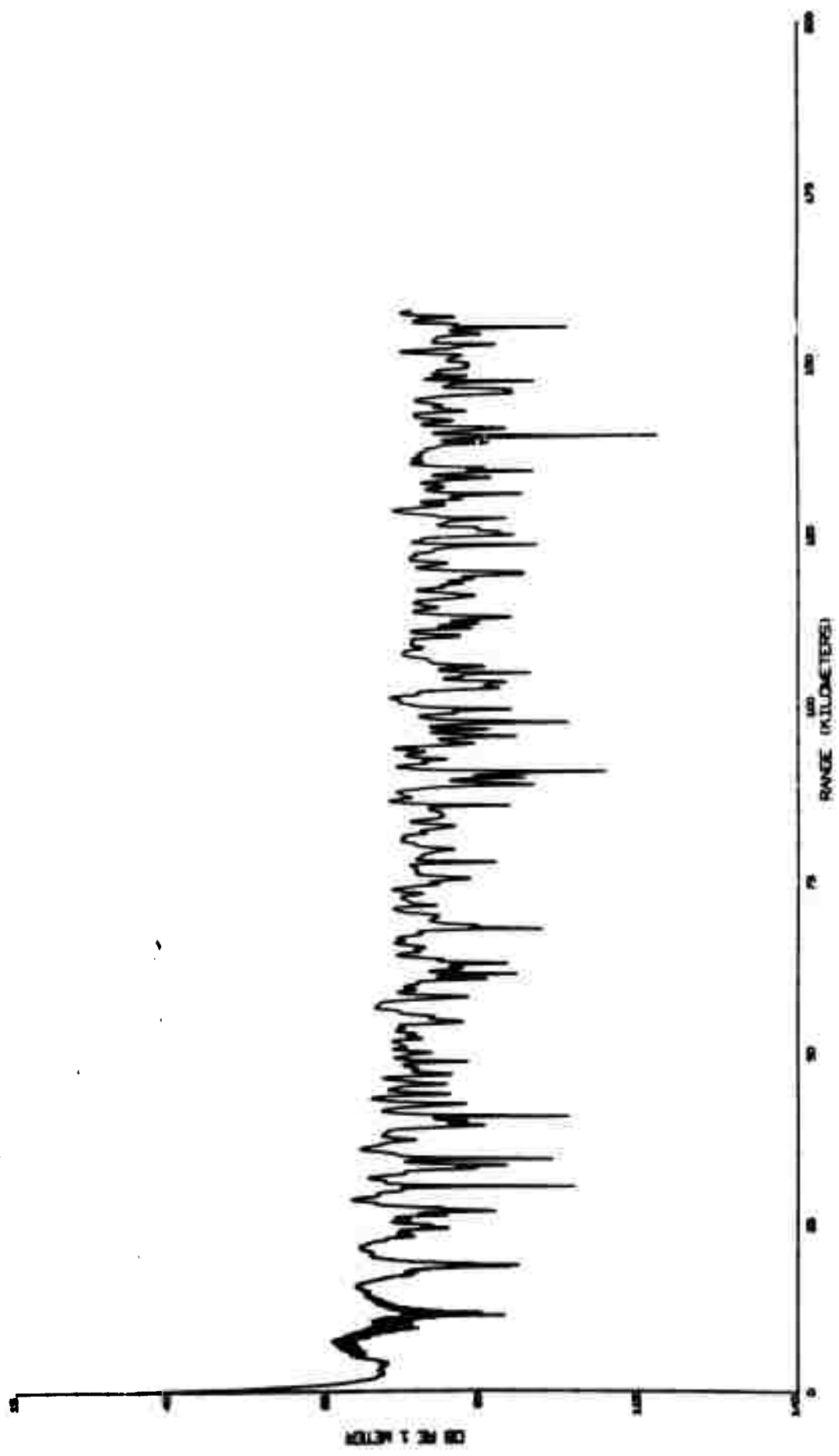


Fig. 13



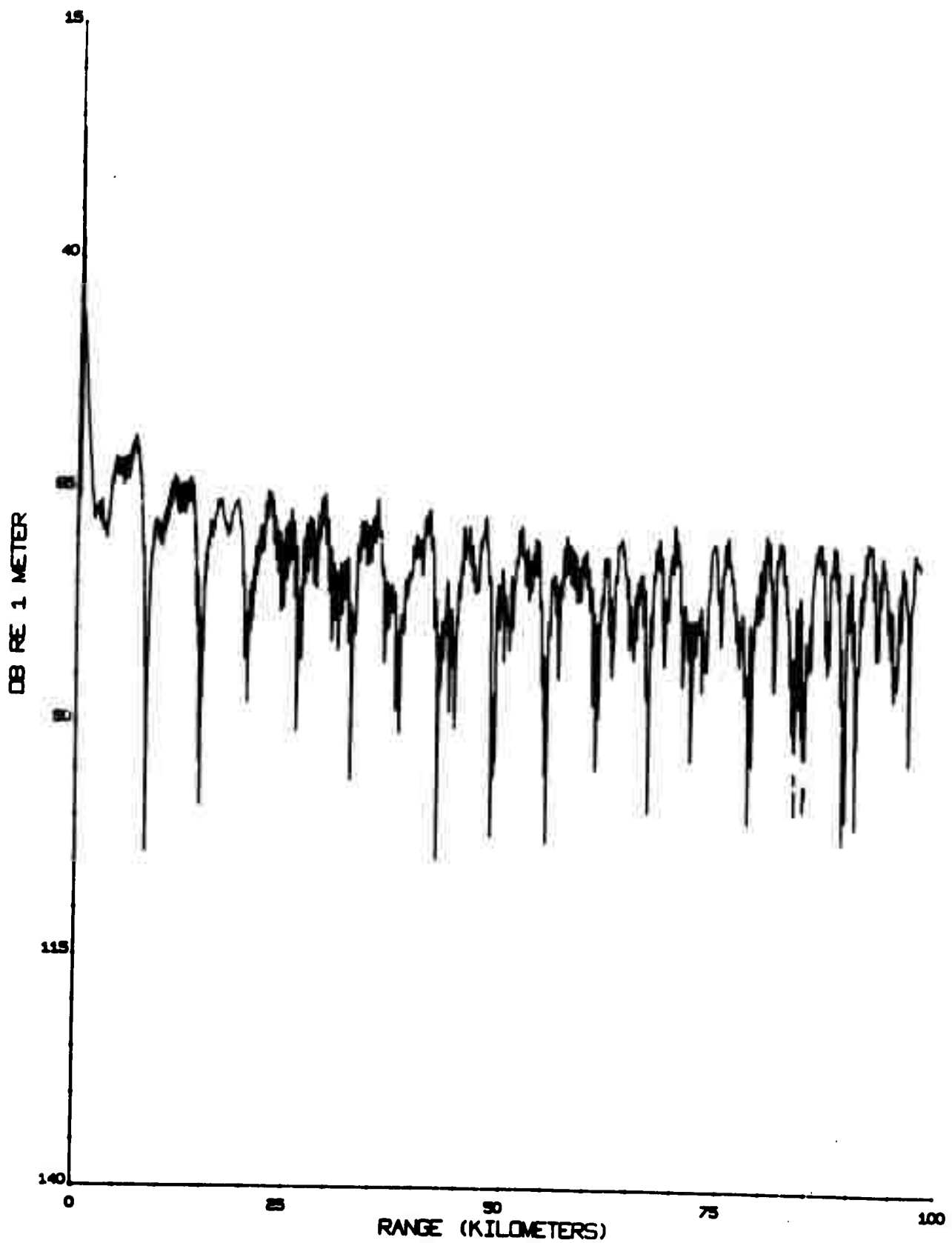


Fig. 15

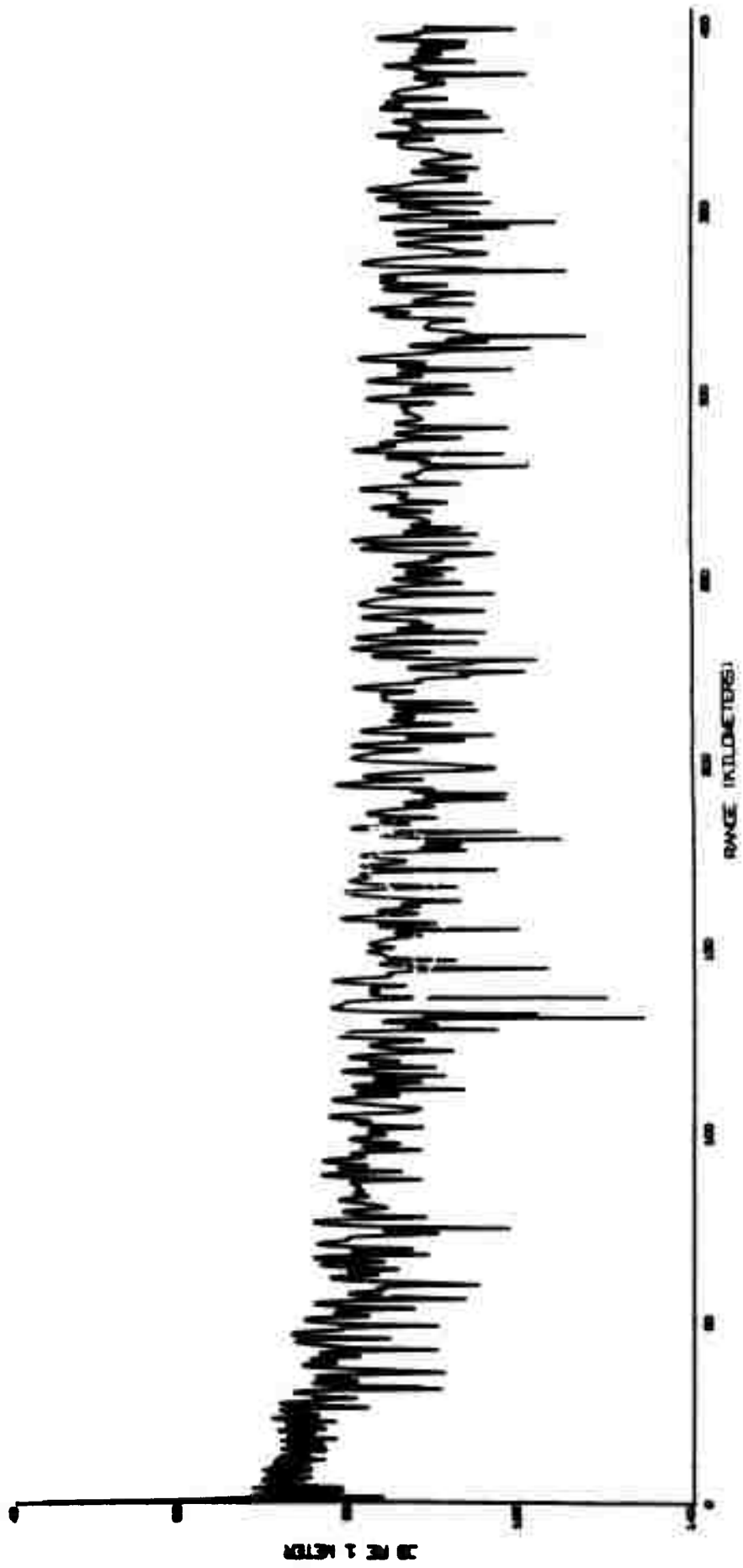


Fig. 16

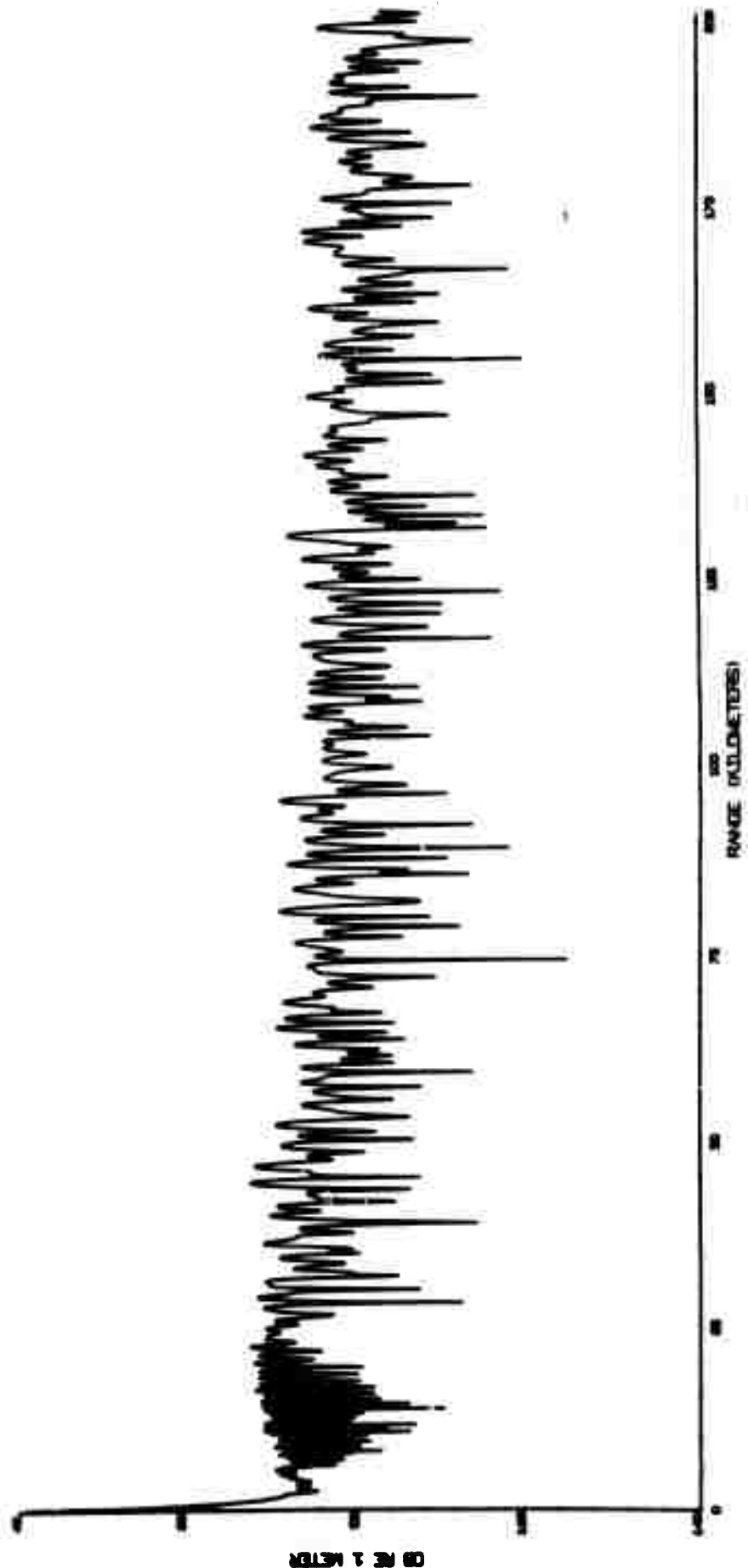


Fig. 17

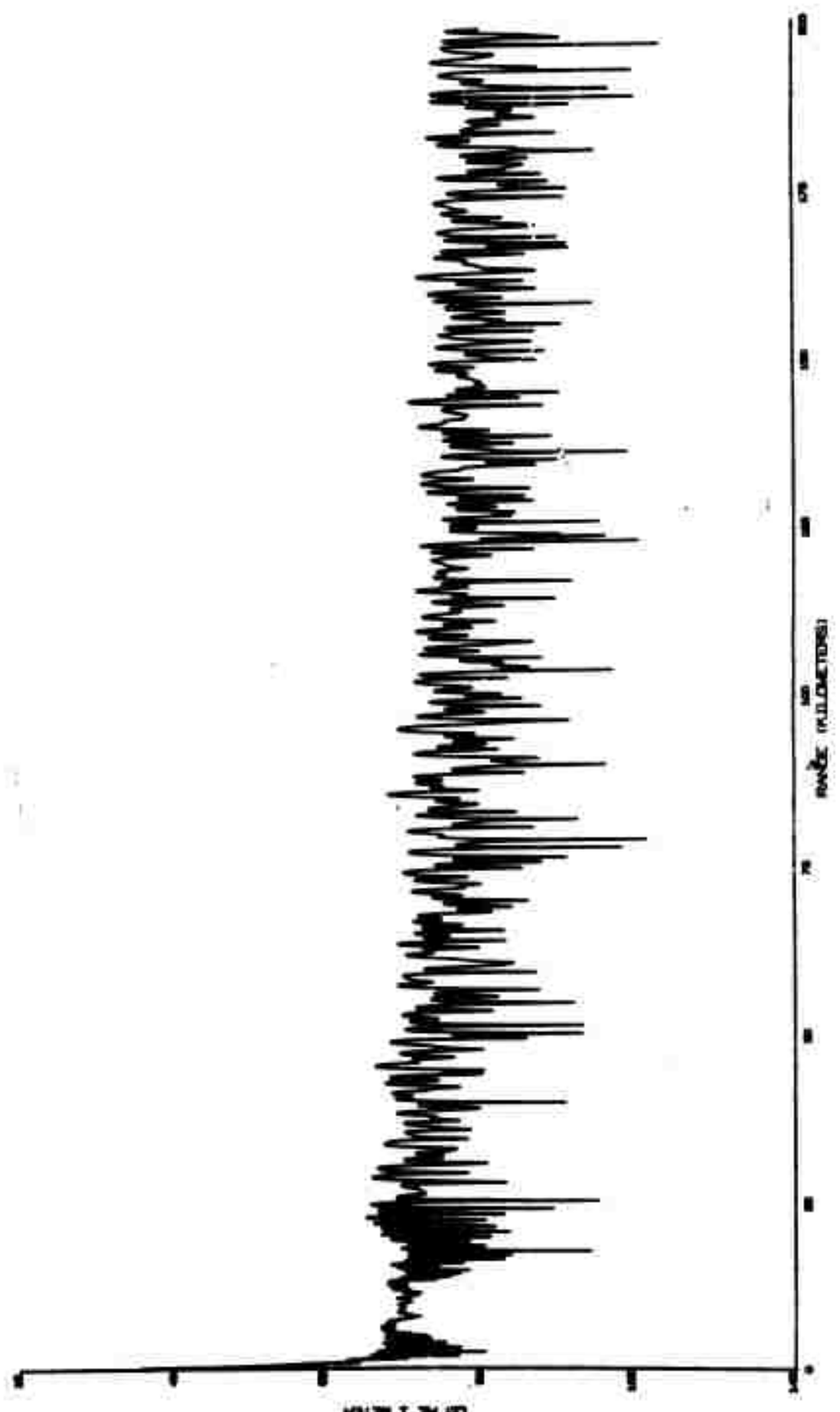
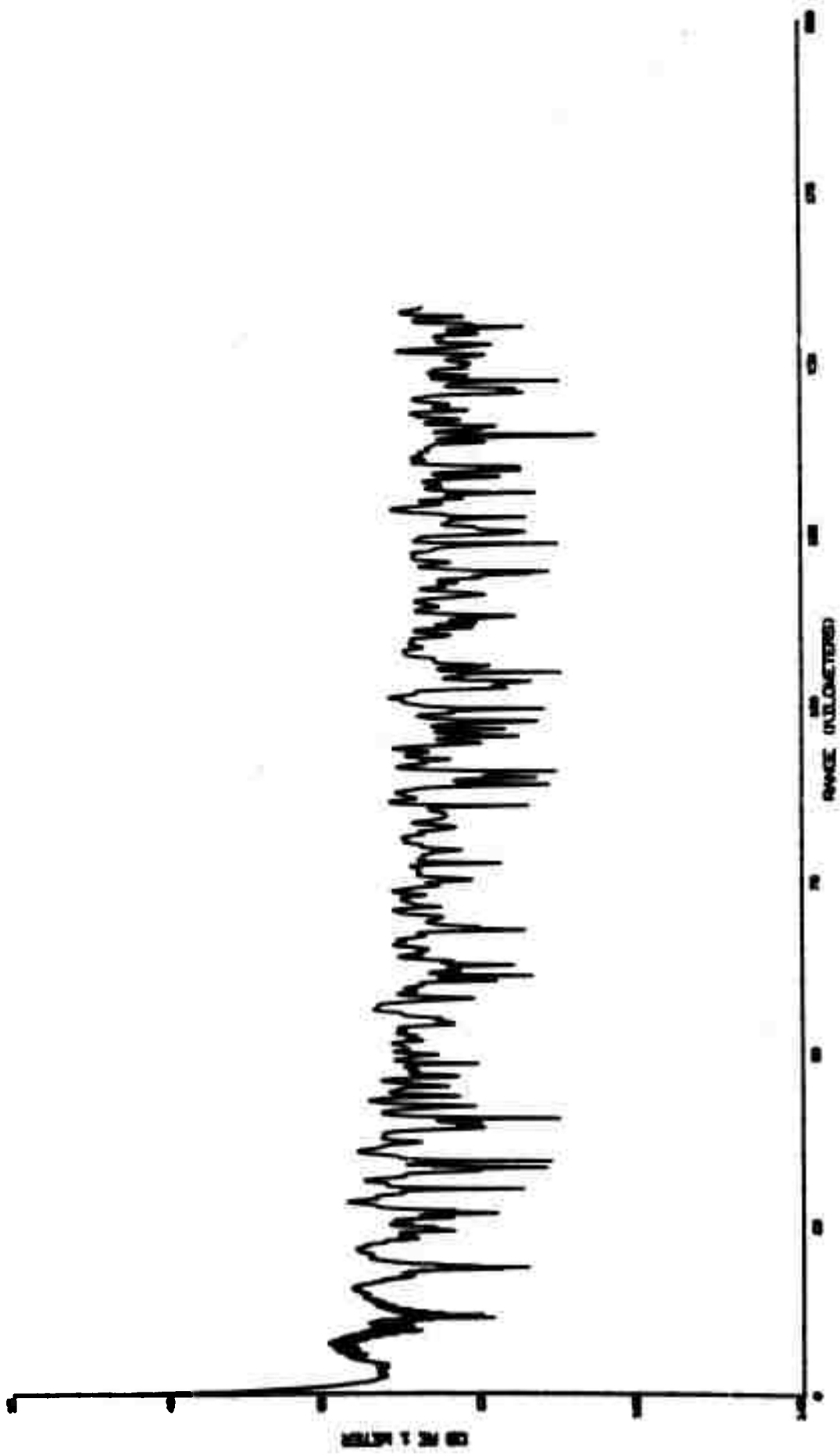
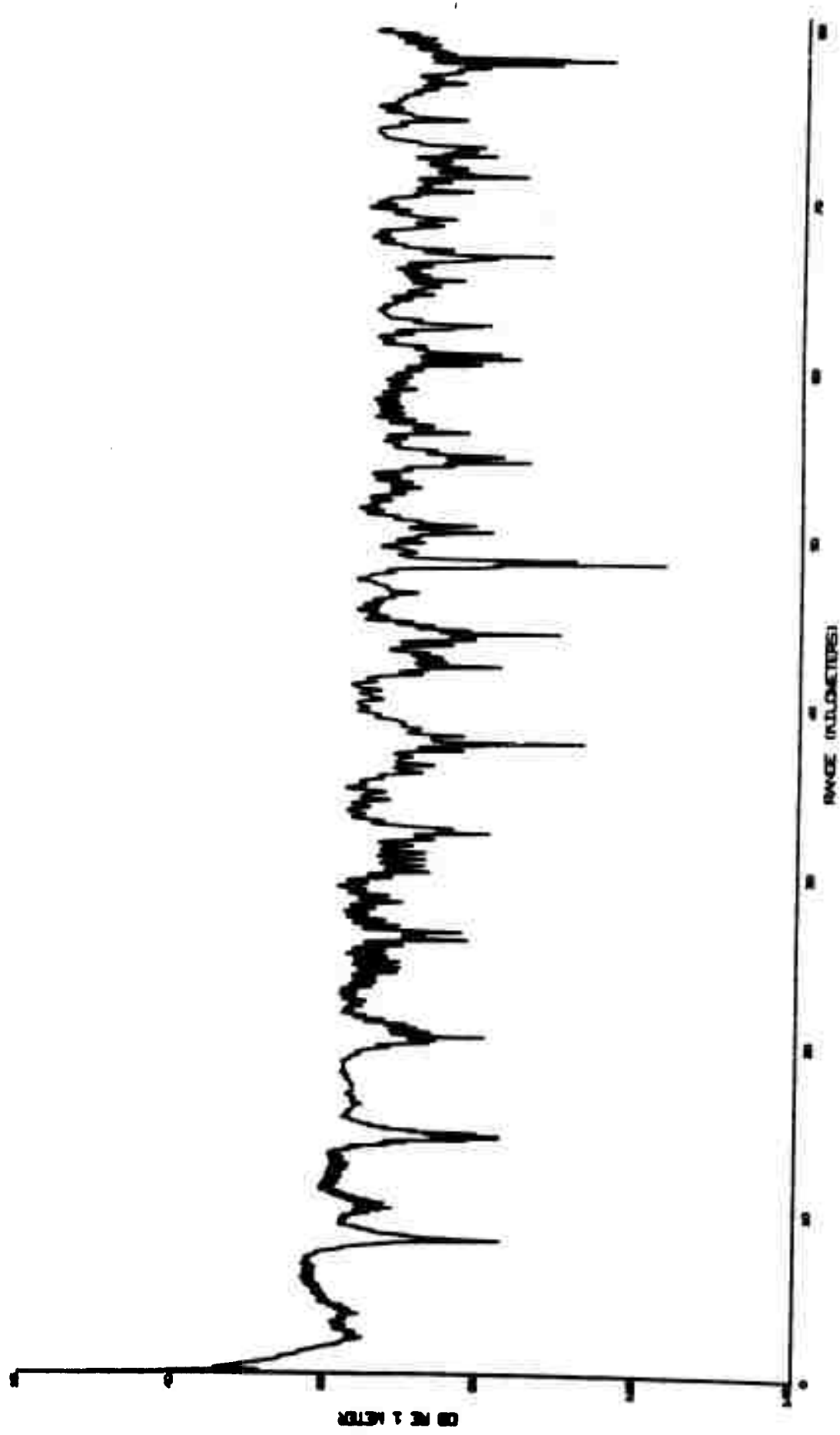
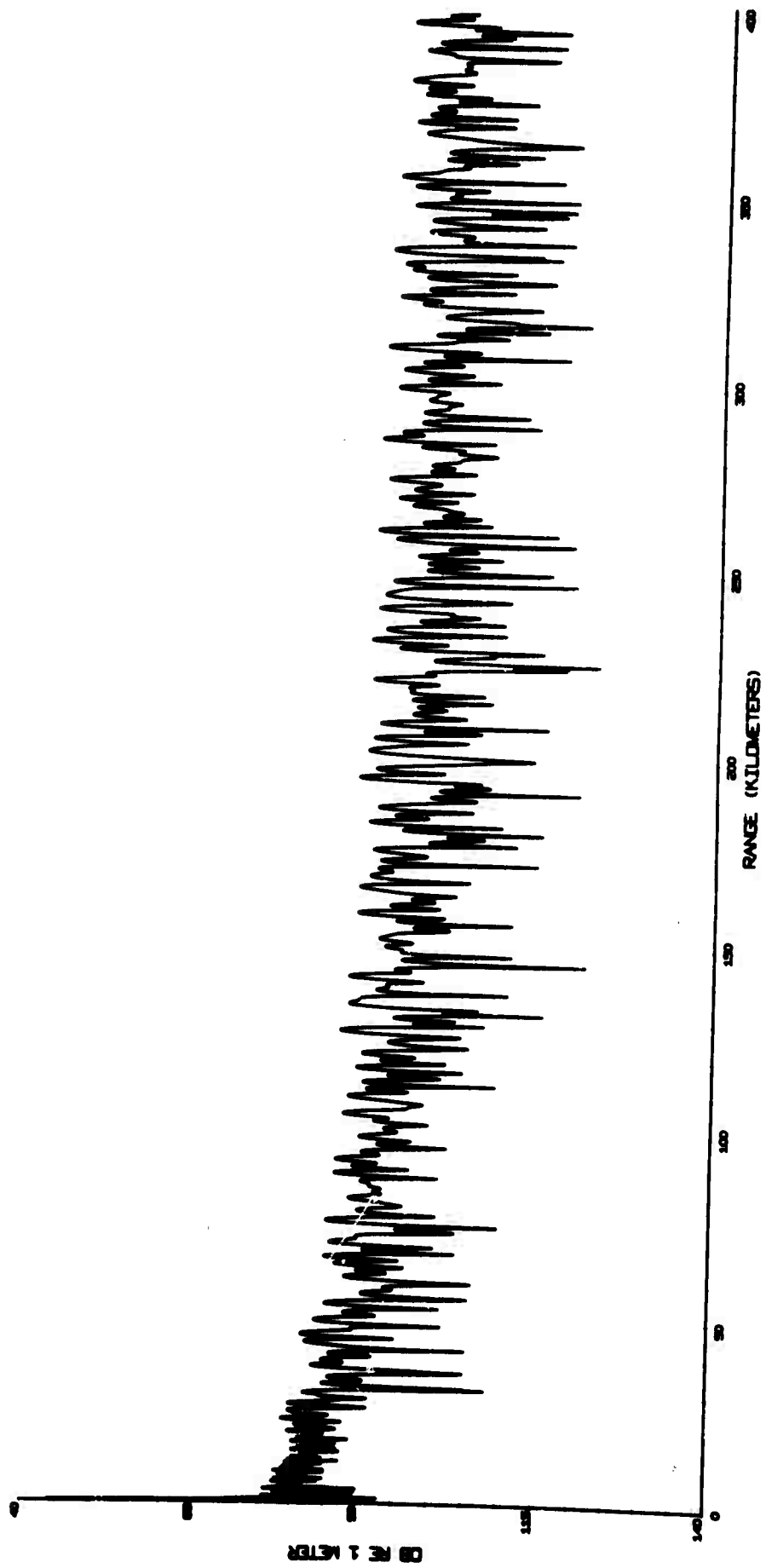


Fig. 18



MILITARY TIME





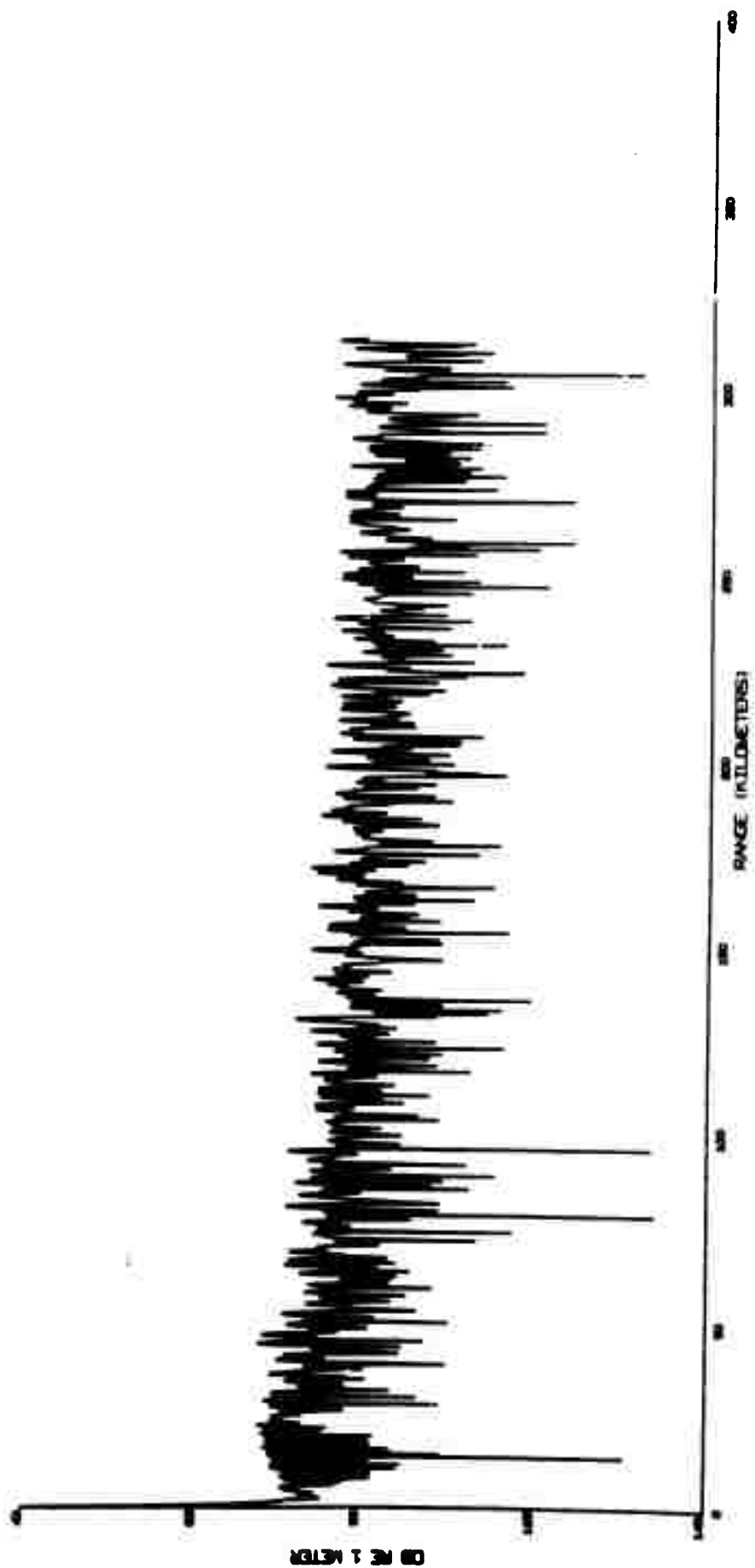


Fig. 22

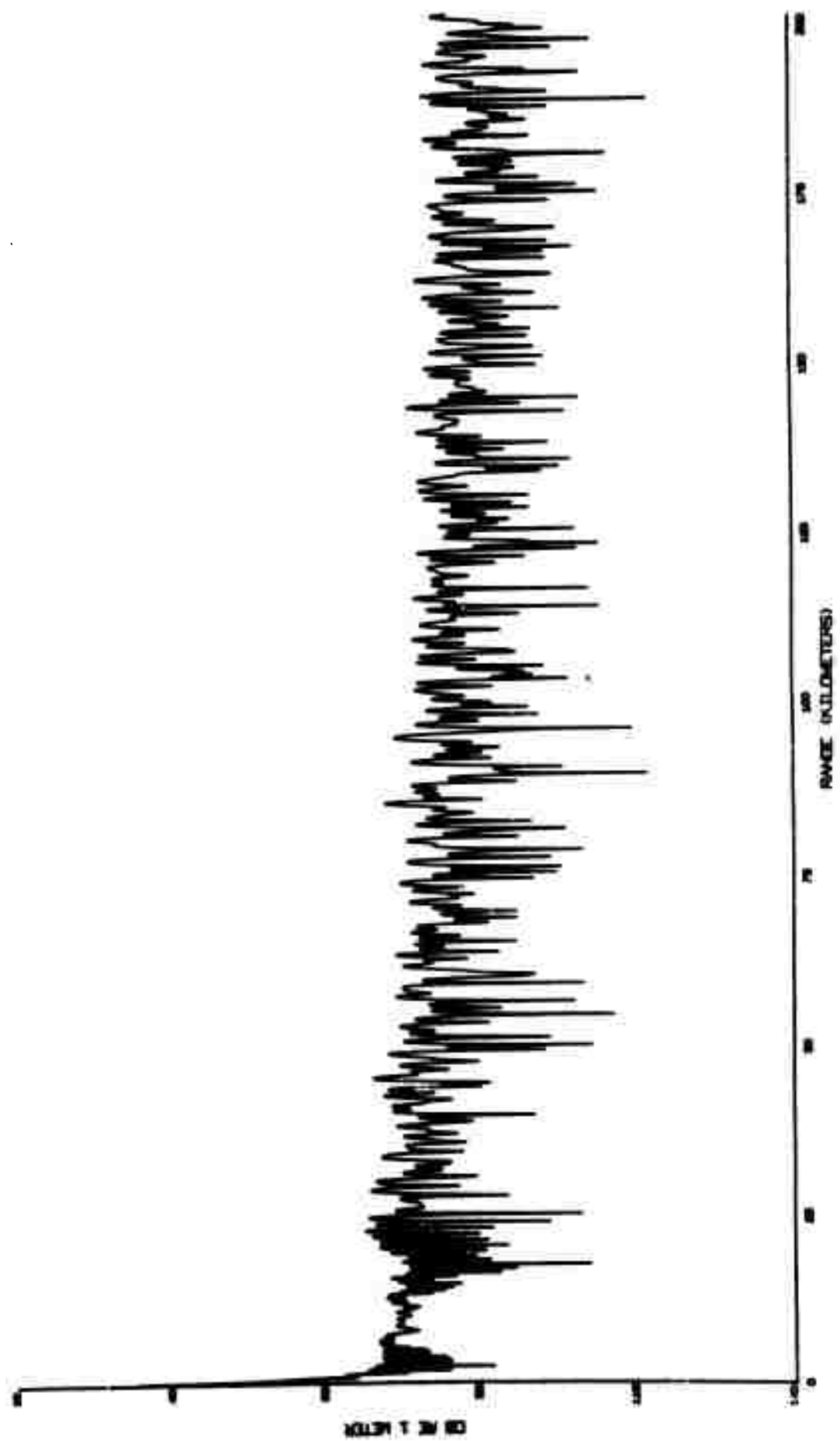


Fig. 23

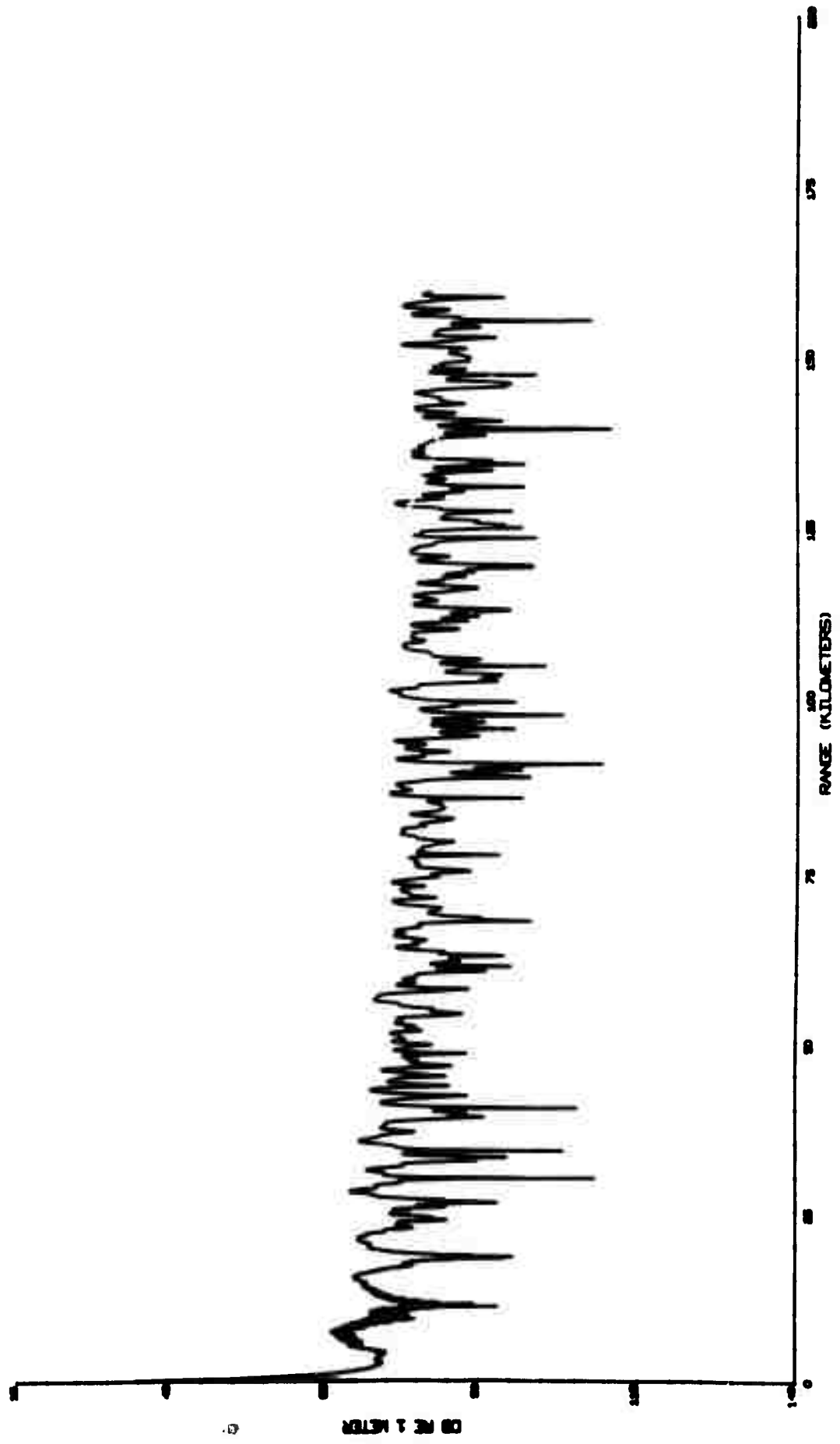


Fig. 24

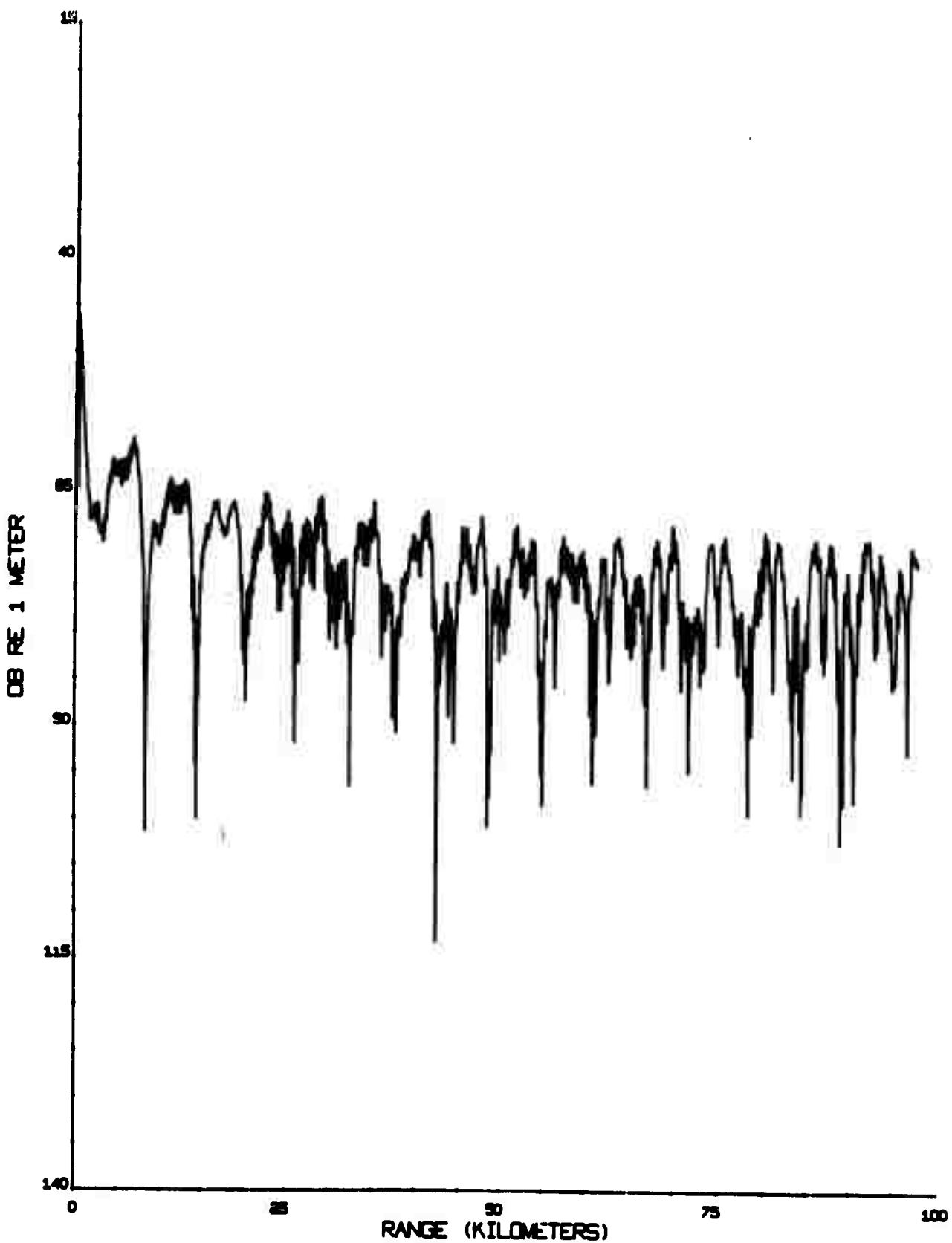


Fig. 25

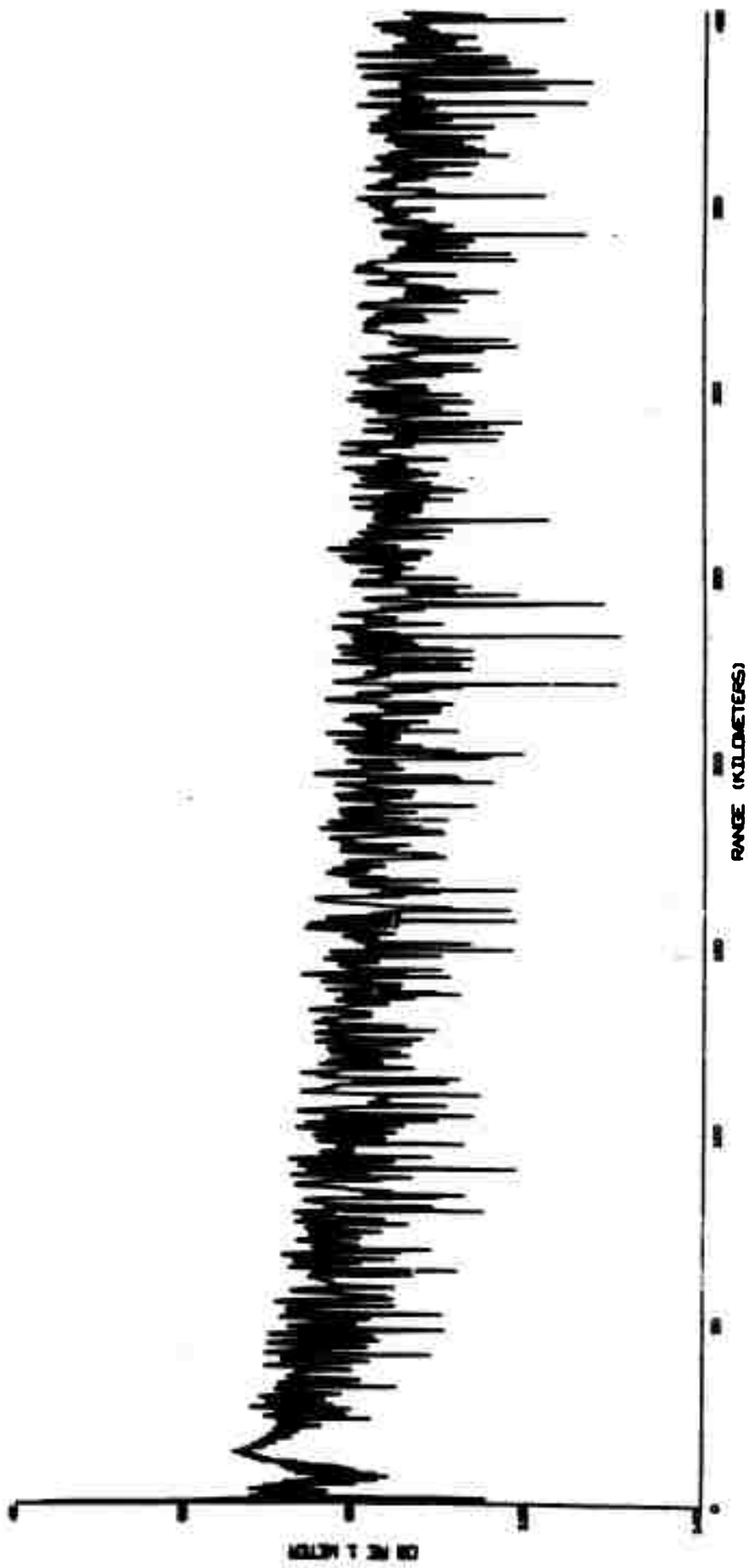


Fig. 26

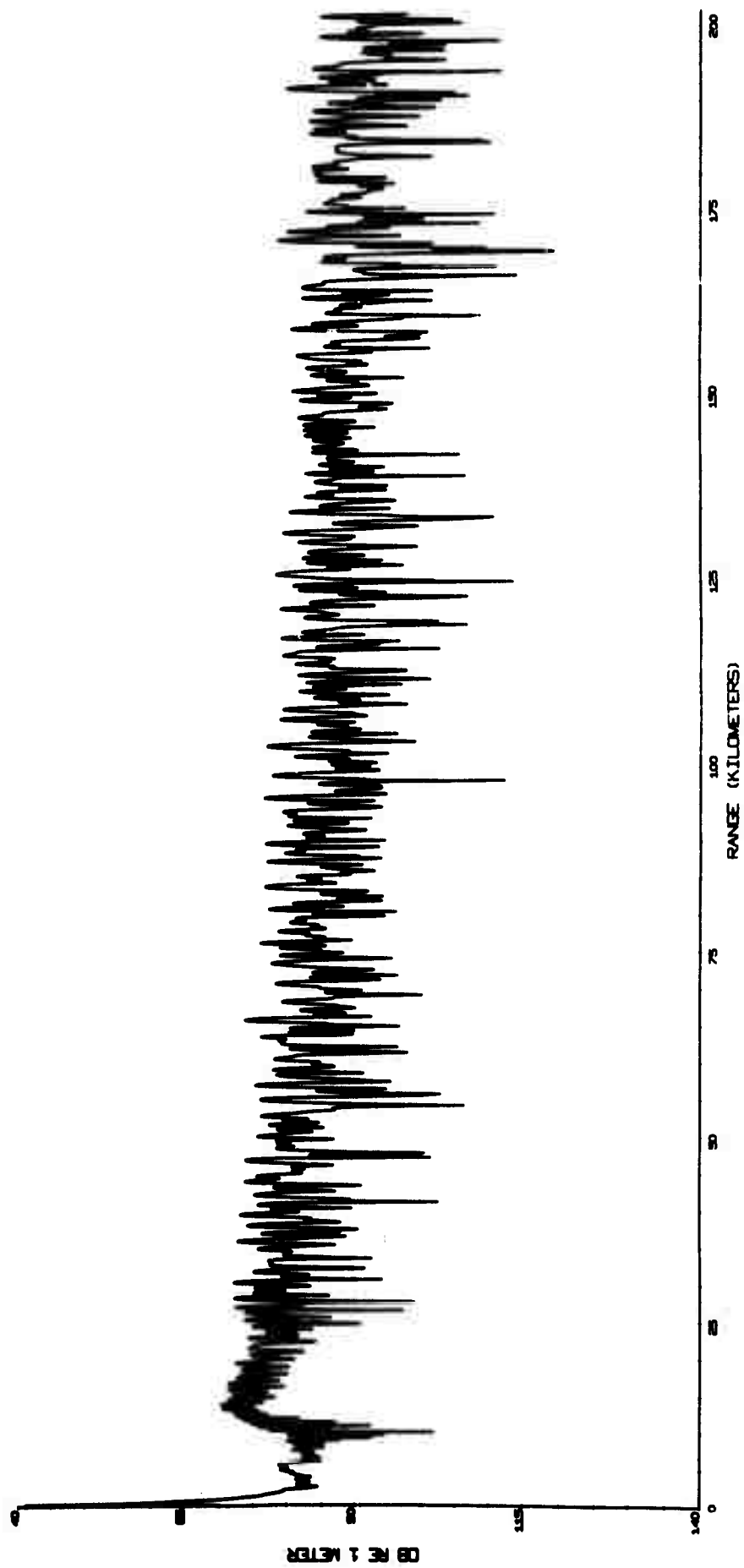
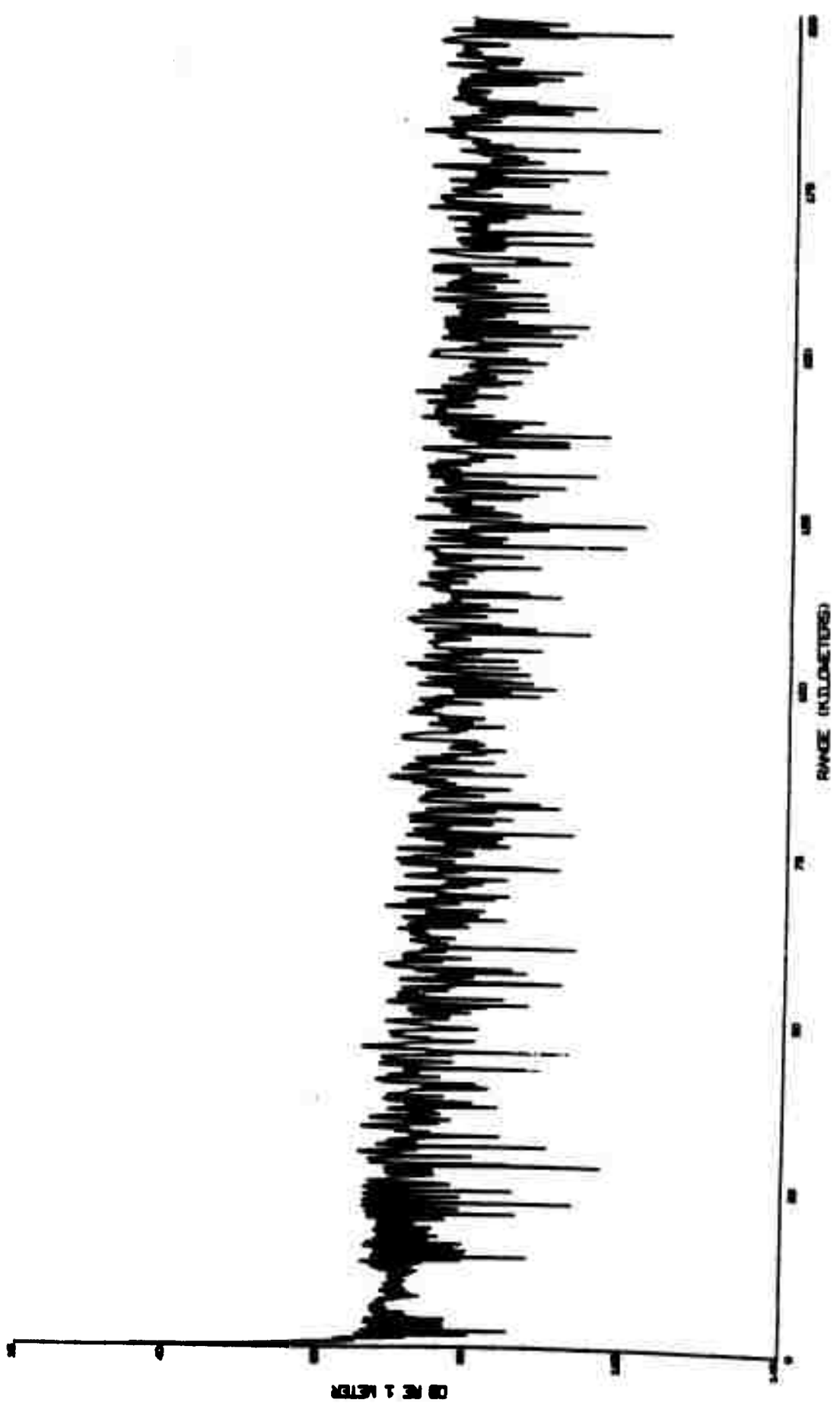


Fig. 27



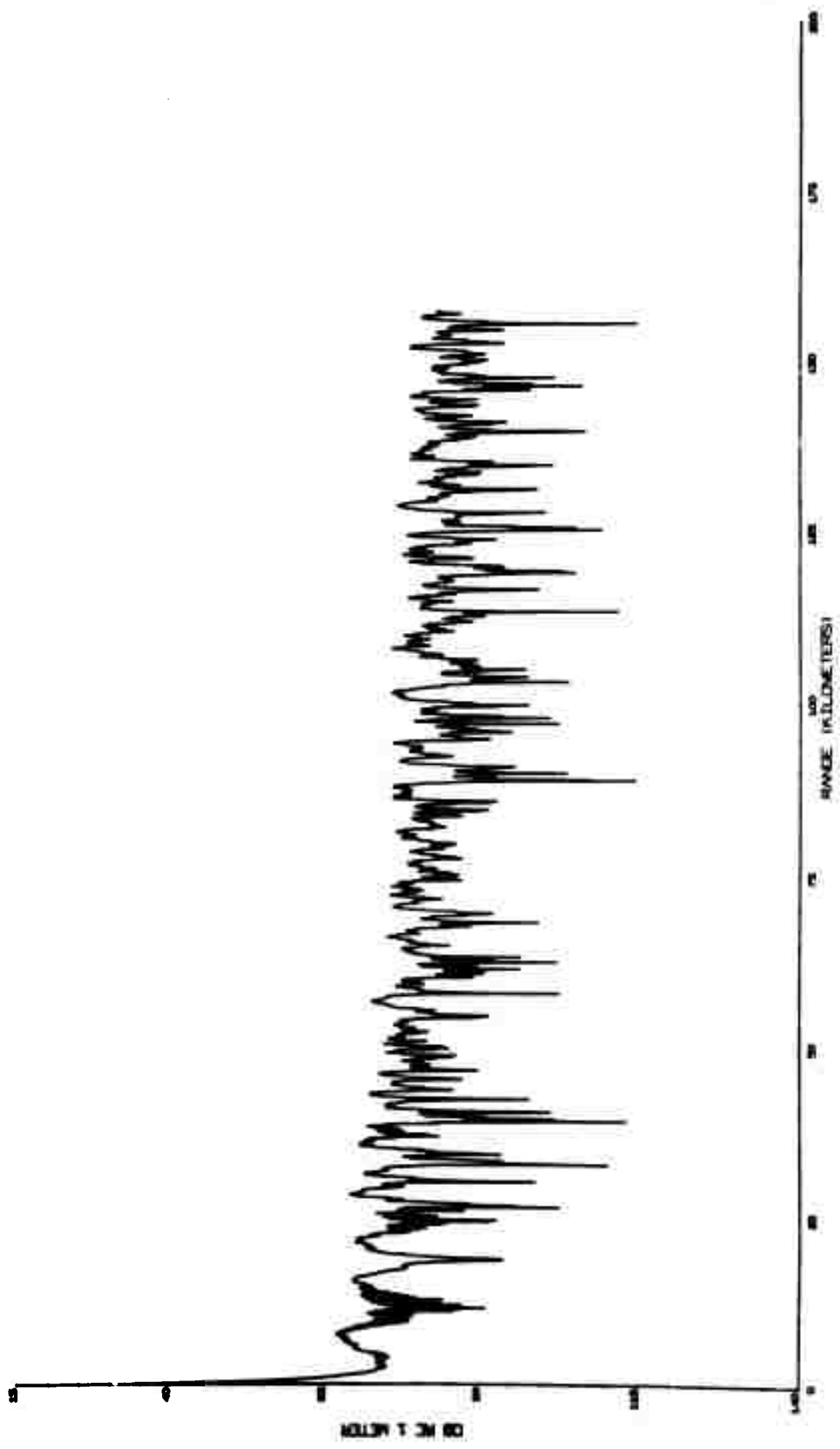


Fig. 29

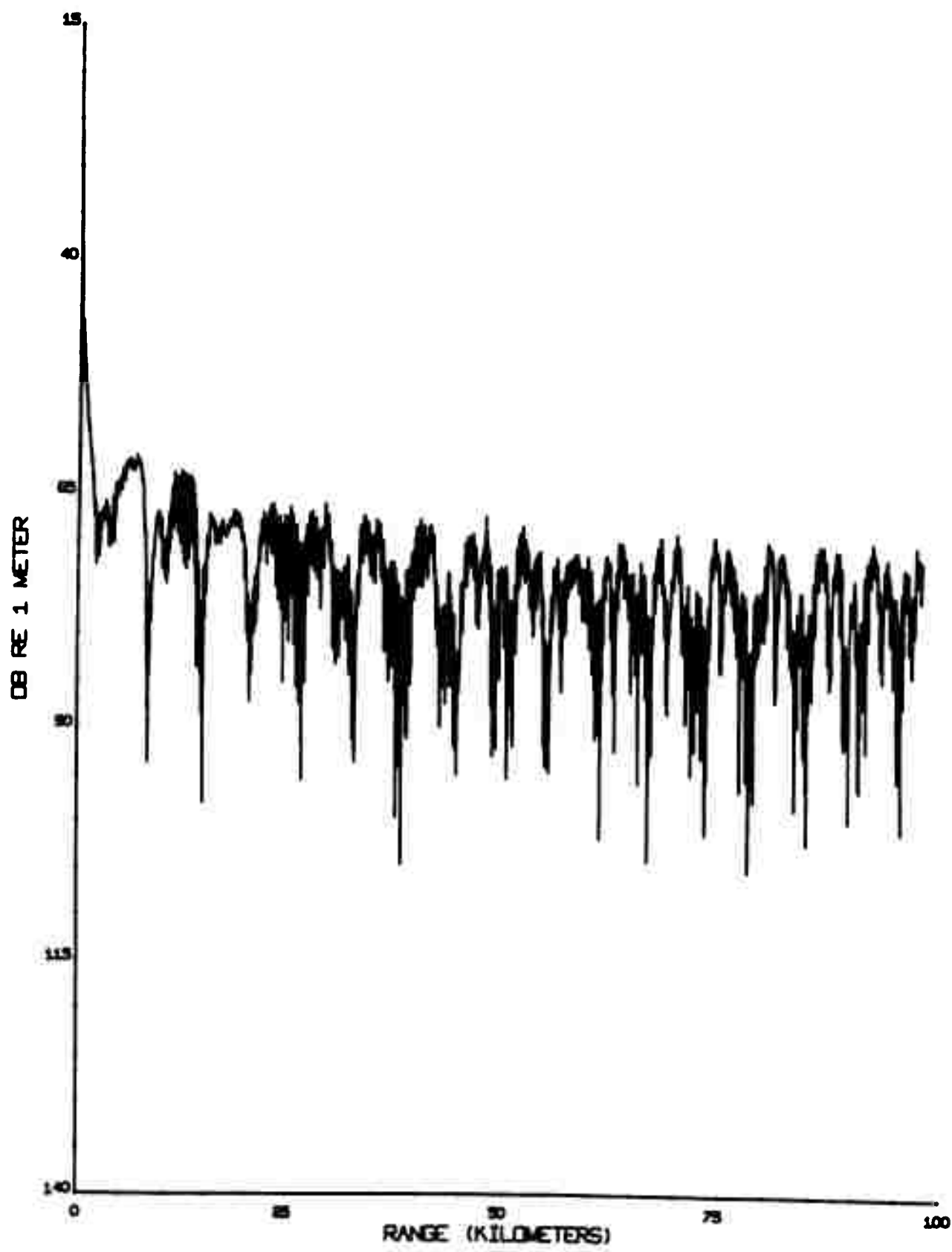


Fig. 30

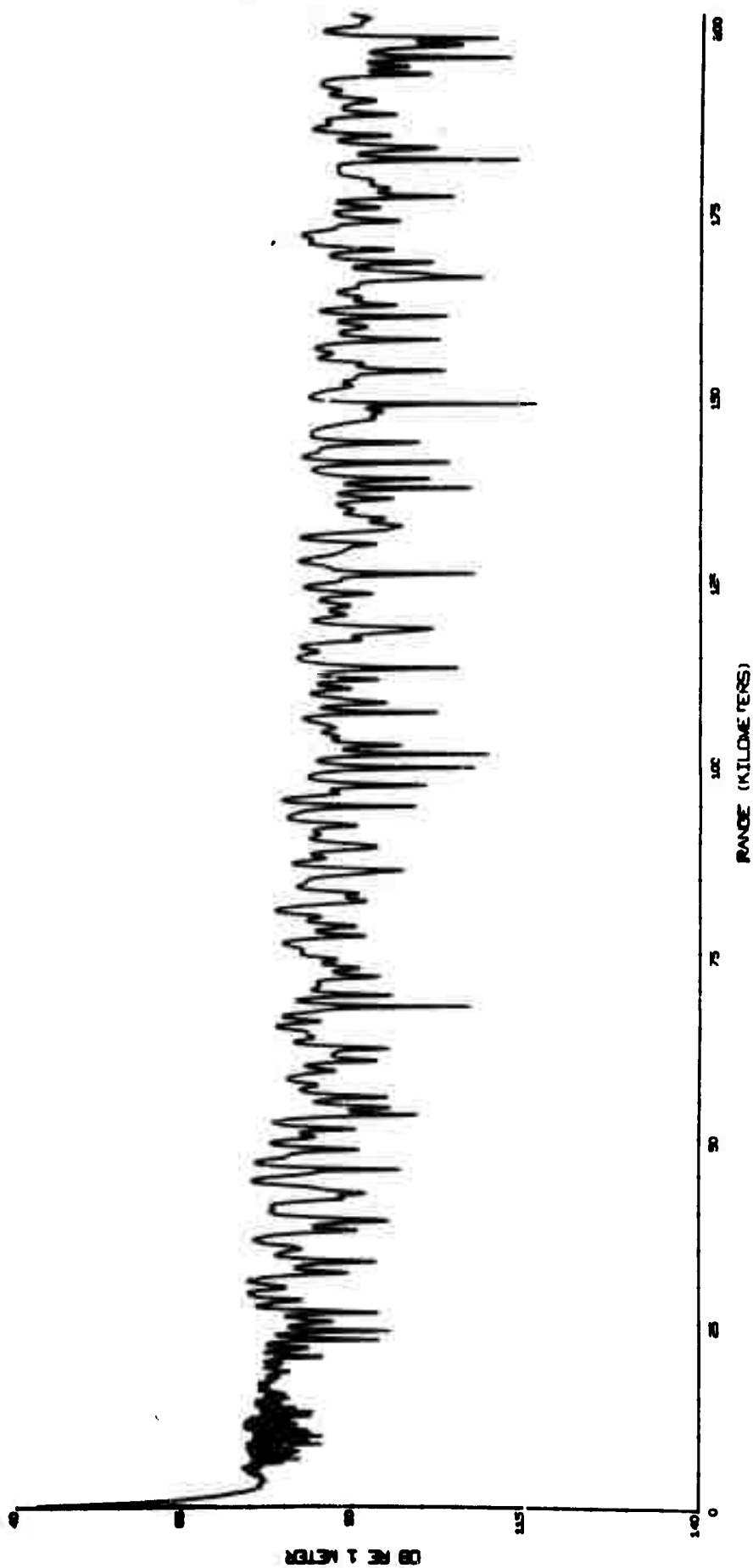


Fig. 31

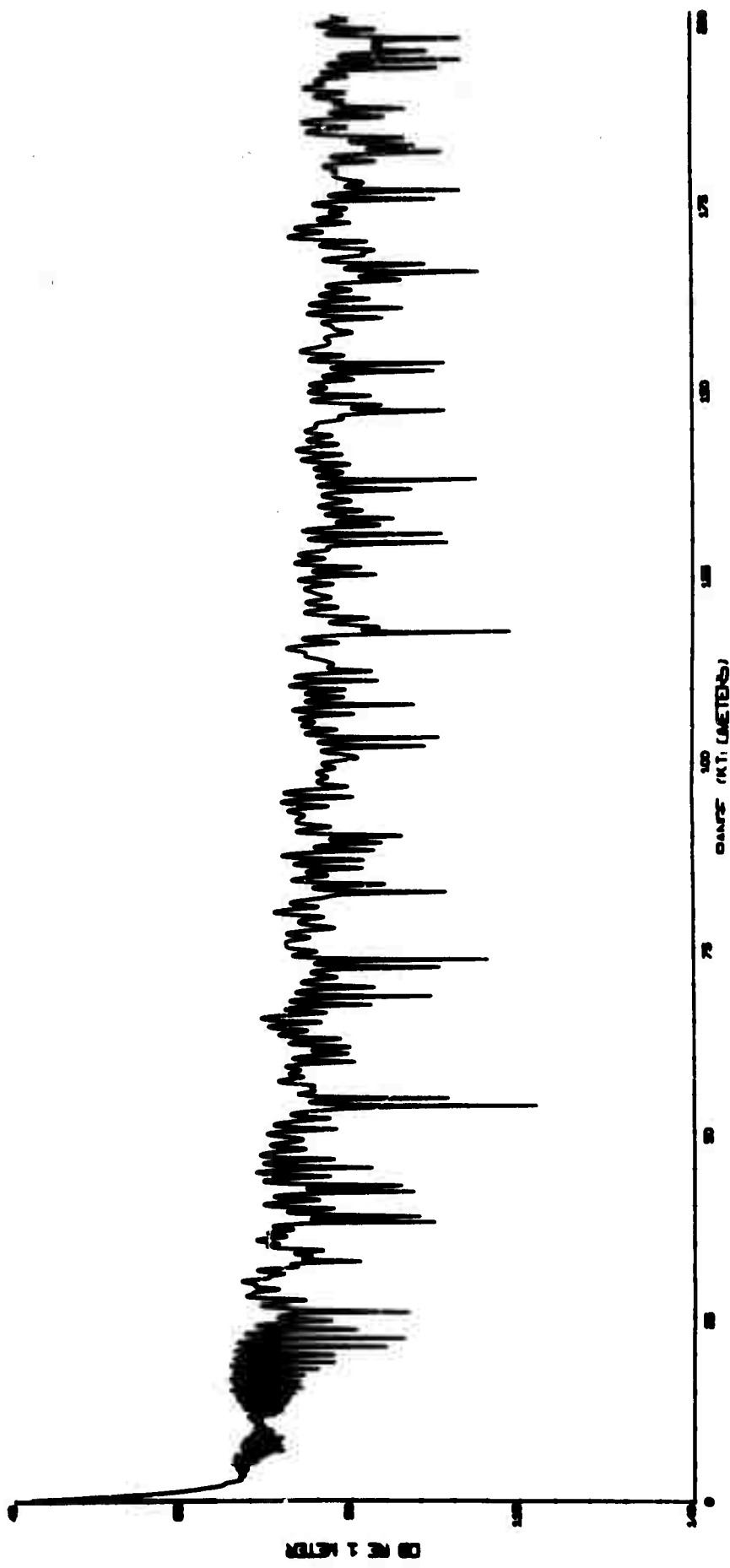


Fig. 32

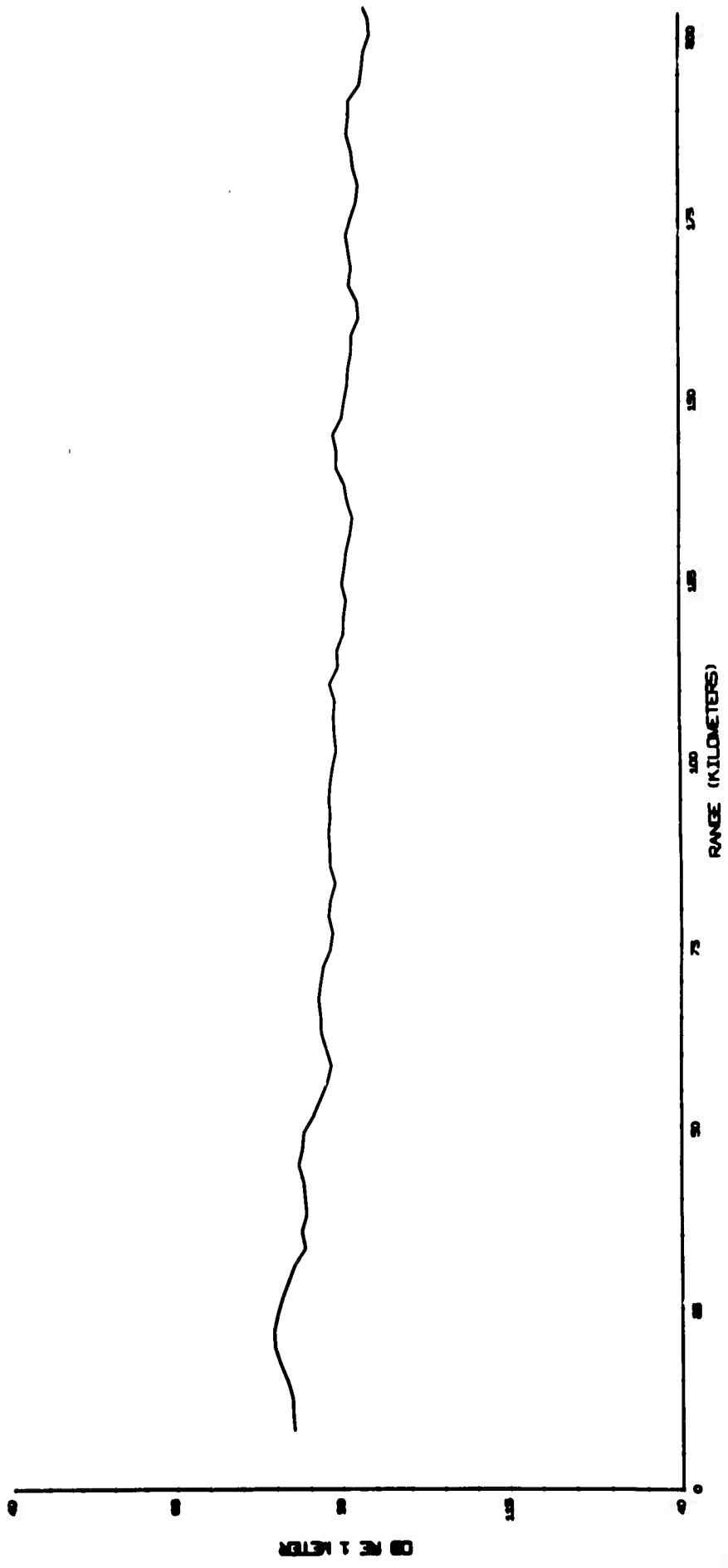


Fig. 33

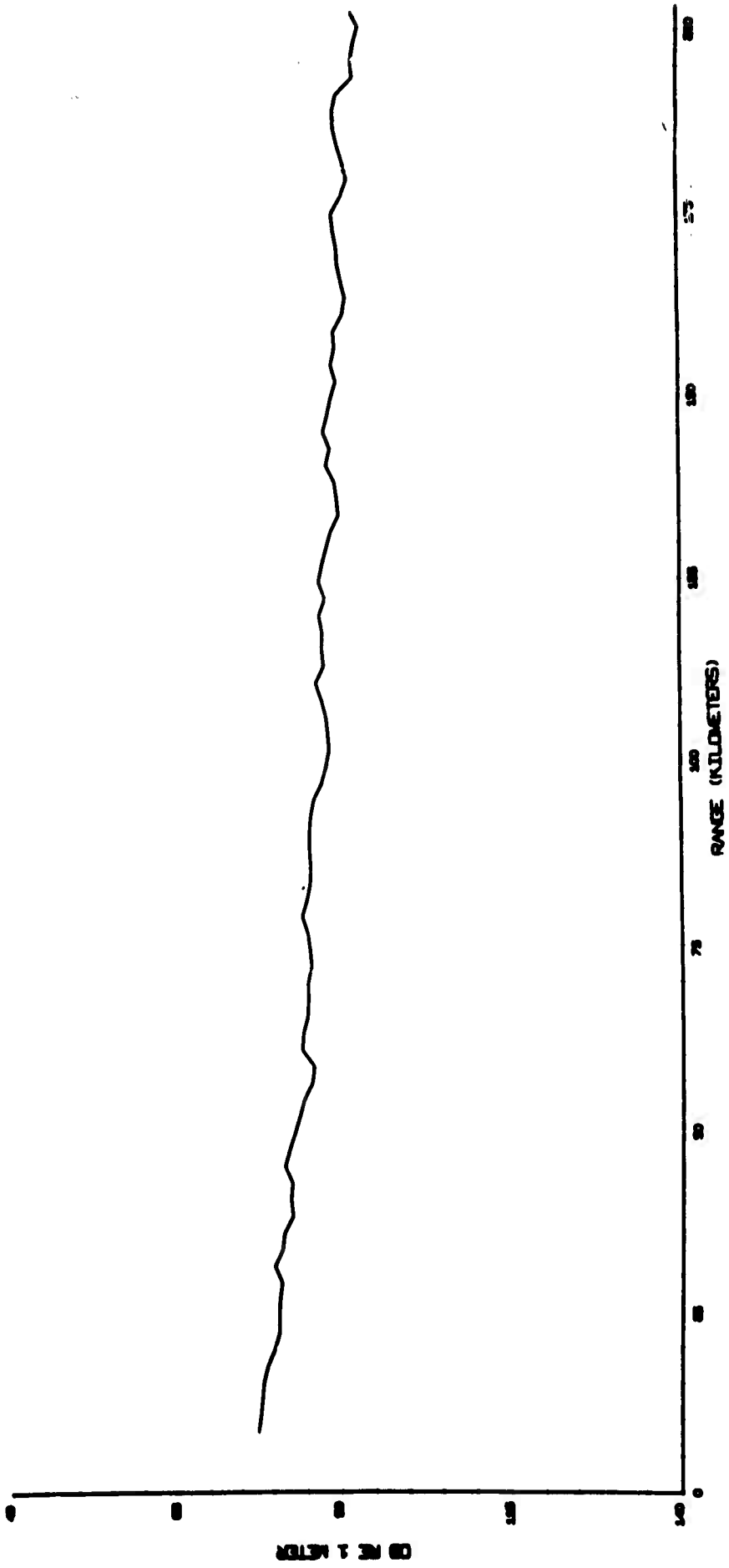
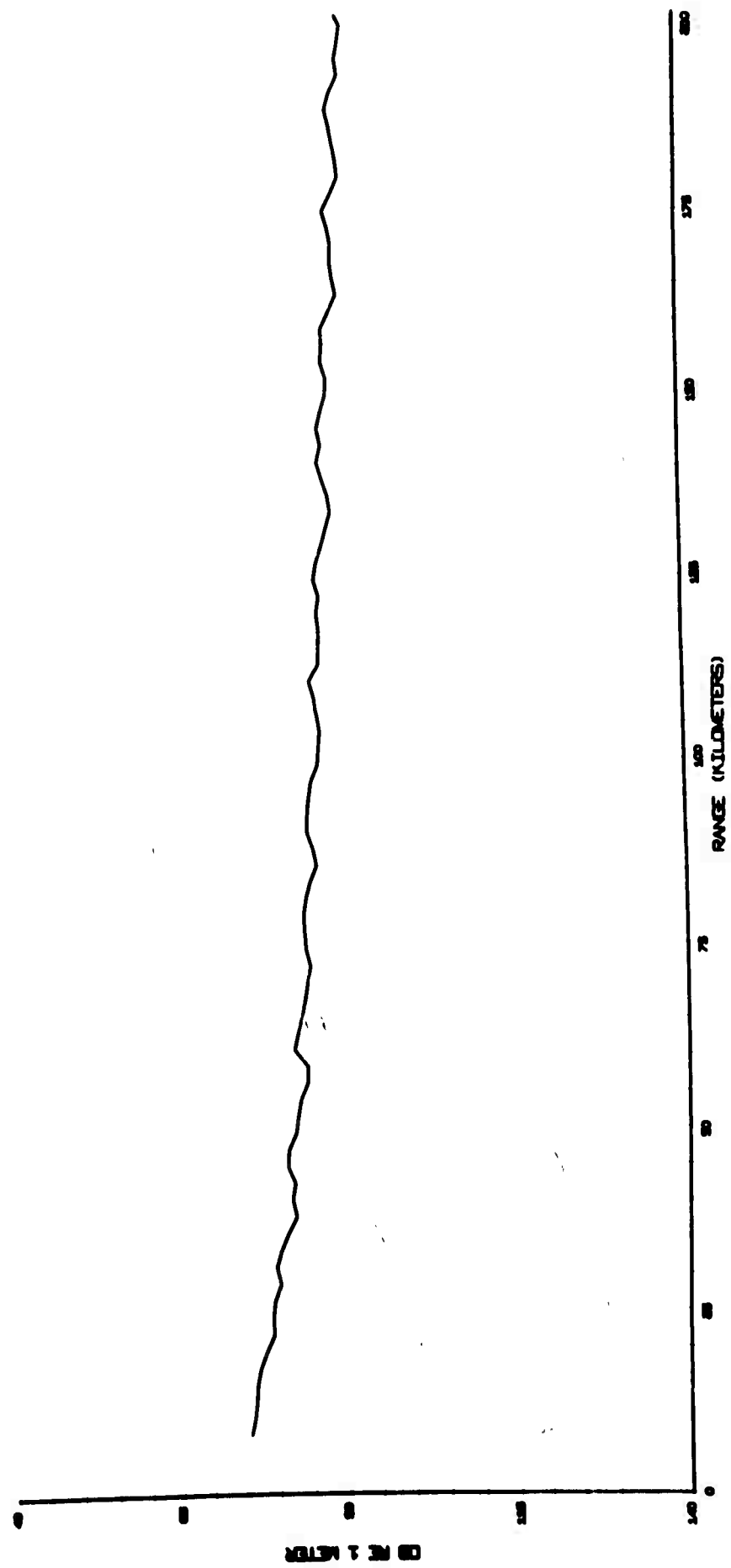


Fig. 34



Pig. 35

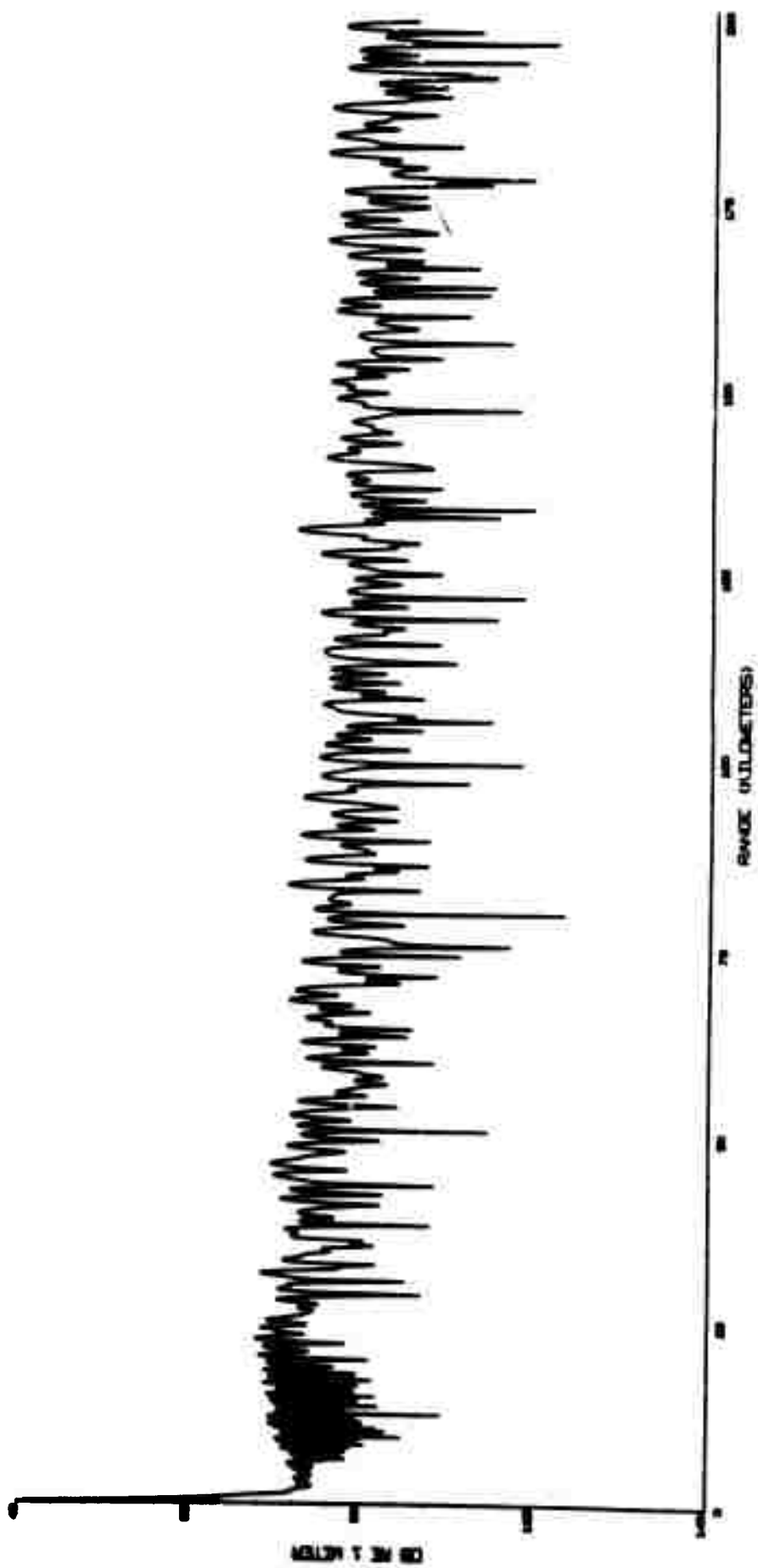
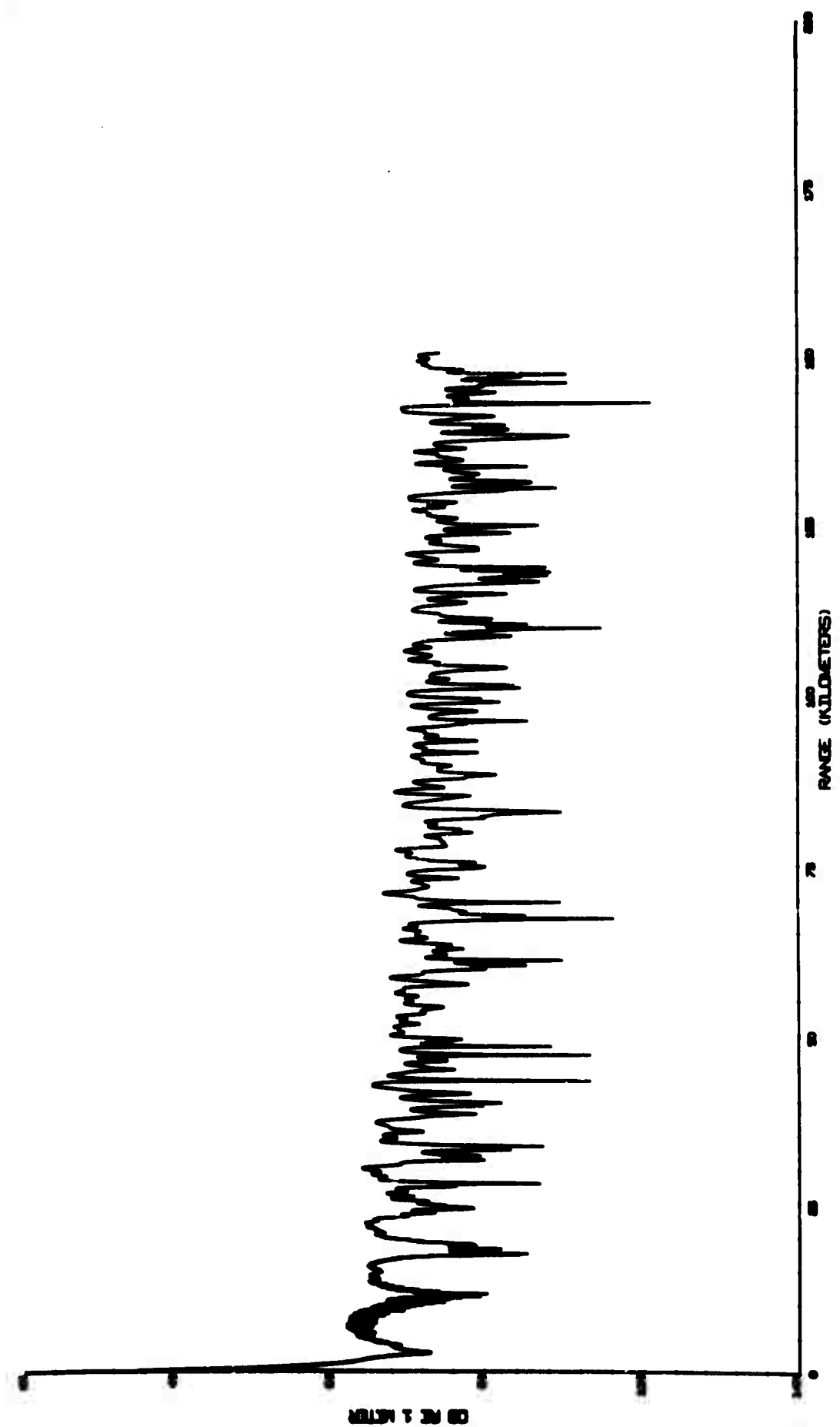
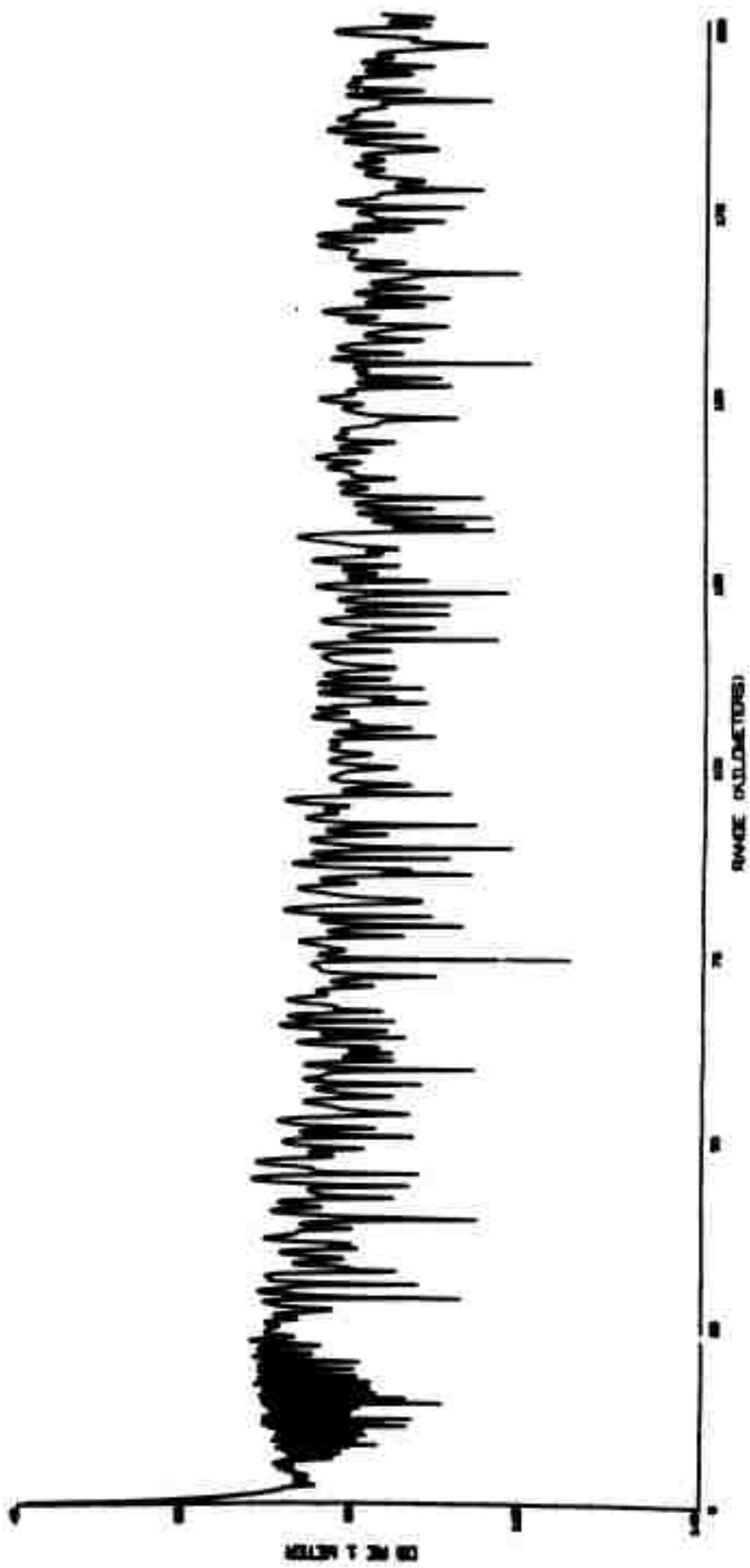
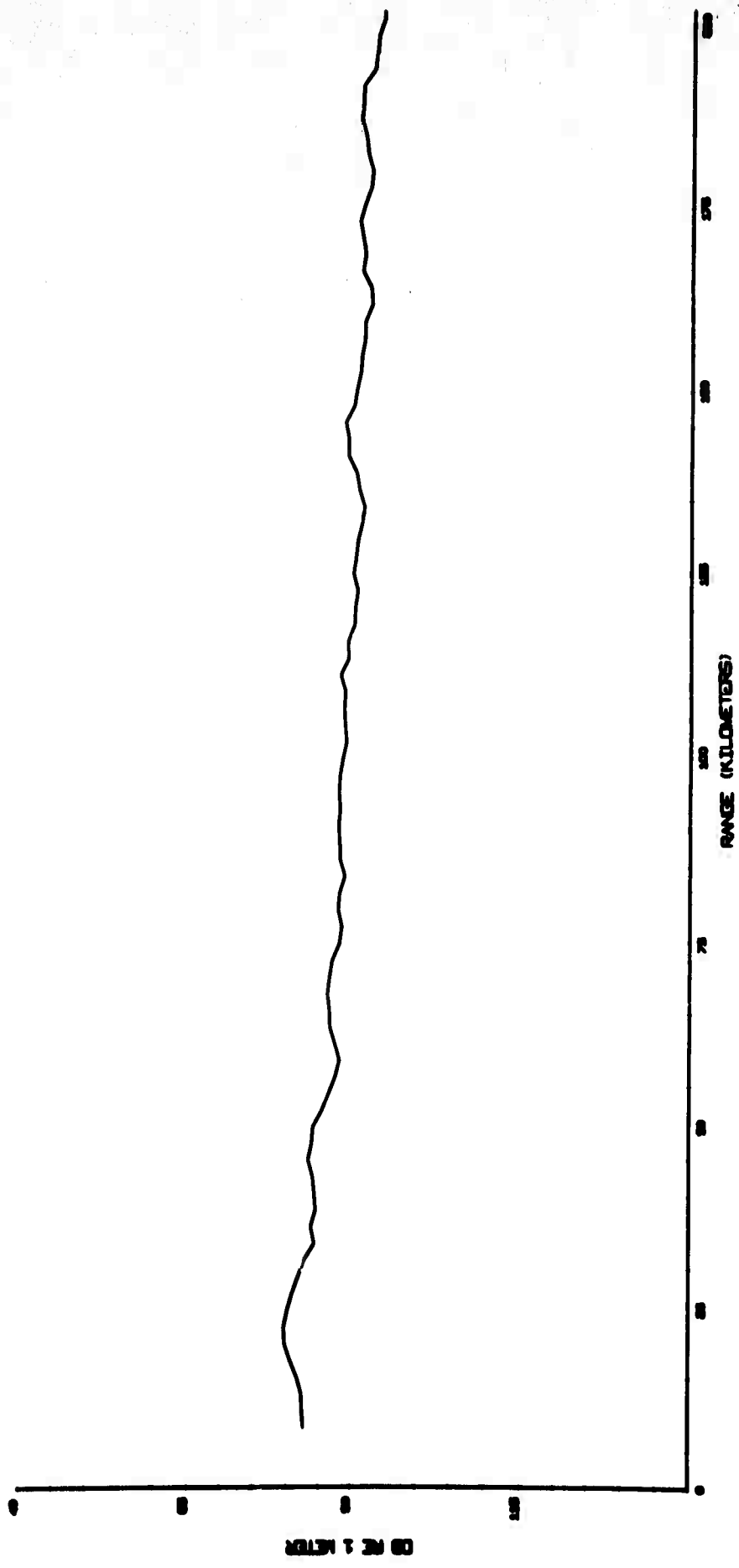
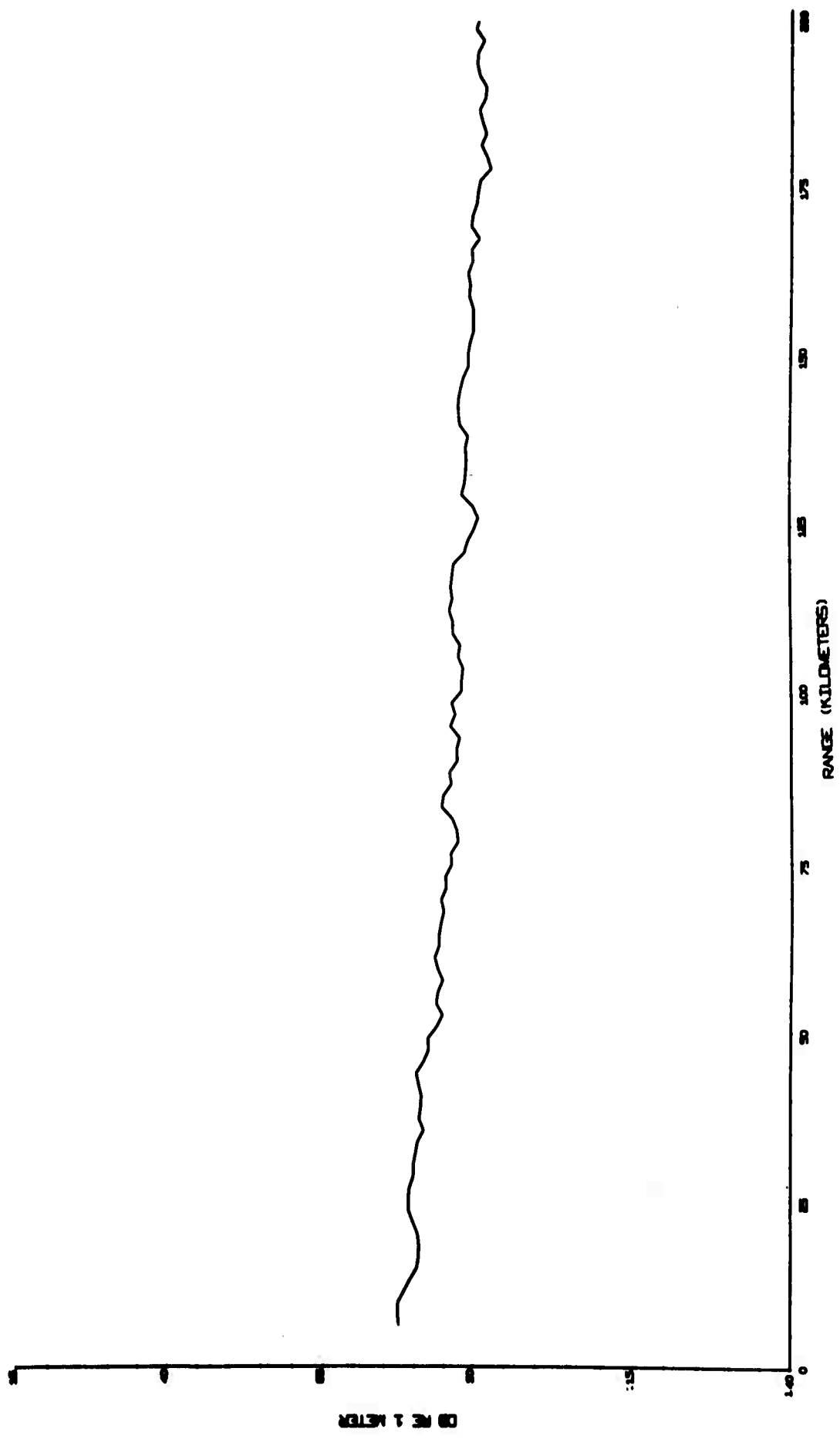


Fig. 36









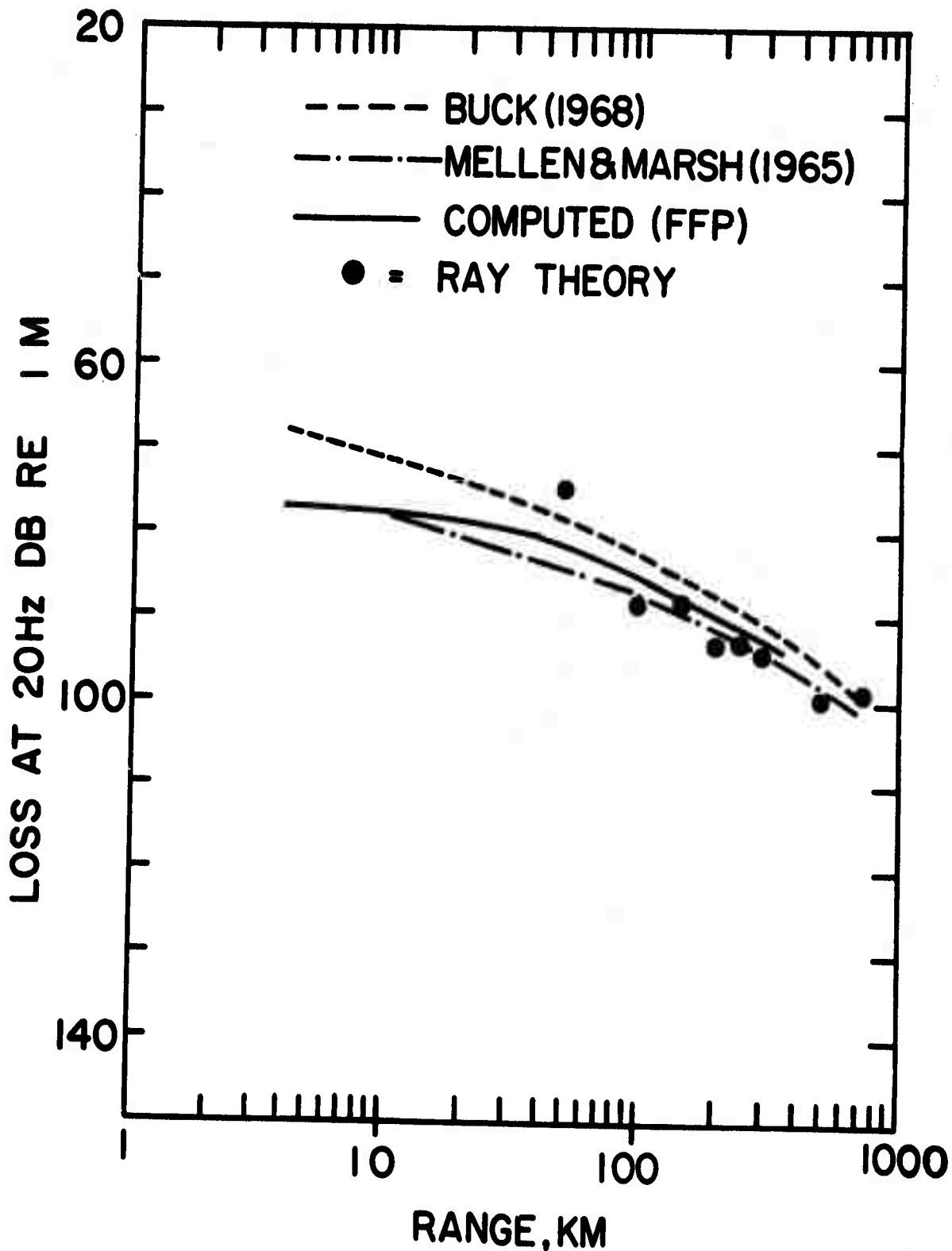


Fig. 41

DEFINITION OF SYMBOLS FOR  
APPENDIX A AND APPENDIX B

$\alpha_m$  : compressional-wave velocity in the m-th layer

$\beta_m$  : shear-wave velocity in the m-th layer

$\mu_{dm}$  : compressional-wave attenuation coefficient in the m-th layer

$\mu_{\beta_m}$  : shear wave attenuation coefficient in the m-th layer

$h_m$  : thickness of the m-th layer

$Z$  : vertical coordinate

$r$  : range between source and detector

$t$  : time

$\omega$  : angular frequency

$c$  : phase velocity

$k$  : wave number

$i$  :  $\sqrt{-1}$

$Re$  : real part of a complex number

$Im$  : imaginary part of a complex number

$|Z|$  : magnitude of a complex number  $z$

$\phi_m$  : velocity potential in the m-th layer

$(\sigma_{zz})_m$  : normal stress in the m-th layer parallel to z axis

$\tau_m$  : tangential stress in the m-th layer

$f_m$  : pressure in the m-th liquid layer

$u_m$  : horizontal particle displacement in the m-th layer in the radial direction

$w_m$  : vertical particle displacement in the m-th layer

$\dot{u}_m$  : horizontal particle velocity in the m-th layer in the radial direction

$\dot{w}_m$  : vertical particle velocity in the m-th layer

$\rho_m$  : density in the m-th layer

$\rho_s$  : density at the source

$J_0$  : Bessel function of order 0

$Y_0$  : Y Bessel function of order 0

$H_0^{(2)}$  : Hankel function of the second kind of order 0

$$k_{\alpha_m} = \frac{\omega}{\alpha_m}$$

$$k_{\beta_m} = \frac{\omega}{\beta_m}$$

$$\Gamma_{\alpha m} = \sqrt{k_{\alpha m}^2 - k^2}, \quad k < k_{\alpha m}$$

$$\Gamma_{\alpha m} = -i\sqrt{k^2 - k_{\alpha m}^2}, \quad k > k_{\alpha m}$$

$$\Gamma_{\beta m} = \sqrt{k_{\beta m}^2 - k^2}, \quad k < k_{\beta m}$$

$$\Gamma_{\beta m} = -i\sqrt{k^2 - k_{\beta m}^2}, \quad k > k_{\beta m}$$

$$P_m = h_m \Gamma_{\alpha m}$$

$$Q_m = h_m \Gamma_{\beta m}$$

**APPENDIX A****INTEGRAL SOLUTION FROM POINT HARMONIC SOURCES**

The solution of the wave equation presented here, based on the Thomson-Haskell matrix method (Thomson, 1950; Haskell, 1953), follows Harkrider (1964) for the solution of the wave equation in an n-layered solid half space. Layer matrices of the type given by Dorman (1962) for computing dispersion in an n-layered liquid-solid half-space are used for the liquid layers. An application of the theorem that the inverse of the product matrix for the layered system above the source has the same form as the inverse of a layer matrix reduces the integrand of the integral solution to a simple form in terms of elements of product matrices derived in the source-free, plane-wave case.

Consider an interbedded stack of plane parallel liquid and solid layers resting on a solid half space. The layers are shown in Figure A-1.

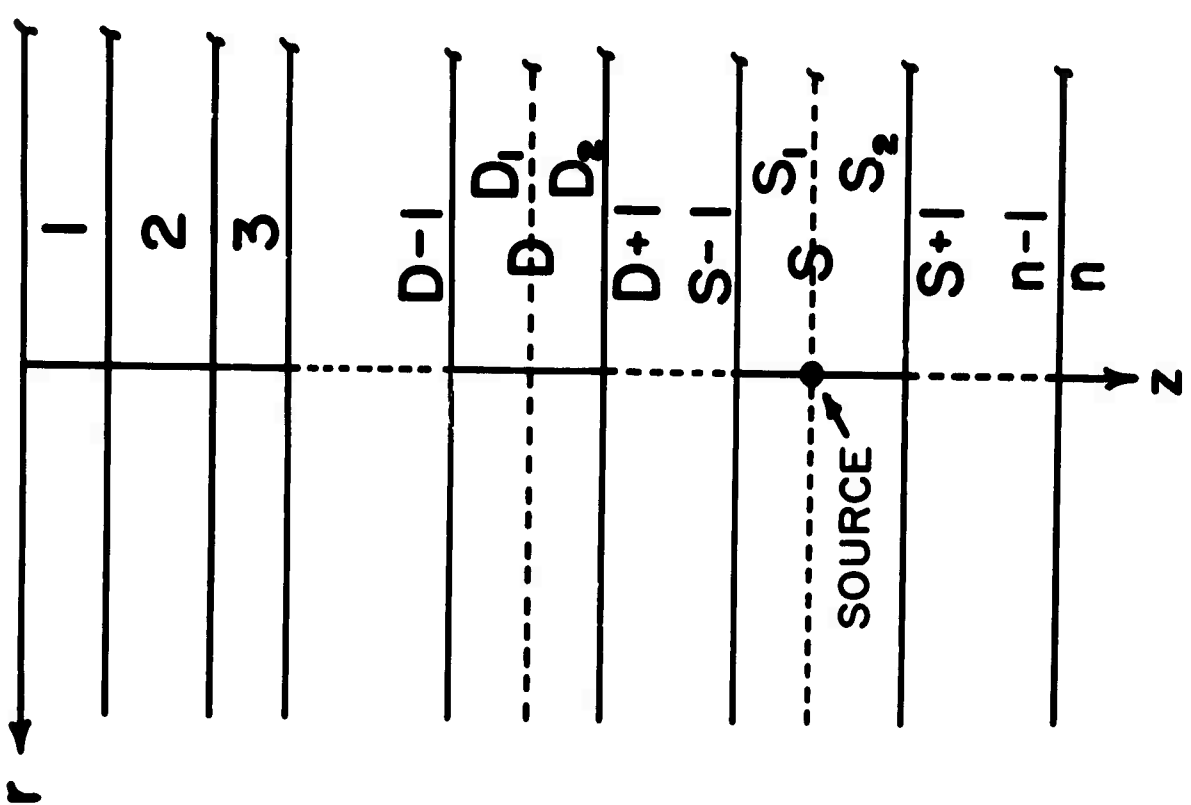
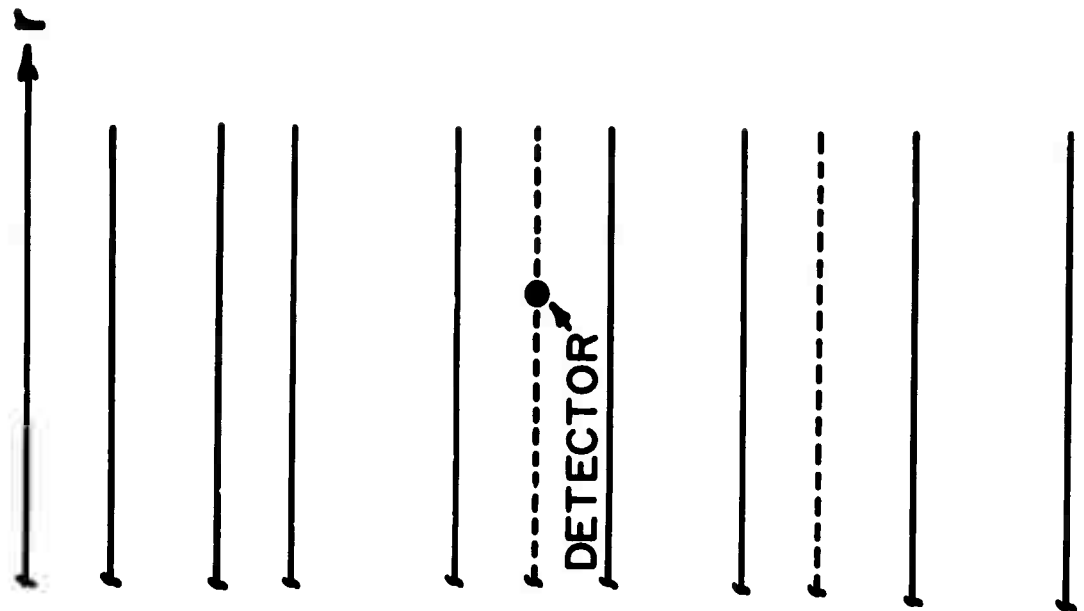


Fig. A-1

Solutions in the  $m$ -th liquid layer of vertical particle velocity and stress are

$$\dot{w}_m = \int_0^\infty \hat{w}_m(z) J_0(kr) e^{i\omega t} dk \quad (1)$$

$$(\hat{\tau}_{zz})_m = \int_0^\infty (\hat{\tau}_{zz})_m(z) J_0(kr) e^{i\omega t} dk \quad (2)$$

We divide the liquid source layer and detector layer each into two layers as shown in Figure A-1. At the bottom of the  $S_1$  layer the pressure is continuous. The vertical particle velocity is continuous everywhere in the plane between the  $S_1$  and  $S_2$  layers except at the point source where the liquid above and below the source moves in opposite directions. This may be expressed by writing

$$\delta(\hat{w}_S) = 2k .$$

In the liquid source layer for the  $\underline{z}$ -dependent particle velocities and stresses

$$\begin{bmatrix} \dot{\hat{u}}_{f-1} \\ \dot{\hat{w}}_{S_2}(D) \\ (\hat{p}_{zz})_{S_2}(D) \\ 0 \end{bmatrix} = \begin{bmatrix} \dot{\hat{u}}_{f-1} \\ \dot{\hat{w}}_{S_1}(D) \\ (\hat{p}_{zz})_{S_1}(D) \\ 0 \end{bmatrix} + \begin{bmatrix} 0 \\ \delta(\hat{w}_s) \\ 0 \\ 0 \end{bmatrix} \quad (3)$$

where  $\dot{\hat{u}}_{f-1}$  is the horizontal particle velocity at the bottom of the first liquid layer above the half space. For the layers below the  $S_1$  layer

$$\begin{bmatrix} \dot{\hat{u}}_{n-1} \\ \dot{\hat{w}}_{n-1} \\ (\hat{p}_{zz})_{n-1} \\ \hat{C}_{n-1} \end{bmatrix} = A_{S_2} \begin{bmatrix} \dot{\hat{u}}_{f-1} \\ \dot{\hat{w}}_{S_2}(D) \\ (\hat{p}_{zz})_{S_2}(D) \\ 0 \end{bmatrix} \quad (4)$$

and for the layers above the  $s_2$  layer

$$\begin{bmatrix} \dot{\bar{u}}_{g-1} \\ \dot{\bar{w}}_{s_1}(D) \\ (\hat{p}_{zz})_{s_1}(D) \\ 0 \end{bmatrix} = A_{s_1} \begin{bmatrix} \dot{\bar{u}}_{g-1} \\ \dot{\bar{w}}_0 \\ 0 \\ 0 \end{bmatrix} \quad (5)$$

At the free surface both  $(\hat{p}_{zz})_0$  and  $\hat{\xi}_0$  are zero.

In Equations 4 and 5

$$A_{s_2} = a_{n-1} \cdot a_{n-2} \cdot \dots \cdot b_{n-6} \dots \cdot a_{s_2}$$

$$A_{s_1} = a_{s_1} \cdot b_{s_1-1} \cdot \dots \cdot a_2 b_1$$

The matrices,  $a_m$ , for liquid layers and  $b_m$ , for solid layers between liquid layers are in terms of  $4 \times 4$  matrices:

$$a_m = \begin{bmatrix} 1 & 0 & 0 & 0 \\ 0 & (a_m)_{22} & (a_m)_{23} & 0 \\ 0 & (a_m)_{32} & (a_m)_{33} & 0 \\ 0 & 0 & 0 & 1 \end{bmatrix}$$

$$b_m = \begin{bmatrix} 1 & 0 & 0 & 0 \\ 0 & (b_m)_{22} & (b_m)_{23} & 0 \\ 0 & (b_m)_{32} & (b_m)_{33} & 0 \\ 0 & 0 & 0 & 1 \end{bmatrix}.$$

The  $(b_m)_{22}, (b_m)_{23}, (b_m)_{32}, (b_m)_{33}$  are derived by

Kutschera (1970, 1972)

$$(b_m)_{22} = (a_m)_{22} - \frac{(a_m)_{21}(a_m)_{42}}{(a_m)_{41}}$$

$$(b_m)_{23} = (a_m)_{23} - \frac{(a_m)_{21}(a_m)_{43}}{(a_m)_{41}}$$

$$(b_m)_{32} = (a_m)_{32} - \frac{(a_m)_{31}(a_m)_{42}}{(a_m)_{41}}$$

$$(b_m)_{33} = (a_m)_{33} - \frac{(a_m)_{31}(a_m)_{43}}{(a_m)_{41}}$$

in terms of elements of the solid layer matrix

$$a_m = \begin{bmatrix} (a_m)_{11} & (a_m)_{12} & (a_m)_{13} & (a_m)_{14} \\ (a_m)_{21} & (a_m)_{22} & (a_m)_{23} & (a_m)_{24} \\ (a_m)_{31} & (a_m)_{32} & (a_m)_{33} & (a_m)_{34} \\ (a_m)_{41} & (a_m)_{42} & (a_m)_{43} & (a_m)_{44} \end{bmatrix}$$

The matrix elements for liquid and solid layers are given in Appendix B.

We now write for the solid half-space (Haskell, 1953)

$$\begin{bmatrix} \Delta_n' + \Delta_n'' \\ \Delta_n' - \Delta_n'' \\ w_n' + w_n'' \\ w_n' - w_n'' \end{bmatrix} = E^{-1} \begin{bmatrix} \hat{u}_{n-1} \\ \hat{w}_{n-1} \\ (\hat{p}_{zz})_{n-1} \\ \hat{c}_{n-1} \end{bmatrix}$$

where

$$E^{-1} = \begin{bmatrix} -2\left(\frac{\beta_n}{\alpha_n}\right)^2 \frac{k}{\omega} & 0 & \frac{1}{\rho_n \alpha_n^2} & 0 \\ 0 & \frac{\omega \left[ 2\left(\frac{k}{k_{pn}}\right)^2 - 1 \right]}{\alpha_n^2 \Gamma_{pn}} & 0 & \frac{k}{\rho_n \alpha_n^2 \Gamma_{pn}} \\ \frac{\omega \left[ 2\left(\frac{k}{k_{pn}}\right)^2 - 1 \right]}{2 \beta_n^2 \Gamma_{pn}} & 0 & -\frac{k}{2 \rho_n \beta_n^2 \Gamma_{pn}} & 0 \\ 0 & \frac{k}{\omega} & 0 & \frac{1}{2 \rho_n \beta_n^2} \end{bmatrix}$$

The  $\Delta_n'$ ,  $\Delta_n''$ ,  $\omega_n'$ ,  $\omega_n''$  are constants for each wave number.

Applying the condition that no sources radiate from infinity

$\Delta_n''$ ,  $\omega_n''$  equal zero and hence

$$\begin{bmatrix} \Delta_n' \\ \Delta_n'' \\ \omega_n' \\ \omega_n'' \end{bmatrix} = E^{-1} \begin{bmatrix} \hat{u}_{n-1} \\ \hat{w}_{n-1} \\ (\hat{p}_{zz})_{n-1} \\ \hat{e}_{n-1} \end{bmatrix} \quad (6)$$

From Equation 4, Equation 6 may be written

$$\begin{bmatrix} \Delta_n' \\ \Delta_n' \\ w_n' \\ w_n' \end{bmatrix} = E^{-1} A_{S_2} \begin{bmatrix} \hat{\omega}_{q-1} \\ \hat{w}_{S_2}(D) \\ (\hat{p}_{zz})_{S_2}(D) \\ 0 \end{bmatrix}$$

or from Equation 3

$$\begin{bmatrix} \Delta_n' \\ \Delta_n' \\ w_n' \\ w_n' \end{bmatrix} = E^{-1} A_{S_2} \left\{ \begin{bmatrix} \hat{\omega}_{q-1} \\ \hat{w}_{S_1}(D) \\ (\hat{p}_{zz})_{S_1}(D) \\ 0 \end{bmatrix} + \begin{bmatrix} 0 \\ \delta(\hat{w}_S) \\ 0 \\ 0 \end{bmatrix} \right\}$$

and from Equation 5

$$\begin{bmatrix} \Delta_n' \\ \Delta_n' \\ w_n' \\ w_n' \end{bmatrix} = E^{-1} \left\{ A_{S_2} A_{S_1} \begin{bmatrix} \hat{\omega}_{q-1} \\ \hat{w}_0 \\ 0 \\ 0 \end{bmatrix} + A_{S_2} \begin{bmatrix} 0 \\ \delta(\hat{w}_S) \\ 0 \\ 0 \end{bmatrix} \right\}$$

$$= E^{-1} A \left\{ \begin{bmatrix} \hat{w}_{q-1} \\ \hat{w}_0 \\ 0 \\ 0 \end{bmatrix} + A_{S_1}^{-1} \begin{bmatrix} 0 \\ \delta(\hat{w}_s) \\ 0 \\ 0 \end{bmatrix} \right\} \quad (7)$$

where  $A = A_{S_2} A_{S_1} = a_{n-1} a_{n-2} \cdots a_2 b,$

Let

$$\begin{bmatrix} W \\ X \\ Y \\ Z \end{bmatrix} = \begin{bmatrix} \hat{w}_{q-1} \\ \hat{w}_0 \\ 0 \\ 0 \end{bmatrix} + A_{S_1}^{-1} \begin{bmatrix} 0 \\ \delta(\hat{w}_s) \\ 0 \\ 0 \end{bmatrix}.$$

We may prove following Harkrider (1964) that the inverse of the product matrix  $A_{S_1}$  has the same form as the inverse of a layer matrix and hence

$$A_{S_1}^{-1} = \begin{bmatrix} 1 & 0 & 0 & 0 \\ 0 & (A_{S_1})_{33} & -(A_{S_1})_{23} & 0 \\ 0 & -(A_{S_1})_{32} & (A_{S_1})_{22} & 0 \\ 0 & 0 & 0 & 1 \end{bmatrix}$$

Therefore

$$\begin{bmatrix} W \\ X \\ Y \\ Z \end{bmatrix} = \begin{bmatrix} \hat{w}_{q-1} \\ \hat{w}_0 \\ 0 \\ 0 \end{bmatrix} + \begin{bmatrix} 1 & 0 & 0 & 0 \\ 0 & (A_{S_1})_{33} & -(A_{S_1})_{23} & 0 \\ 0 & -(A_{S_1})_{32} & (A_{S_1})_{22} & 0 \\ 0 & 0 & 0 & 1 \end{bmatrix} \begin{bmatrix} 0 \\ \delta(\hat{w}_s) \\ 0 \\ 0 \end{bmatrix}$$

or in terms of matrix elements

$$W = \hat{w}_{q-1} \quad (8)$$

$$X = \hat{w}_0 + (A_{S_1})_{33} \delta(\hat{w}_s) \quad (9)$$

$$Y = -(A_{S_1})_{32} \delta(\hat{w}_s) \quad (10)$$

$$Z = 0 \quad (11)$$

We define  $J = E^{-1}A$  and write Equation (7)

$$\begin{bmatrix} \Delta_n' \\ \Delta_n' \\ W_n' \\ W_n' \end{bmatrix} = \begin{bmatrix} J_{11} & J_{12} & J_{13} & J_{14} \\ J_{21} & J_{22} & J_{23} & J_{24} \\ J_{31} & J_{32} & J_{33} & J_{34} \\ J_{41} & J_{42} & J_{43} & J_{44} \end{bmatrix} \begin{bmatrix} W \\ X \\ Y \\ Z \end{bmatrix}$$

Eliminating  $\Delta_n'$

$$(J_{11} - J_{21})W + (J_{12} - J_{22})X + \quad (12)$$

$$(J_{13} - J_{23})Y + (J_{14} - J_{24})Z = 0$$

and eliminating  $W_n'$

$$(J_{31} - J_{41})W + (J_{32} - J_{42})X + \quad (13)$$

$$(J_{33} - J_{43})Y + (J_{34} - J_{44})Z = 0$$

If we let

$$L = J_{11} - J_{21}$$

$$K = J_{12} - J_{22}$$

$$G = J_{13} - J_{23}$$

$$R = J_{14} - J_{24}$$

$$N = J_{31} - J_{41}$$

$$M = J_{32} - J_{42}$$

$$H = J_{33} - J_{43}$$

$$S = J_{34} - J_{44}$$

and solve Equations (12) and (13) for W and X respectively,

$$W = -\frac{K}{L}X - \frac{G}{L}Y - \frac{R}{L}Z \quad (14)$$

$$X = -\frac{N}{M}W - \frac{H}{M}Y - \frac{S}{M}Z \quad (15)$$

or substituting Equation 14 in Equation 15

$$X = -\frac{N}{M} \left( -\frac{K}{L} X - \frac{G}{L} Y - \frac{R}{L} Z \right) - \frac{H}{M} Y - \frac{S}{M} Z$$

and solving for X

$$X = \frac{(GN - HL)Y + (RN - SL)Z}{ML - NK}$$

and therefore from Equations (10) and (11)

$$X = \frac{(GN - HL)(A_{s1})_{32} \delta(\dot{\bar{w}}_s)}{NK - ML}$$

or from the Equation 9

$$\dot{\bar{w}}_o = \frac{(GN - HL)(A_{s1})_{32} \delta(\dot{\bar{w}}_s) - (A_{s1})_{33} f(\dot{\bar{w}}_s)}{NK - ML}$$

Hence, the integral solution for  $\dot{w}_o$  is from Equation 1,  
 dropping the  $e^{i\omega t}$  term,

$$\dot{w}_o = \int_0^\infty \left\{ \frac{(GN - HL)(A_{S,32})}{(NK - ML)} - (A_{S,33}) \right\} J_o(kr) \alpha k dk$$

If a hydrophone or vertical particle velocity detector is located in a liquid layer at the bottom of the  $D_1$  layer in Fig-

ure A-1.

$$\begin{bmatrix} \dot{u}_{f-1} \\ \dot{w}_{D_1} \\ (\dot{p}_{zz})_{D_1} \\ 0 \end{bmatrix} = \begin{bmatrix} 1 & 0 & 0 & 0 \\ 0 & (A_{D_1,22}) & (A_{D_1,23}) & 0 \\ 0 & (A_{D_1,32}) & (A_{D_1,33}) & 0 \\ 0 & 0 & 0 & 1 \end{bmatrix} \begin{bmatrix} \dot{u}_{f-1} \\ \dot{w}_o \\ 0 \\ 0 \end{bmatrix}$$

where

$$A_{D_1} = a_{D_1} \cdot a_{D_1-1} \cdot \dots \cdot a_2 b_1$$

or

$$(\hat{p}_{zz})_{D_1} = -\hat{p}_{D_1} = (A_{D_1})_{32} \dot{\hat{w}}_o$$

Hence, the integral solution for pressure at the bottom of layer

$D_1$  is

$$\hat{p}_{D_1} = - \int_0^\infty \left\{ \frac{(GN - HL)(A_{S_1})_{32}}{(NK - ML)} - (A_{S_1})_{33} \right\} \cdot (16)$$

$$(A_{D_1})_{32} J_0(kr) 2 k dk$$

which is the desired integral solution (Equation 2).

For a constant pressure source of amplitude  $P_o$  dynes/cm<sup>2</sup> at 1 m we multiply Equation 16 by  $\frac{P_o}{i w \rho_s}$  and get

$$\hat{p}_{D_1} = -\frac{1}{i} \left( \frac{P_o}{w \rho_s} \right) \int_0^\infty \left\{ \frac{(GN - HL)(A_{S_1})_{32}}{(NK - ML)} - (A_{S_1})_{33} \right\} \cdot$$

$$(A_{D_1})_{32} 2 J_0(kr) k dk$$

If the bottom is liquid the corresponding formula is (Kutschale

1970) in terms of 4 by 4 layer matrices of Appendix B

$$P_{D_1} = -\frac{1}{i} \left( \frac{P_0}{W_P S} \right) \left\{ \frac{(W_P n A_{23} + F_{dn} A_{33})(A_{S_1})_{32}}{(W_P n A_{22} + F_{dn} A_{32})} - (A_{S_1})_{33} \right\}$$

$$(A_{D_1})_{32} \propto J_0(kr) k dk .$$

Carrying out the matrix multiplication

$$\begin{bmatrix} \Delta_n' \\ \Delta_n' \\ W_n' \\ W_n' \end{bmatrix} = E^{-1} A \begin{bmatrix} W \\ X \\ Y \\ Z \end{bmatrix}$$

and eliminating  $\Delta_n'$  and  $W_n'$  explicit expressions for

L, K, G, N, M and H are

$$L = -2 \frac{k^2}{k_{\beta n}^2} A_{11} - k \left[ \frac{2 \left( \frac{k}{k_{\beta n}} \right)^2 - 1}{r_{\alpha n}} \right] A_{21} +$$

$$\frac{k}{w_{pn}} A_{31} - \frac{k^2}{\rho_n w r_{\alpha n}} A_{41}$$

$$K = -2 \frac{k^2}{k_{\beta n}^2} A_{12} - k \left[ \frac{2 \left( \frac{k}{k_{\beta n}} \right)^2 - 1}{r_{\alpha n}} \right] A_{22} +$$

$$\frac{k}{w_{pn}} A_{32} - \frac{k^2 A_{42}}{\rho_n w r_{\alpha n}}$$

$$G = -2 \frac{k^2}{k_{\beta n}^2} A_{13} - k \frac{\left[ 2 \left( \frac{k}{k_{\beta n}} \right)^2 - 1 \right]}{r_{\alpha n}} A_{23} +$$

$$\frac{k}{\omega \rho n} = \frac{k^2 A_{43}}{\rho_n \omega r_{\alpha n}}$$

$$N = \frac{\left[ 2 \left( \frac{k}{k_{\beta n}} \right)^2 - 1 \right] k}{r_{\beta n}} A_{11} - 2 \frac{k^2}{k_{\beta n}^2} A_{21} -$$

$$\frac{k^2}{\rho_n \omega r_{\beta n}} A_{31} - \frac{k}{\omega \rho n} A_{41}$$

$$M = \frac{\left[ 2\left( \frac{k}{k_{\beta n}} \right)^2 - 1 \right] k}{r_{\beta n}} A_{12} - 2 \frac{k^2}{k_{\beta n}^2} A_{22} -$$

$$\frac{k^2}{\rho_n w r_{\beta n}} A_{32} - \frac{k}{w \rho_n} A_{42}$$

$$H = \frac{\left[ 2\left( \frac{k}{k_{\beta n}} \right)^2 - 1 \right] k}{r_{\beta n}} A_{13} - 2 \frac{k^2}{k_{\beta n}^2} A_{23} -$$

$$\frac{k^2}{\rho_n w r_{\beta n}} A_{33} - \frac{k}{w \rho_n} A_{43}$$

We now introduce attenuation coefficients  $\mu_{\alpha m}$ ,  $\mu_{\beta m}$  in each layer which removes the singularities in the integrand from the real  $k$  axis. This is done by setting  $k_{\alpha m}^2$ ,  $k_{\beta m}^2$  complex in each layer:

$$\bar{k}_{\alpha m}^2 = k_{\alpha m}^2 - 2i\mu_{\alpha m} k_{\alpha m}$$

$$\bar{k}_{\beta m}^2 = k_{\beta m}^2 - 2i\mu_{\beta m} k_{\beta m}$$

since  $H_0^{(2)}(kr) = J_0(kr) - iY_0(kr)$

the integral solution for a constant power source may be written

$$P_D = -\frac{1}{c} \int_0^\infty \frac{P_0}{wps} \left\{ \frac{(GN - HL)(A_{S1})_{32}}{(NK - ML)} - (A_{S1})_{33} \right\} dk$$

$$(A_{D1})_{32} \int H_0^{(2)}(kr) k dk$$

if we remember that only the part of  $H_0^{(2)}(kr)$  corresponding to  $J_0(kr)$  is desired.

Let

$$F(k) = -\frac{P_0}{\omega \rho_s} \left\{ \frac{(GN - HL)(A_{S_1})_{32}}{(NK - ML)} - (A_{S_1})_{33} \right\} .$$

$(A_{D_1})_{32} \propto k$

and set

$$H_0^{(2)}(kr) = \left(\frac{2}{\pi}\right)^{\frac{1}{2}} \frac{1}{(kr)^{\frac{1}{2}}} e^{-i(kr - \frac{\pi}{4})}$$

This approximation of  $H_0^{(2)}(kr)$  is valid beyond a wavelength from the source. The integral solution is then

$$f_{D_1} = \int_0^\infty F(k) \left(\frac{2}{\pi}\right)^{\frac{1}{2}} \frac{1}{(kr)^{\frac{1}{2}}} e^{-i\frac{\pi}{4}} e^{-ikr} dk \quad (17)$$

Let

$$k_m = k_0 + m \Delta k, \quad m=0, \dots, N-1$$

and

$$r_n = r_0 + n \Delta r, \quad n=0, \dots, N-1$$

with

$$\Delta k \Delta r = \frac{2\pi}{N}$$

N must be an integral power of two.

Substituting

 $k_m, r_n$  in Equation 17

$$f_D(r_n) = \left(\frac{2}{\pi}\right)^{\frac{1}{2}} \frac{\Delta k}{r_n^{\frac{1}{2}}} e^{-ik_0 r_n} \sum_{m=0}^{N-1} \left\{ \frac{F(k)}{k_m^{\frac{1}{2}}} \cos\left(\frac{\pi}{4} + m\Delta kr_0\right) \right.$$

$$\left. -i \frac{F(k)}{k_m^{\frac{1}{2}}} \sin\left(\frac{\pi}{4} + m\Delta kr_0\right) \right\} e^{-2\pi i mn/N}$$

$$F(k) = \operatorname{Re}[F(k)] + i \operatorname{Im}[F(k)],$$

or

$$f_D(r_n) = \left(\frac{2}{\pi}\right)^{\frac{1}{2}} \frac{\Delta k}{r_n^{\frac{1}{2}}} e^{-ik_0 r_n} \sum_{m=0}^{N-1} (X + iY) e^{-2\pi i mn/N}$$

This formula is rapidly evaluated at  $n$  range points  $r_n$  by

the FFT for the complex input  $X + iY$ .

The upper limit of integration is chosen to include waves corresponding to nonzero values of the integrand in the layered system.

The upper limit of integration is

$$k_{UP} = k_0 + (N-1)\Delta k$$

from which

$$\Delta k = \frac{k_{up} - k_0}{N - 1}$$

and

$$\Delta r = \frac{2\pi}{N \Delta k}$$

Propagation loss at range  $r_n$  is defined by

$$PL(r_n) = -20 \log_{10} \frac{|P_{D_i}|}{P_0}$$

If the attenuation coefficients are equal in each layer the effect

on propagation loss of the attenuation is removed by multiplying

$$P_{D_i} \quad \text{by} \quad f(r_n) = e^{2\mu_{dm} r_n} \quad e^{2\mu_{pm} r_n}$$

In this case

$$PL(r_n) = -20 \log_{10} \frac{|P_{D_i}(r_n)f(r_n)|}{P_0}$$

The effect of attenuation by a rough ice sheet is introduced in the propagation loss computations by multiplying  $|P_D(r) f(r_n)|$  by

$$e^{-(1.29 \times 10^{-4} f^{\frac{3}{2}} H^{\frac{8}{5}} \sqrt{1 - \frac{c_0^2}{c^2}} \frac{r_n}{r_i})}$$

where

$f$  = wave frequency

$H$  = RMS ice roughness in m

$c_0$  = surface sound velocity in the water in m/sec

$r_i$  = range for one cycle of a ray of phase velocity  $c$ .

This formula is derived by Marsh et al (1961) and was used by

Mellen and Marsh (1965) for their work on Arctic propagation. It

has proved useful at low frequencies if  $c$ , and  $r_i$

are computed from a ray vertexing at 1000 m for deep water propagation.

## APPENDIX B

## LAYER MATRIX ELEMENTS

Solid Layers:

$$(a_m)_{11} = (a_m)_{44} = 2 \left( \frac{k}{k_{\beta m}} \right)^2 \cos P_m -$$

$$\left[ 2 \left( \frac{k}{k_{\beta m}} \right)^2 - 1 \right] \cos Q_m$$

$$(a_m)_{12} = (a_m)_{34} = i \left\{ k \left[ \frac{2 \left( \frac{k}{k_{\beta m}} \right)^2 - 1}{r_{\alpha m}} \right] \sin P_m \right.$$

$$\left. + \frac{2}{k} \left( \frac{k}{k_{\beta m}} \right)^2 r_{\beta m} \sin Q_m \right\}$$

$$(a_m)_{13} = (a_m)_{24} = -\frac{k}{\rho_m w} (\cos P_m - \cos Q_m)$$

$$(a_m)_{14} = i \left( \frac{\frac{k^2 \sin P_m}{\rho_m w r_{\alpha m}} + \frac{r_{\beta m}}{w P_m} \sin Q_m}{1} \right)$$

$$(a_m)_{21} = (a_m)_{43} = -i \left\{ 2 \left( \frac{k}{k_{\beta m}} \right)^2 \frac{r_{\alpha m}}{k} \sin P_m + \left[ 2 \left( \frac{k}{k_{\beta m}} \right)^2 - 1 \right] \frac{k \sin Q_m}{r_{\beta m}} \right\}$$

$$(a_m)_{22} = (a_m)_{33} = \left\{ - \left[ 2 \left( \frac{k}{k_{\beta m}} \right)^2 - 1 \right] \cos P_m \right\}$$

$$+ 2 \left( \frac{k}{k_{pm}} \right)^2 \cos Q_m \} \quad \quad \quad$$

$$(A_m)_{23} = \frac{i}{\rho_m \omega} \left[ r_{\alpha m} \sin P_m + \frac{k^2 \sin Q_m}{r_{\beta m}} \right]$$

$$(a_m)_{31} = (a_m)_{42} = \frac{2\beta_m w}{k} \left( \frac{k}{k_{\beta m}} \right)^2 \left[ 2 \left( \frac{k}{k_{\beta m}} \right)^2 - 1 \right]$$

$$\cdot (\cos P_m - \cos Q_m)$$

$$(a_m)_{32} = i \rho_m \omega \left\{ \left[ 2 \left( \frac{k}{k_{\beta m}} \right)^2 - 1 \right]^2 \frac{\sin P_m}{r_{\alpha m}} \right.$$

$$\left. + \left[ 2 \left( \frac{k}{k_{\beta m}} \right)^2 \right]^2 \frac{r_{\beta m} \sin Q_m}{k^2} \right\}$$

$$(a_m)_{41} = i \omega \rho_m \left\{ \left[ 2 \left( \frac{k}{k_{\beta m}} \right)^2 \right]^2 \frac{r_{\alpha m} \sin P_m}{k^2} \right.$$

$$\left. + \left[ 2 \left( \frac{k}{k_{\beta m}} \right)^2 - 1 \right]^2 \frac{\sin Q_m}{r_{\beta m}} \right\}$$

Liquid layers:

$$(a_m)_{11} = (a_m)_{44} = 1$$

$$(a_m)_{12} = (a_m)_{13} = (a_m)_{14} = (a_m)_{21} =$$

$$(a_m)_{24} = (a_m)_{31} = (a_m)_{34} = (a_m)_{41} =$$

$$(a_m)_{42} = (a_m)_{43} = 0$$

$$(a_m)_{22} = (a_m)_{33} = \cos P_m$$

$$(a_m)_{23} = \frac{i r_{dm} \sin P_m}{\omega P_m}$$

$$(a_m)_{32} = \frac{i \omega P_m \sin P_m}{r_{dm}}$$

REFERENCES

Buck, B. M., "Arctic Acoustic Transmission Loss and Ambient Noise", In: J. E. Sater, ed., Arctic Drifting Stations, Montreal: The Arctic Institute of North America, pp. 427-438, 1968.

DiNapoli, F. R., "Fast Field Program for Multilayered Media", Naval Underwater Systems Center Report No. 4103, 1971.

Dorman, J., "Period Equation for Waves of Rayleigh Type on a Layered Liquid-Solid Half-Space," Bull Seismol. Soc. Am., 52, pp. 389-397, 1962.

Haskell, N. A., "The Dispersion of Surface Waves on Multilayered Media," Bull. Seismol. Soc. Am., 43, pp. 17-34, 1953.

Harkrider, D. G., "Surface Waves in Multilayered Elastic Media I. Rayleigh and Love Waves from Buried Sources in a Multilayered Elastic Half-Space," Bull. Seismol. Soc. Am., 54, pp. 627-679, 1964.

Kutschale, H. W., "Long-range Sound Transmission in the Arctic Ocean", Jour. of Geophys. Res., 66, pp. 2189-2198, 1961.

Kutschale, H. W., "Arctic Hydroacoustics," Arctic, 22, pp. 246-264, 1969.

Kutschale, H. W., "Effect of an Ice Layer on Arctic SOFAR Propagation", Jour. Acoust. Soc. Am., 52, p. 137, 1972 (abstract)

Kutschale, H. W., "Further Investigation of the Integral Solution of the Sound Field in Multilayered Media; A Liquid-Solid Half Space with a Solid Bottom", Lamont-Doherty Geol. Obs. of Columbia University Tech. Rept. No. CU-6-71, 1972.

Kutschale, H. W., "Rapid Computation of Propagation Loss of Ice Vibrations from Underwater Sources in the Arctic Ocean (Report in preparation).

Kutschale, H. W., "The Integral Solution of the Sound Field in a Multilayered Liquid-Solid Half Space with Numerical Computations for Low-Frequency Propagation in the Arctic Ocean", Lamont-Doherty Geol. Obs. of Columbia University Tech. Rept. No. CU1-1-70, 1970.

## REFERENCES (cont'd)

Marsh, H. W. and S. R. Elam, Internal Document Raytheon Company,  
Marine Research Laboratory, New London, Connecticut, 1967.

Marsh, H. W., M. Schulkin, and S. G. Kneale, "Scattering of Underwater Sound by the Sea Surface, Jour. Acoust. Soc. Am., 33, pp. 334-340, 1961.

Mellen, R. H. and H. W. Marsh, Underwater Sound in the Arctic Ocean, New London, Connecticut, U. S. Navy Underwater Sound Laboratory Report MED-65-1002, 1965.

Thomson, W. T., "Transmission of Elastic Waves through a Stratified Solid Medium", J. Appl. Phys., 21, pp. 89-93, 1950.